2009

# Pretest 3-D finite element analysis of the girder-to-cap-beam connection of an inverted-tee cap beam designed for seismic loadings

Zachary John-william Thiemann
*Iowa State University*

# Pretest 3-D finite element analysis of the girder-to-cap-beam connection of an inverted-tee cap beam designed for seismic loadings

by

Zachary John-William Thiemann

A thesis submitted to the graduate faculty

in partial fulfillment of the requirements for the degree of

MASTER OF SCIENCE

Major: Civil Engineering (Structural Engineering)

Program of Study Committee:

Sri Sritharan, Major Professor
Fouad Fanous
Lester Schmerr

Iowa State University

Ames, Iowa

2009

## Table of Contents

## Table of Figures

## Table of Tables

# Chapter 1. INTRODUCTION

## 1.1 General

An integral part to any roadway system is the bridge structures used to connect roadways over obstacles. Many of these bridges are present in areas of high seismic activity. One of these areas is the state of California. The roadway system in the state of California contains more than 24,000 bridges (Federal Highway Administration, 2008). More than twenty different types have been used in the design of the bridges in the state of California, with the most commonly used being: slabs, multi-girder, tee beam and box beam (Federal Highway Administration, 2008). The median age of the bridges in California is forty years (State of California, 2007).

The cast-in-place box-girder is the most popular of the bridge types; however, an increasingly popular bridge style is an inverted-tee bent cap, shown in Figure 1.1. This style includes a cast-in-place column and cap beam and precast girders that are set on the ledges, or corbel, of the cap beam. The stem of the cap beam is the middle portion, with a total height typically equal to the height of the superstructure, and the ledges are shorter to allow for the dapped end of a girder to rest on it. The inverted-tee bent cap has been used in design by Caltrans for decades. A common use of the inverted-tee bent cap is in widening projects of existing structures. In the widening process, precast concrete girders are placed on the ledges of the cap beam and then the bridge deck is cast-in-place.

The use of precast girders allows the total construction time to be reduced, when compared to cast-in-place girders, which allows for less disruption to the traffic system and greater safety on the jobsite (Internation Federation of Structural Concrete, 2007). Also, another benefit of the inverted-tee bent cap is in regard to clearance issues. Since the girders are placed on the ledge of the bent cap, and not on top of the bent cap, the overall depth of the sub-structure is reduced. However, with the

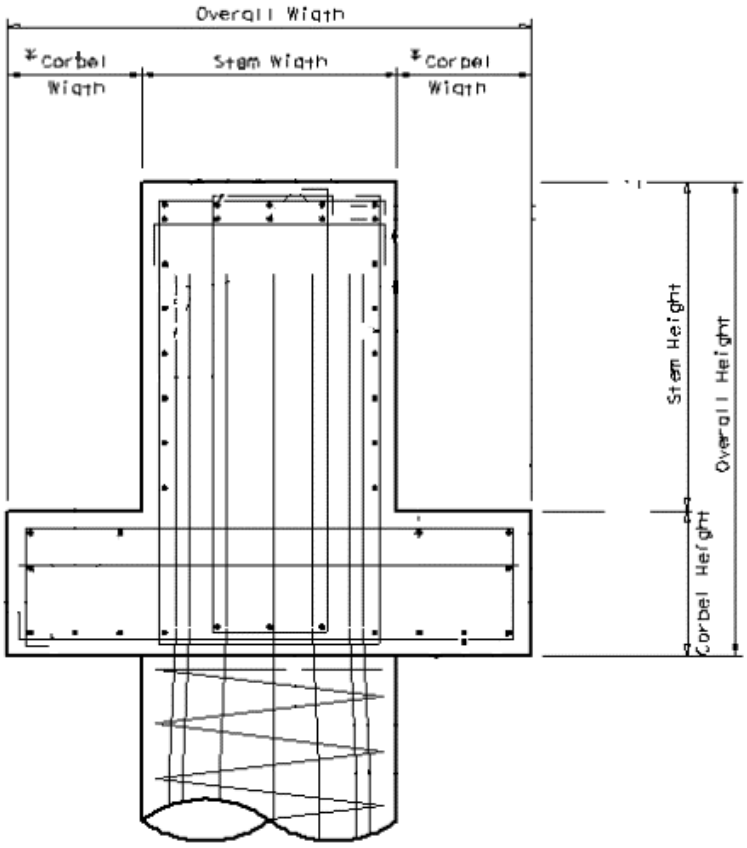


Figure 1.1. Inverted-Tee cap beam diagram

Figure 1.2. Example of the use of precast I-girders on a highway bridge widening project in California. (Internation Federation of Structural Concrete, 2007)

application of the load to the ledge, special reinforcing needs to be detailed for shear, flexure and anchorage of the cap beam (Caltrans, 1995).

The current design assumption, used by Caltrans in the design of inverted-tee cap beam systems, is that the cap-to-girder connection has zero moment resistance. This is uneconomical because it will require a larger column and foundation, the base must be fixed and the structure will have increased sensitivity to seismic displacements. The increased sensitivity is due to the top of the column being considered pinned, which allows for more displacement when compared to a column with a fixed top. Additionally, fixing the top and bottom of the column results in less displacement as it places the column in double-bending as opposed to single-bending. Also, assuming no moment resistance, the natural period of the system will be miscalculated to be longer due to a smaller stiffness value. However, as the cap beam experiences large rotations, there becomes a greater possibility of the girder closing any gap between the girder and cap causing negative moment resistance. Therefore, the assumption of zero moment resistance in the cap-beam-to-girder connection and inaccurate estimate of the seismic design forces will likely result in possible damage to the superstructure

In the last forty years, the seismic design philosophy has changed dramatically. The original philosophy, dating back to before 1970, led to three main deficiencies: underestimated seismic deflections, artificially low gravity to seismic load ratio and insufficient mechanisms of inelastic response. All these deficiencies can be traced back to the use of an elastic design philosophy. In the design, the assumed seismic forces were significantly underestimated. The result of this assumption was drastic. Once the forces in the structure exceeded the sections capacity, very little inelastic action occurred which caused the bridge to experience catastrophic damage (Priestley, Seible, & Calvi, 1996). The actual deflections experienced were significantly larger than expected, causing pounding of nearby structures and unseating of the superstructure. Since the seismic load was underestimated,

the seismic moment profile was significantly misrepresented and the flexural reinforcement was subsequently incorrectly placed. Also, the locations of reinforcement termination were inappropriate and possibly terminated well within the moment region in which it was needed. This resulted in insufficient moment capacity at some locations, anchorage and lap-splice failures at other locations. The bars were anchored and spliced in areas where the moment was thought to be low but actually were areas of high moment. As a result, the reinforcement often failed, causing significant damage as the structure was not designed to experience the inelastic action in that area. However, when the design forces were exceeded, the system had little inelastic capacity or ductility. The ductility of a structure allows the energy generated in a seismic event to be dissipated; the higher the ductility, the more the structure can dissipate excess energy before catastrophic consequences occur. The lack of design for inelastic action led to confinement failures in the column. Sufficient confinement will allow the structure to experience a significant ductile behavior to dissipate the seismic energy. Without confinement, the concrete will crush at lower strains and lose strength rapidly. When reconsidering the design philosophy, after the major earthquakes in California in the 1980's and 1990's, the idea of designing plastic hinges in the columns, while keeping the superstructure elastic, became the recommended practice. Allowing the column to experience a plastic action will provide greater energy dissipation and allow for sufficient ductility. This greater ductility will help ensure that the column will not experience a brittle failure due to the flexural demand. However, for this to be possible, sufficient and effective detailing must be provided in order to not allow other types of brittle failure to occur. Also, for a plastic hinge to fully develop, adequate confinement must be provided. After examining damage from previous earthquakes, the lack of confining steel has been a contributing factor in some of the collapses. The confining steel is placed around the plastic hinge area, in hoops or spirals, and helps prevent the concrete from expanding laterally. This allows the core of the concrete to experience higher compressive stresses and strains. If the plastic hinge area is incorrectly placed or insufficiently detailed, the resulting damage can be catastrophic. Another result

of low design forces was the shear resistance provided in the columns. As the structure experienced the seismic activity, the columns failed in a brittle manner once the shear force exceeded the capacity. The capacity design philosophy is based on allowing the structure to respond inelastically through flexural yielding and not allowing undesirable failure mechanisms, such as shear, bond and confinement failure, to occur.

Considering the inverted-tee bent cap to girder connection, possible damage may include unseating, pounding and confinement failure among others. As the bridge undergoes a seismic event, the columns will displace at the foundation. Once this happens, the columns will bend due to the inertial resistance of the superstructure and, with an assumed pinned column to superstructure connection, the cap beam will rotate. As the cap beam rotates, a gap may be formed between the bottom of the girder and cap beam on the positive moment side. As the cap beam experiences large rotations and displacements, the girders may unseat themselves from the cap beam or bearing pad, as shown in Figure 1.3. If the girders fully unseat themselves from the cap beam, the span will fall

Figure 1.3. Girder Unseating

down. If this were to happen, the bridge will need to be replaced, which will be a lengthy and expensive process. More importantly, it is possible that the collapse of the bridge could also result in a loss of human life. If the girder unseats itself from the bearing pad only, that will cause the girder to drop 1" or more and damage the bridge deck.

However, as the cap beam rotates on the negative moment side the girders will close any gap present and strike the cap beam or abutment which is referred to as pounding. An example of pounding can be seen in Figure 1.4, where two girders can be seen impacting against each other. As the girder strikes the cap beam, the concrete in the impact area may crack and damage the girders or cap beam. Depending on the location of pounding, the damage can lead to additional failures. The costs to repair the superstructure of the bridge are high because the traffic will need to be diverted so construction crews can repair the area, leaving this as an unwanted scenario.

Figure 1.4. Girder to Girder pounding

If the connection is partially or fully moment resistant, which it is assumed not to be, the moment transferred to the top of the column maybe large enough to cause a confinement failure in the top of the column, which can be seen in Figure 1.5. As stated previously, the confinement will allow for a greater ductility without significant strength loss, which is one of the principles of the current design

philosophy. Given the current cap-beam-to-girder connection of the inverted-tee bent cap, it is likely that the aforementioned failures may be experienced in a future seismic event.

Figure 1.5. Confinement failure at the top of the column

The importance of practical and economical designs within seismic regions has been increased due to the catastrophic damage experienced by bridge structures during seismic events over the last twenty years. Previous earthquakes have accounted for billions of dollars of economic losses along with the loss of human life. Part of the economic losses is attributed to the closure of bridges which then disrupt the transportation infrastructure. As discussed above, the inverted-tee bent cap

Table 1.1. Estimated Earthquake Economic Costs

| Earthquake | Date | Magnitude | Total Loss[1] |
|---|---|---|---|
| San Fernando | February 9, 1971 | 6.7 | 2,240 |
| Imperial Valley | October 15, 1979 | 6.5 | 79 |
| Coalinga | May 2, 1983 | 6.4 | 18 |
| Loma Prieta | September 18, 1989 | 7 | 8,000 |
| Northridge | January 17, 1994 | 6.7 | 23,000-46,000 |
| [1] Total loss in millions of 2000 dollars | | | |

is the optimal choice when widening existing roadways because of the ability to utilize precast girders, minimizing construction time. As the population continues to grow in California, the

potential for using these bents to meet the expanding highway system increases. Therefore, if the inverted-tee cap beams do not perform adequately, the losses from a future seismic event can be greater.

## 1.2 Current Design Procedure

The current design procedure for bridges, including the inverted-tee, for the State of California follows details presented in the Seismic Design Criteria (SDC), along with the Bridge Design Specifications (BDS) and AASHTO LRFD Bridge Design Specifications (AASHTO). While the BDS and AASHTO provide detailed steps for the design of a standard bridge, the SDC is a compilation of design criteria, either newly or previously developed, that is reflective of the current practice for seismic bridge design in California (Caltrans, 2006). The SDC is applicable for all Ordinary Standard bridges, which are bridges that meet the following criteria (Caltrans, 2006):

- Span lengths less than 300 ft
- Constructed with normal weight concrete girders and columns or piers
- Horizontal members either rigidly connected, pin connected or supported on conventional bearings
- Dropped bent caps or integral bent caps terminating inside the exterior girder
- Foundations supported on spread footing, pile cap with piles or pile shafts
- Soil that is not susceptible to liquefaction, lateral spreading or scour

The connection being considered in this study is used on bridges classified as Ordinary Standard bridges. Upon further review of the SDC, it is noted that for precast girders, the lack of a sufficient positive moment connection between the girder and cap beam may lead to degradation of the connection to a pinned connection during seismic actions. The conclusion drawn from this information was to require a fixed base condition, for the case of the inverted-tee bent cap. It is also

mentioned that the mild reinforcement to resist a positive moment in the girder bottom should be placed during the casting of the precast girders, where the required steel in the top shall be placed in the slab and made continuous.

The bridge system currently designed uses a cast-in-place column and inverted-Tee cap beam constructed in the field. Then, the dapped end of the precast girder is set on bearing pads, which rest on the ledge of the cap beam. After the girders are set in place, three 4-foot pieces of rebar are inserted through the interior girders and three 1-inch diameter bolts are threaded into the inside face of the exterior girders, near the edge of the cap beam, to act as dowels. A diaphragm is poured between the girders and around the cap beam, which produces a rectangular section instead of a tee-shaped section. The deck is then poured on top of the girders and cap beam. Once the diaphragm and deck have cured, a connection between the girder and diaphragm and cap beam is formed, which will allow the transfer of forces from the superstructure to the cap beam and column. Additional description of the bridge system will be discussed in Chapter 3.

The moment being transferred from the superstructure to the column is not preferred when the column was designed as a pinned top connection. This could possibly lead to a failure at the top of the column due to the flexural demand exceeding the capacity. It is also possible that a confinement failure would occur, since little confinement was designed in that section. If the connection is transferring moment as suspected, then the column needs to be detailed adequately to withstand these forces.

The performance of the current connection needs to be established so that the design of future bridges can be performed adequately and, if needed, current bridges can be retrofitted. Analytical investigation into the behavior of the cap-beam-to-girder connection will be conducted. The objectives are detailed in the next section.

## 1.3 Scope and Objective

The scope of this research is to investigate the actual behavior of the current girder-to-inverted-tee- bent-cap-beam connection and to recommend an improved connection detail to better utilize the whole system for seismic resistance such that it will lead to an efficient and cost effective design practice.

A prototype bridge was developed using the current connection details. The prototype bridge was then used to develop a fifty percent scale test unit. A single-girder model was developed in ABAQUS, a 3-D finite element analysis program, using the prototype structure details and dimensions to capture the moment capacity of the current connection. A single-girder model with the test unit dimensions was then modeled to develop the moment-rotation characteristics of the existing connection. Then, a two-and-one-half girder model was developed to investigate the additional effects from the slab, diaphragm and cap beam on the behavior of the system. A new girder-to-cap-beam connection was then developed in order to provide a moment resistant connection so that a plastic hinge can be developed at the top of the column. The proposed connection was then modeled to capture the behavior and ensure the effectiveness.

The test unit will include the old connection details on one side and a newly developed connection detail on the other. Prior to the testing a grillage model was developed to understand the behavior of the prototype structure. These analytical results were used to ensure that the design of the test unit was such that the behavior during the testing would accurately correspond to that of the prototype bridge. In order to more accurately predict the test results, the cap beam to girder connection of the test unit was modeled using the moment-rotation properties developed in this thesis.

The results were implemented into the grillage analysis to enhance the capabilities of the model in predicting the overall seismic performance.

In a future report, the validation of the analysis models will be presented with data collected from the laboratory testing of the test unit. Once the validation is complete, the results will be reintroduced into the prototype models and used to assess the adequacy of both the current and proposed connection. The completed grillage model will also be used as a tool in future designs and analysis.

## 1.4 Report Layout

The research outlined in the previous section is presented in seven chapters including the current chapter. A literature review performed to gather knowledge about previous cap-beam-to-superstructure moment connection research and the seismic related applications. Also, modeling techniques are discussed to capture the specific behavior of moment connections. A Prototype structure design is presented in Chapter 3. Chapter 4 presents information on the development of the Test Unit for the large-scale testing portion of the project. The finite element model development is presented in Chapter 5. Analysis results are presented in Chapter 6 including the analysis of the Prototype structure and Test Unit. For the Test Unit analysis, multiple analyses are presented in attempts to capture the difference behaviors affecting the structural response. Also, the proposed connection is presented and analyzed. The conclusions are summarized and presented in Chapter 7. The Prototype and Test Unit drawings are presented in Appendix A and B, respectively. Appendix C contains the material properties used in the finite element model.

# Chapter 2. LITERATURE REVIEW

## 2.1 Introduction

In order to better understand the seismic performance of an I-Girder to inverted-tee bent cap connection, as well as the various finite element models and details required to complete the project, an in-depth literature review was performed. It was found that little research has been performed on precast girder-to-cap connections under seismic loading. The previous research mainly focused on the use of integrally cast cap beams, some with the use of precast girders, both steel and concrete, while no research was discovered relating to the use of inverted-tee cap beams or a complete precast system for seismic regions.

It is now widely known that the use of precast components offers a substantial amount of benefits to both contractors and designers. For example, construction time is reduced, less falsework is required, the construction requires less of an impact on the surrounding environment, and the components are constructed in a more controlled environment, which results in a higher quality of craftsmanship. However, it could be argued that the use of spliced girders with an integral cap beam could be a disadvantage in terms of constructability, when compared to an inverted-tee cap. If an adequate moment resisting connection can be developed and practically implemented in the field in order to achieve continuity with an inverted-tee system, then this type of system may be used more frequently than it is currently. Since the girders would not need to be supported by falsework while constructing the integral cap beam for an inverted-tee concept, a smaller environmental impact, less labor intensive construction procedures, and improved cost savings could be achieved with this system compared to those described in the studies presented above.

As these precast systems become more common, the need for experimental studies to predict their behavior during seismic events becomes an increasing priority. Specifically, the connection

behavior between the precast girders and cap system is of interest as it will govern the placement and possibly the formation of the column plastic hinges as well as the generalized behavior. Previous experimental studies, which will be discussed in more detail below, have indicated that the negative moment resistance provided by these connections can most often be developed by the reinforcement placed within the deck slab. However, more information is still desired regarding the formation of any positive moment resistance within the connection.

The use of lab testing, of any scale, is of common use in engineering research. A search of bridge research proves that a high percentage of the research projects include lab testing, either exclusively or for validation. This method can effectively predict the true response of a bridge as long as any scaling has been done properly. The use of lab testing to validate other analytical models has been a common practice in the past. Superstructure to cap beam connection testing by (Almer & Sanders, 2007) has shown that a scaled test unit can be used to validate the analytical work done using more simplified means. The research focused on precast girder to cast-in-place bent caps and they were able to investigate the performance of the superstructure to cap beam connection, for both positive and negative moment, when subjected to a seismic application. They have tested two test units at the time of the paper publishing and will design the next two to improve upon the response of the first tests. The information gathered from testing in the lab for research is valuable and, as long as the setup is correct, is the best indicator of true response of a system. However, lab testing is not always the most efficient way to gather the response of a system. The cost of a few bridge test units can become very costly when considering the labor, materials, lab space, etc. The ability to secure funding to test multiple designs is challenging, now that other more cost effective means have been found to analytically predict the same response.

The following literature review begins with a brief background on the experimental research that has been conducted on the seismic performance of bridges made continuous for positive moment

at the girder-to-cap connection. Information regarding positive moment connection and then the use of finite element analysis techniques to predict and understand the behavior of various aspects of the bridge, such as the rotation, strains and displacements, will be presented. Finally, the need, benefits, and means for establishing positive moment connections between girders and bent cap systems, as well as related previous experimental studies, are discussed.

## 2.2 Positive Moment Connection

### 2.2.1 Background

The use of precast girders has become a common place in bridge design, as it allows for the construction time to be greatly reduced. However, careful consideration has to be given to the area over the cap beams to ensure that sufficient continuity is provided through the girder-to-cap connection. For negative moment resistance, reinforcing bars are typically placed in the deck over the cap beam to provide the necessary moment resistance (Miller, Castrodale, Mirmiran, & Hastak, 2004). Mechanical splices, provided directly between the girder top flanges and the cap beam, have also been used in order to develop negative moment resistance. Testing of the connection from the superstructure to cap beam has been conducted by Portland Cement Association, and discussed in the NCHRP 519 report (Miller, Castrodale, Mirmiran, & Hastak, 2004), that showed that using the reinforcing in the deck for negative moment was adequate in design. During the aforementioned testing, cracking was observed in the diaphragms and the cause was believed to be from positive moment. The positive moment was caused from time-dependent effects on the girders. Therefore, a recommendation was made that a connection from the bottom of the diaphragm, next to the girder, to the girder should be provided. Multiple positive moment connections, which are discussed later, were then constructed and tested. During the testing, it was observed that the formation of cracks in the slab were the first signs of failure of the positive moment connection. Once the connection failed, the slab acted as a hinge during further loading (Miller, Castrodale, Mirmiran, & Hastak, 2004).

Many states currently use precast, prestressed girders for continuous highway bridges (Freyermuth, 1969). A survey of 150 agencies in Japan, Canada and the United States was performed regarding the use of positive moment connections. One-third of the surveys were returned and about half of the respondents said they had designed less than 200 continuous precast girder bridges while seven-percent responded indicating that they had designed more than 1,000 (Hastak, Mirmiran, Miller, Shah, & Castrodale, 2003). The main application of continuous, precast bridges was on interstates and high volume urban highways. Another observation from the survey was that over 60 percent of the respondents reported that they consider positive moment continuity for live load and superimposed dead load during their design process. For seismic regions, most of the respondents preferred positive moment continuity to be provided in all multi-span bridges. The connections were used with girders primarily of the AASHTO Type III and IV size. Other girder sizes that have been used were the PCI-BT, Quad-T, NEBT, U-Beams and Texas shapes. Finally, for the design of the cap beam to superstructure connections, half the respondents replied that a standard detail was used regardless of the application while the majority of the remaining responses used the PCA Method developed by Freyermuth, which is briefly discussed below. It was reported that some found the PCA Method to be conservative in design.

One of the first research projects undertaken to provide details for moment connections was performed to develop what is known as the PCA method, which provided details for designing connection between the superstructure and cap beam to resist creep, shrinkage and live load moments at the cap beam (Freyermuth, 1969). Testing was conducted on the connection that was considered most practical, shown in Figure 2.1, was performed both in a static manner and a fatigue test with a stress range of 20,000 psi. Based on the results, some design recommendations were presented. During the design of the structure, it is recommended that the stress on the bottom face of the girder be limited to 80 percent of the modulus of rupture. A similar recommendation was stated to limit the stress in the connection reinforcing bars to 0.6 times the yield stress. The limit was developed to keep

the diaphragm concrete from cracking under positive moments. Also, multiple connections were tested and it was found that most of the bars failed at 670,000 applications of the load. The failure was of the brittle manner at knee of the hooks. As a result, in order to avoid this mode of failure, a recommendation was made that the maximum stress where the bar bends begin should be limited to 50 percent of the fatigue strength (Freyermuth, 1969). Also, it was recommended that, due to the amount of design calculations, standard details to be used in all loading scenarios should be recommended for each common girder types.

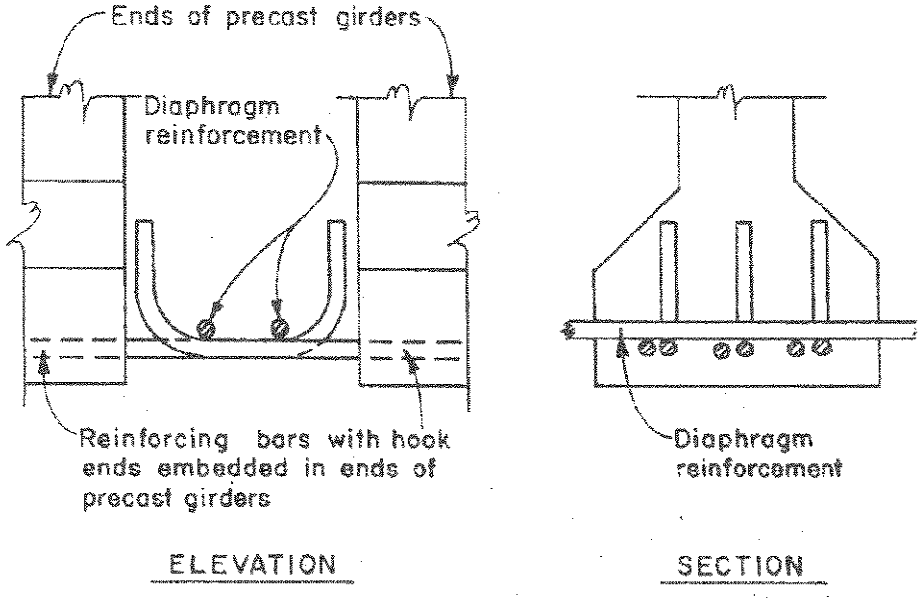


Figure 2.1. Tested connection for testing by Freyermuth (1969)

### 2.2.2 Causes of Positive Moment at Connections

The cause of positive moment comes from multiple effects, while each could appear minor, they can have large effects on the behavior of the structure. A few common causes of positive moment are creep, shrinkage and temperature strain in the decks and girders (Miller, Castrodale, Mirmiran, & Hastak, 2004). In the testing performed for the NCRHP 519 Report, creep, shrinkage and temperature strains were assumed to produce a positive moment equivalent to the nominal

cracking moment at the beam-diaphragm interface (Miller, Castrodale, Mirmiran, & Hastak, 2004). The combined creep, shrinkage and thermal effects may cause the girder to camber up resulting in end rotations of the girders. When this occurs, a positive moment develops at the diaphragm next to the grider and may be large enough to crack the diaphragms as seen in Figure 2.2 (Hastak, Mirmiran, Miller, Shah, & Castrodale, 2003). However, it was found that the creep effects are partially counteracted by the differential shrinkage between the precast girders and the cast-in-place deck (Freyermuth, 1969).

In some cases the shrinkage did not appear to cause any negative moment, the reactions actually showed that additional positive moment was forming (Miller, Castrodale, Mirmiran, & Hastak, 2004). The thermal effects were found to be significant as it caused a daily moment change of over one-half the cracking moment capacity of the diaphragm (Miller, Castrodale, Mirmiran, & Hastak, 2004). Finally, once the spans are made continuous, the effects in one span will cause positive moment in remote spans leading to additional positive moment demands. In addition to those investigations, seismic excitation of a structure was also found to produce positive moments in the connection regions (Priestley, Seible, & Calvi, 1996). As the superstructure displaces laterally from the seismic excitation, one side of the cap beam will experience positive moment while the other will undergo negative moment.

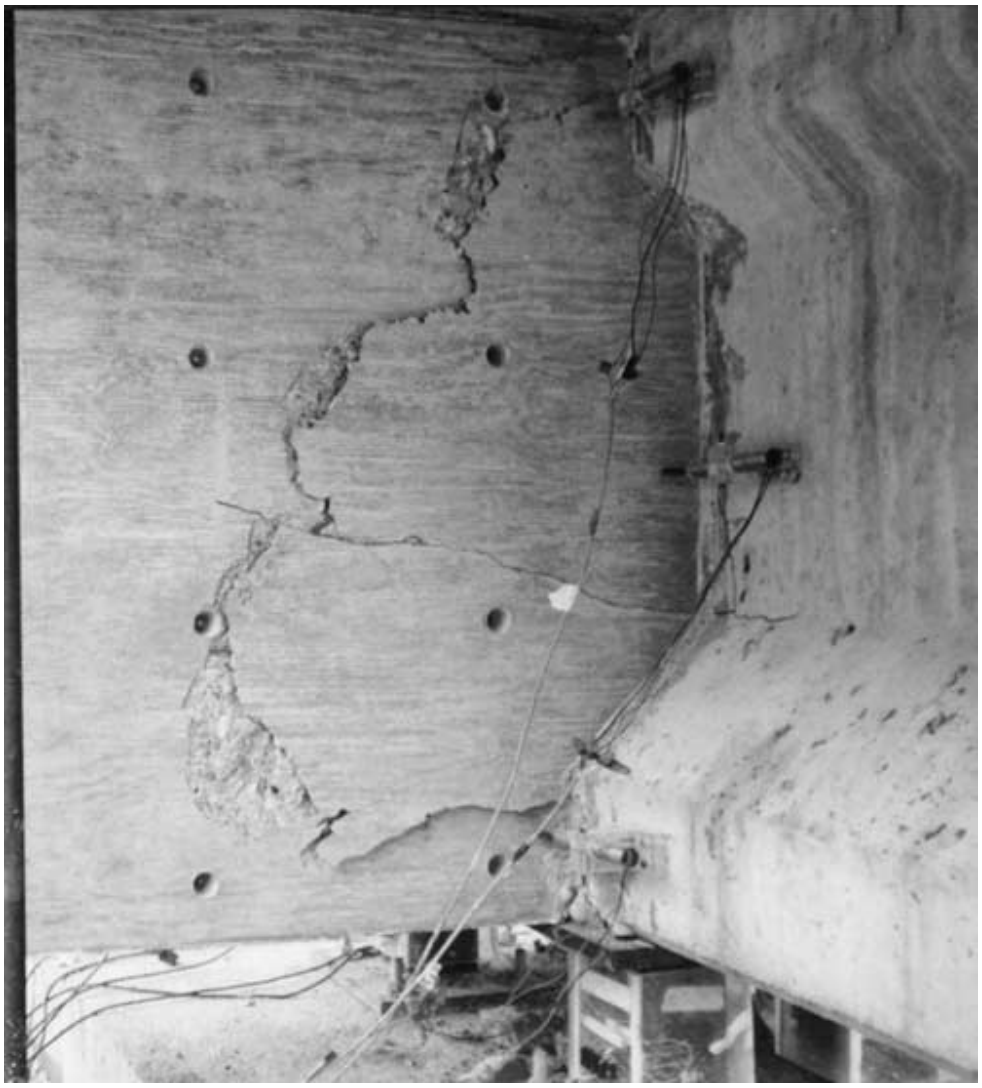

Figure 2.2. Diaphragm cracking from positive moment

### 2.2.3 Benefits of Positive Moment Connections

A general goal that many state DOTs is to make bridges continuous-for-live-load using prestressed, precast concrete components. The obvious reasons for this goal are to counteract the aforementioned causes of positive moment in order to prevent cracking of the diaphragm, deck and girders. A structure with a sufficient positive moment connection will exhibit enhance seismic resistance (Tadros, Ficenec, Einea, & Holdsworth, 1993). In addition, superior structural integrity and lower deflection levels can result when a positive moment connection between the superstructure and

cap beam is active. Also, providing positive moment continuity between the girders and cap beam via integral bents, or connecting the girder ends across the depth of the cap beam, allows for the combined depth of the cap beam and girders to be reduced (Sritharan, Vander Werff, Abendroth, Wassef, & Greimann, 2005). Providing integral connections also eliminates girder bearings which, in turn, reduce future maintenance costs. In general, the benefits of a continuous bridge are the improved durability, elimination of bridge deck joints and reduced maintenance costs (Hastak, Mirmiran, Miller, Shah, & Castrodale, 2003).

Several additional advantages of a positive moment connection directly benefit the seismic performance of the bridge (Priestley, Seible, & Calvi, 1996). The redundancy in the bridge structure is increased, which allows for additional plastic hinges to be formed. With additional plastic hinges forming, the potential for energy dissipation increases. When the response of the bridge in the longitudinal direction is concerned, the columns will be under double bending when the plastic hinges are formed at the top and bottom of the column. This allows for greater shear resistance of a given section size and reinforcement content of the columns. Additionally, a double bending behavior of multi-column bents is preferred because the stiffness in the longitudinal and transverse direction is equal, which is the optimum condition for seismic design. Also, by allowing a moment transfer at the top of the column, a pin connection can be designed at the column base; this will significantly lower the cost of the substructure. Furthermore, a pinned base is preferred for bridge columns in areas of low soil stiffness and a positive moment connection will allow for that to occur. Finally, under small seismic displacements, the connection is insensitive to the seismic displacement.

### 2.2.4 Types of Connections

A number of systems have been developed in order to establish a positive moment connection between the superstructure and cap beam; most of which require a connection mechanism to be developed between the girder and the diaphragm, in order to resist moment at the connection due to

the applied loading. The following are examples of systems that have been incorporated into a bridge structure in order to establish the desired positive moment connection: bent bars and untensioned prestressing strands, straight bars, welded bars, reinforcement placed through the web of the girders and into the diaphragms, additional stirrups placed in the diaphragms, mechanical strand connectors, a partial diaphragm to pre-compress the section, and embedding the ends of the girders into the diaphragms at the cap (all sources). However, the use of bent bars and bent strands extending into the diaphragm is the most commonly used system for the superstructure to cap beam connection, both of which are used equally as frequent (Hastak, Mirmiran, Miller, Shah, & Castrodale, 2003). Therefore, the advantages, limitations, and applications of these two systems will be of focus in the following text. The research has mainly been performed for non-seismic applications, to resist creep, shrinkage and vehicular live loads; however, some experimental research has been performed and will be discussed in the next section.

#### *2.2.4.1 Bent Bars*

According to (Freyermuth, 1969), the most practical positive restrain moment connection was the hooked bar connection. This type of connection was further tested, under monotonic and cyclic loading, and the results were published, in NCHRP 519 (NCHRP) (Miller, Castrodale, Mirmiran, & Hastak, 2004). The 90 degree hooks used in the testing, were designed using the AASHTO Standard Specifications regarding hooked bars (Miller, Castrodale, Mirmiran, & Hastak, 2004). It should also be noted, according to (Freyermuth, 1969), that the maximum bar size used for this connection, if the bars are bent in the field, should be limited to No. 6 (diameter = 0.75 in.). The full scale test specimen used in the NCHRP report consisted of two I-girders, which were connected using eight hooked No. 5 bars (diameter = 0.625”). The girders were placed 10 in. away from each other and a diaphragm and deck was poured around the girders in order to establish the connection, shown in Figure 2.3. Though some cracking occurred at the connection during the testing, the end reactions and strains within the section demonstrated that continuity was achieved and that the connection

detail was effective for the dead and live loading cases (Miller, Castrodale, Mirmiran, & Hastak, 2004). This test focused on the use of bars hooked at a 90 degree angle; however, it was also noted in this report that the use of a 180 degree bend might also be a viable option.

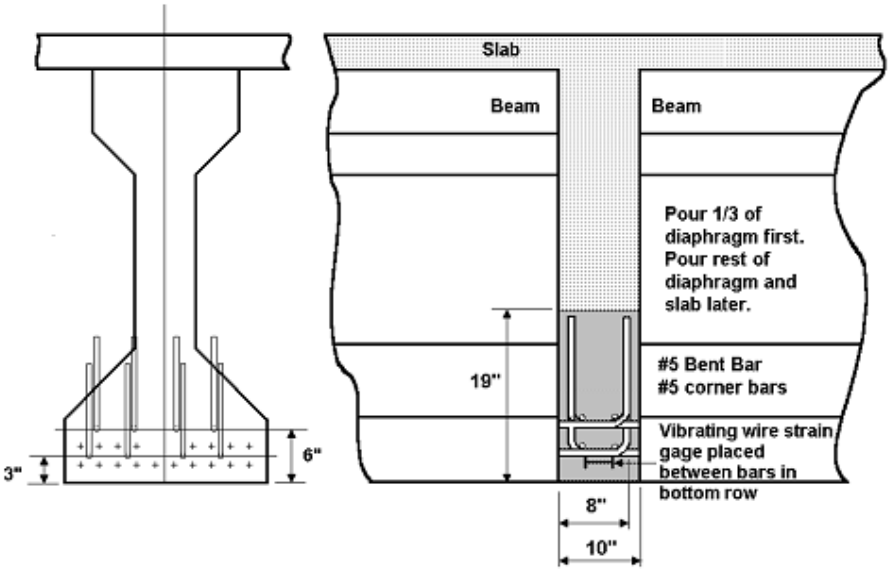


Figure 2.3. NCHRP Bent Bar Specimen

*2.2.4.2 Bent Strands*

The aforementioned NCHRP report also performed a positive moment connection test, under monotonic and cyclic loading, on a similar full scale test specimen incorporating bent strands as the connection mechanism; shown in Figure 2.4. Scaled pullout tests were also conducted on specimens using 90 degree bent, straight, and frayed strands. The results of the full scale test demonstrated that bent strands can effectively establish positive moment continuity in the system, even if cracking occurs at the joint. Continuity was only lost when the slab and diaphragm cracked and the connection was near failure. The scaled tests also showed that the bent strands resulted in the optimum anchorage when compared to the straight or frayed strands, which slipped twice as much as the bent strands. Additionally, these tests found that systems involving bent strands and girder ends that were

not embedded in a diaphragm, had a tendency for the girders to separate from the face of the diaphragm. However, this separation from the diaphragm did not result in any damage. Finally, the results of the testing did show that though the specimens did provide continuity, the bent strands also had a tendency to slip under cyclic loading. As a result, it may be concluded the bent strand detail would not be preferred for seismic applications.

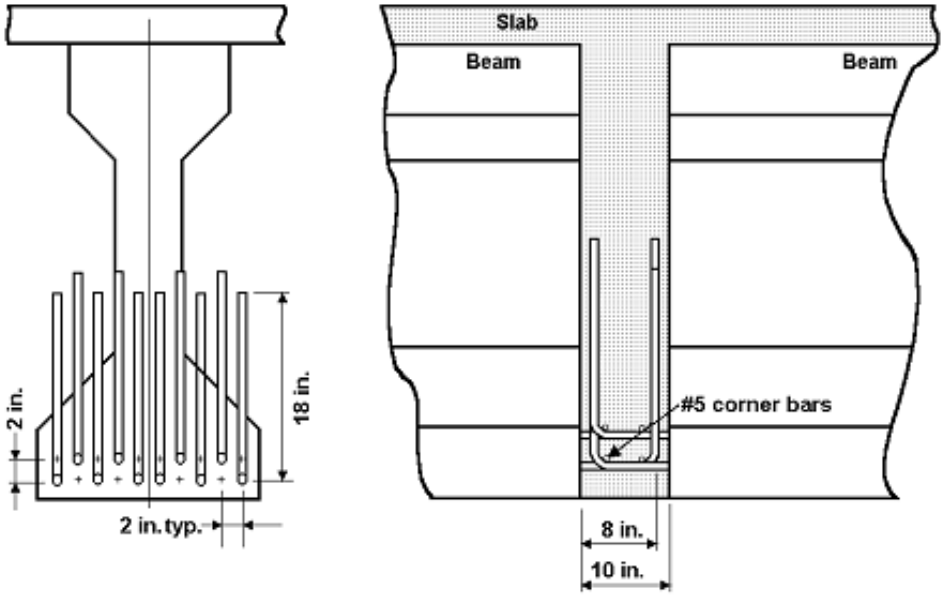


Figure 2.4. NCHRP Bent Strand Specimen

The behavior of untensioned prestressing strands for use in positive moment connection details was also investigated by Salmons and McCrate (Salmons & McCrate, 1977). Their findings showed that the helical orientation of the strands tended to unscrew the strand from the surrounding concrete. Additionally, under high stress levels, local crushing at the strand-concrete interface was observed, which contributed to both creep and slipping effects on the strand. However, under cyclic loading, additional creep was not experienced until the load returned to its previous maximum. Similar to the findings presented in the NCHRP report, Salmons and McCrate concluded that bent strands provided a higher strength and stiffness when compared to straight and frayed strand configurations. Salmons

and McCrate went further to investigate which characteristic of the section had an influence on the slip behavior experienced by the untensioned strands. First, it was concluded that the relationship between stress within the strand and slip were independent of the embedment length of the strand. Second, varying the concrete between 3750 and 6900 psi did not have a significant effect on the bond characteristics of the strand before slipping occurred. Finally, the diameter of the strand also did not have a significant effect on the stress-slip behavior of the steel strands. Based on these findings, Salmons and McCrate were able to develop and present a series of equations pertaining to the embedment length of the untensioned strands to establish a superstructure to cap beam moment connection.

#### *2.2.4.3 Embedded Girder Ends*

The aforementioned NCHRP report also investigated the effect that embedding the ends of the girders into the diaphragm had on establishing a positive moment connection. In general, it was determined that embedding the ends of the girders 5 in. into the diaphragm reduced the stresses in the connection and allowed for a higher number of cycles to be reached before failure of the positive moment connection. Girders that were connected using bent strands and embedded ends failed at a number of cycles that was three times greater than that required for the same detail without embedded ends as the strains in the embedded details were lower than those in the non-embedded. As a result, it appeared as though embedding the ends of the girders for sections connected with bent strands was beneficial. However, the general effects of the embedded were hard to quantify, specifically for the bent bar details, and as a result, it was recommended that the effects of embedment be ignored in the design process.

#### *2.2.4.4 Additional Stirrups*

A few other connection components were also examined as a part of the NCHRP report, one of which was the placement of additional stirrups within diaphragm in the joint region. During

testing, it was noted that the additional stirrups helped to control diagonal cracking and increase ductility after the main bars fractured. However, in general, the stirrups had little effect on the overall strength of the connection. Finally, the report suggested that the ends of the girders should be embedded in order for the stirrups to provide the additional ductility.

#### *2.2.4.5 Through Web Reinforcement*

Another NCHRP connection component was the use of reinforcement placed through the webs of the girders and into the diaphragm. It was found that, though the web reinforcement improved the performance of the connection, the bars caused cracks to develop in the webs of the girders, which is undesirable.

#### *2.2.4.6 Partial Diaphragm*

The final connection component that was investigated as a part of NCHRP 519 was the use of a partial diaphragm to improve the connection performance. It was initially assumed that the partial diaphragm would place the bottom of the diaphragm in compression, which would reduce the tension in the section caused by the positive moments within the joint and increase the capacity of the connection. However, it was found that though the concept worked, it was not by the originally assumed mechanism and that it did not provide continuity. Based on the results of the testing, it was implied that more research regarding the use of partial diaphragms needed to be performed in order to better understand this mechanism.

### 2.2.5 Concerns Regarding Positive Moment Connections

Though methods for establishing a positive moment connections and their respective behaviors have been established, there are still a number of concerns and issues associated with positive moment connections. This primarily includes fabrication issues, the lack of a well-defined design procedure, and the age at which the connection is established.

#### *2.2.5.1 Fabrication Issues*

In general, the additional reinforcement that is required in order to achieve continuity in the connection often results in congestion within the section, which causes difficulties related to construction in the field. However, it was found that, though the diaphragm may be congested, the connection should still have adequate strength. Additionally, the bent connection bars are difficult to construct, labor intensive, and are often asymmetrical, which can lead to uneven stresses and failure in the section (Miller, Castrodale, Mirmiran, & Hastak, 2004). The asymmetry is due to the fact that the bent connection bars must be installed straight and then be bent in the field. Also, it is not uncommon for the extended bars or strands to be damaged or fractured during fabrication and transport. In the event of a fractured piece of reinforcement, holes must be drilled into the girder ends in which the new reinforcement is embedded in epoxy. Finally, it has been observed that strands that are detensioned have a tendency to experience a "bird cage" effect, where the wires unravel, which renders the section ineffective.

#### *2.2.5.2 Lack of a Well-defined Design Procedure*

Though NCHRP 519 makes design recommendations based on the results of their extensive testing of positive moment connections, a design method for determining the amount and spacing of reinforcement for the connection has not yet been accepted. As a result, there are often concerns associated with placing too many reinforcing bars in one area without an adequate spacing within the diaphragm. It is typically assumed that cracking will occur at the interface of the beam-to-diaphragm connection region, but the failure will not occur within the diaphragm. However, it is unclear as to whether or not this cracking will affect the continuity of the system. Furthermore, it has been found that the cracking did not affect the negative moment capacity, but it did reduce the negative cracking moment. Therefore, in order to help ensure an adequate capacity, designers recommend that the positive moment connection at the diaphragm have a capacity no greater than 1.2 times the cracking moment of the section. This limit is imposed in order to prevent the section from being overdesigned

as additional reinforcement in the section will only increase congestion, while providing little impact on the overall behavior of the connection.

*2.2.5.3 Age at which the Connection is Established*

Based on the results of the NCHRP testing, it was found that the age of the girders at the time at which continuity was established was the "single most important factor in the behavior" of the section. If the girder is relatively young, creep can produce significant positive moments within the connection. Conversely, if the girders are older, the differential shrinkage that will be experienced between the girder and the deck can produce significant negative moments within the connection. Therefore, it was decided that it would be unnecessary to limit the age of the girder, but rather a minimum advisable limit for the age is advisable in order to limit the formation of large positive moments, which might be generated during aging.

## 2.3 Experimental Research

One example of previous research regarding the use of precast components in a bridge structure made continuous was report and research completed by Holombo et. al. (1998) regarding the use of precast sliced-girder bridges. In his report, an investigation on the seismic behavior of bridges using precast girder segments, which are spliced together using prestressing tendons and made continuous for seismic loading as well as any live load or self-weight, was presented. The benefits of using spliced precast girders over a more conventional, cast-in-place or simply supported precast girder system are that longer spans may be achieved and that the design moment may be reduced, resulting in a reduced superstructure depth, smaller foundation, and ultimately the cost.

The results of the testing by Holombo et al. showed that spliced precast girders, both the bulb-tee and bathtub, could be used effectively in areas of high seismic activity with a high degree of performance. Both of the test units used in this research achieved a level of ductility ($\mu_\Delta$= 8 for the

bulb-tee unit and $\mu_\Delta$= 6 for the bathtub unit) that was significantly greater than that of the design value ($\mu_\Delta$=4), while only minor cracking in the superstructure was observed.

Another example is the experimental research performed in order to develop design guidelines for integrally constructed cap beam to steel girder joint regions (Patty, Seible, & Uang, 2002). Four specimens were tested with combinations of cap reinforcement, either post-tensioning or conventional reinforcement, and girder stiffeners, with or without. The study focused on the torsional behavior of the cap beam with the different concepts, as shown in Figure 2.5.

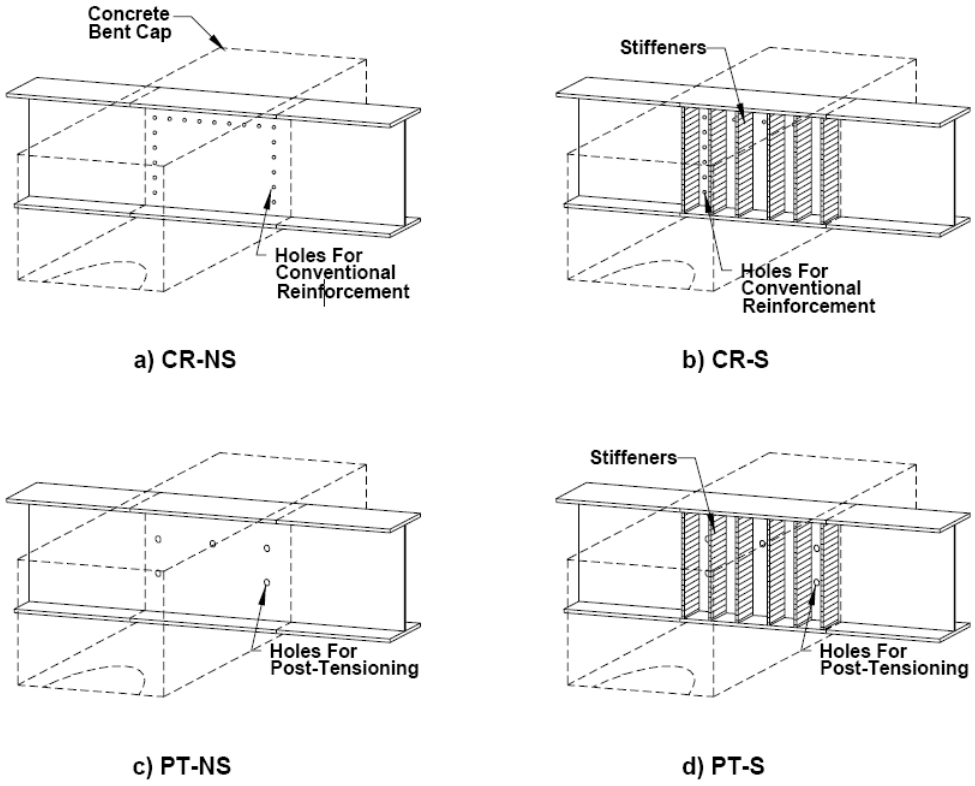


Figure 2.5. Test concepts for torsional behavior of integral cap beam

After testing the four concepts, the results showed that the torsional moment capacity of the component with stiffeners increased by 25%. The strain gauges recorded higher strains on the outer stiffeners than the inner stiffeners, indicating the outer stiffeners are more effective in transferring the

flexural moment of the girders to the cap beam, resulting in a torsional moment. The stiffeners also contributed in reduced dilation of the bent cap by approximately 33% compared to the specimens without stiffeners. Next, the effect of the post-tensioning from the concept testing was discussed. Bent caps with post-tensioning experienced almost zero dilation and significantly less cracking up to maximum moment. Also, the bent caps with post-tensioning instead of conventional reinforcement are easier to construct.

Additional research was conducted at Iowa State University into the behavior of concrete cap beam and steel girders constructed integrally (Sritharan, Vander Werff, Abendroth, Wassef, & Greimann, 2005). A connection was used that made the girders continuous across the cap beam by using flange and web plate connections. The girders were welded to steel splice plates that were in line with the flanges and girder web. After the testing of two test units was completed, it was noted that the superstructure, girder-to-cap-beam connection and the column-to-cap beam connection all remained essentially elastic. Minor spalling in the deck was observed, which was attributed to the punching column longitudinal bars through the bridge deck. The failure of the test units was measured to occur at a displacement ductility of 4; however, modification to the shear connectors that extended from outside of the cap beam into the column would have allowed for greater ductility.

## 2.4 Detailed Modeling Introduction

The ability to understand the response of a bridge to its prescribed loads is important to formulate the best design. To achieve the best design, testing of the structure should be performed to understand the response components, such as, stress-strain behavior, deflections and rotations. To ensure that the forces are transmitted from the superstructure to the column, an effective connection must be designed to pass the forces from one component to the other. Without a sufficient connection, the response of the bridge may change dramatically and have ill-advised effects. To understand the response, research has been undertaken to model the structures in such a manner as to

be able to capture the needed information. Many different means of modeling a structure have been used such as lab testing, strut-and-tie analysis and detailed finite element analysis. Each of these analysis techniques have been proven to be an effective way to model the structural response for a given application. The three analysis techniques listed will be discussed in greater detail below and concerns will be raised regarding their adequacy for joint modeling.

### 2.4.1 Detailed FEA

Detailed finite element analysis has become a more common entity of research and design in the recent years (Roylance, 2001). A detailed analysis can be a powerful tool for engineering purposes only if the user has a sufficient knowledge in its usage. In the modeling, many different options are available for elements, meshing, material properties, contact controls, etc. and sufficient understanding of each of these topics is needed to properly establish a model. When modeling, an incorrect assumption or incorrect technique can lead to a solution, however, it may be incorrect. Therefore, to have full confidence in any finite element analysis, experimental results or a closed-form solution needs to be presented to validate the results. In the following section, the purpose, advantages and challenges of finite element analysis will be discussed.

The finite element method allows for solutions to complicated problems to be obtained with ease. Many programs are available over a wide cost range for microcomputers and supercomputers. This leaves little reason for analysts to write their own software (Roylance, 2001). The commercial codes generally consist of three modules to build a model: preprocessor, analysis and postprocessor. Preprocessors in the commercially available codes undergo continuous upgrades to make the most user-friendly version. Some of the more sophisticated software can import CAD or other drawing files directly to the program and mesh the geometry, making the process of building the model easier. The analysis module imports the code from the preprocessor and analyzes the model. Another advantage of finite element analysis is the ability during analysis to address many different element

types by simply specifying the appropriate element from the library (Roylance, 2001). Finally, the postprocessor compiles the results from the analysis into a user-friendly interface that allows the analyst to visualize the results.

The main advantage of the finite element analysis is the ability to mimic expensive experiments (Prabha, Seetharaman, Arul Jayachandran, & Marimuthu, 2007). In this process, the analyst has to have the knowledge to run the program and accurately model the structure being considered. Once the analyst has finished the modeling, the program will analyze the structure and provide the results. This method is applicable for a wide range of applications: solid mechanics, dynamics, heat problems, fluids, electrostatic, etc. If modeled correctly, indeterminate structures can be solved along with applications with complex loadings and interactions. Once a model has been verified for accuracy, multiple loadings and restraints can be modified and analyzed with relative ease compared to other analysis techniques, such as the strut-and-tie method.

The finite element method provides many advantages; however, the disadvantages need to be considered to ensure the response is applicable. One possible disadvantage is the processing time, depending on the size of the model, the analysis time can become costly and inefficient when compared to other methods, especially when considering non-linearity. However, a detailed finite element analysis can be used in conjunction with a simplified model to reduce processing time. Main areas of interest on the structure can be modeled in detail and the behavior can be inputted into the simpler model to capture the global response accurately, like the moment-rotation characteristics of a connection for example. Another disadvantage of the finite element method is that the model can return results that are inaccurate if an aspect of the structure wasn't modeled correctly. To overcome this, verification needs to be performed to ensure the results being reported are correct (Biggs, Barton, Gomez, Massarelli, & McKeel, 2000). For accurate prediction of the structural behavior, correct geometric and material properties are vital (Chowdhury & Ray, 1995). The geometry of the key

components needs to be accurately inputted to ensure that the correct response is captured. The complexity of the material models is dependent upon the material that is used. Materials with well-defined constitutive properties, such as steel and aluminum, are able to be modeled easily with accurate results in FE programs. However, a material such as concrete does not provide easy analysis. The discrete cracking, different response in compression and the changing stiffness after crushing and cracking occurs provides considerable problems in modeling the behavior (Chen, Yamaguchi, Kotsovos, & Pan, 1993). An extensive study was completed to demonstrate a methodology to analyze reinforced-concrete structures to overcome the previous concerns which will be discussed below (Biggs, Barton, Gomez, Massarelli, & McKeel, 2000).

The FE software ABAQUS was selected to perform the analysis of reinforced-concrete bridge decks (Biggs, Barton, Gomez, Massarelli, & McKeel, 2000). A specific objective of the study was to develop a model that could accurately predict global bridge behavior and strains, stresses and displacements in the deck. The FE model included a plasticity-based constitutive model for concrete. The elements used were shell elements to model the slab and beam elements to model the girders. Reinforcing bars were also included and modeled using one-dimensional truss elements. A uniform load was applied with a maximum near the ultimate load of the beam. Deflections and stresses were determined from the FE model and compared to hand calculations that were performed by the approach given in the American Concrete Institute code. The compressive stress in the beam is presented below in Figure 2.6. In Figure 2.7, the stress in the reinforcing bars is presented and Figure 2.8 presents the deflection of the slab across the span. The difference in the stress in the reinforcing bars near the support was attributed to the tension stiffening effects of the concrete model. Overall, the results from this study prove that the response of the concrete slab can be adequately predicted using the concrete models in ABAQUS. To further validate this conclusion, the model was modified to predict the response of a two-way reinforced, simply supported concrete slab that was

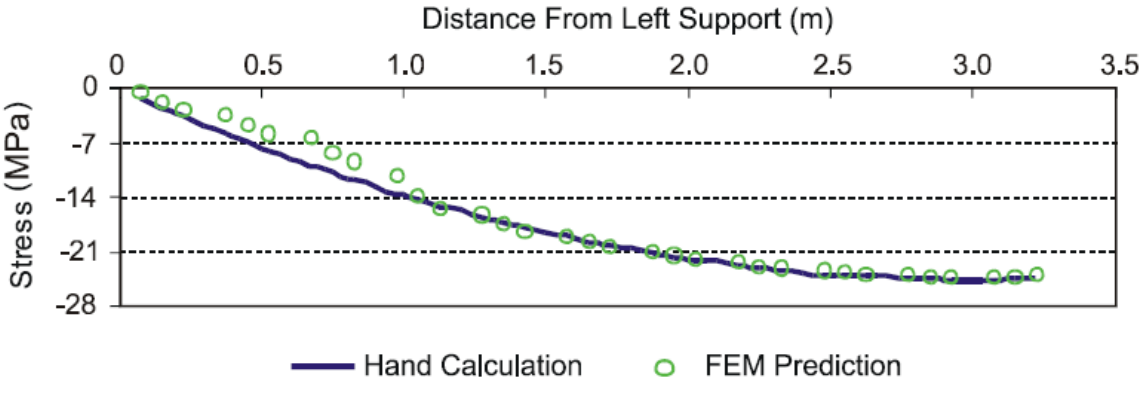


Figure 2.6. Compressive stress in top fiber of the beam

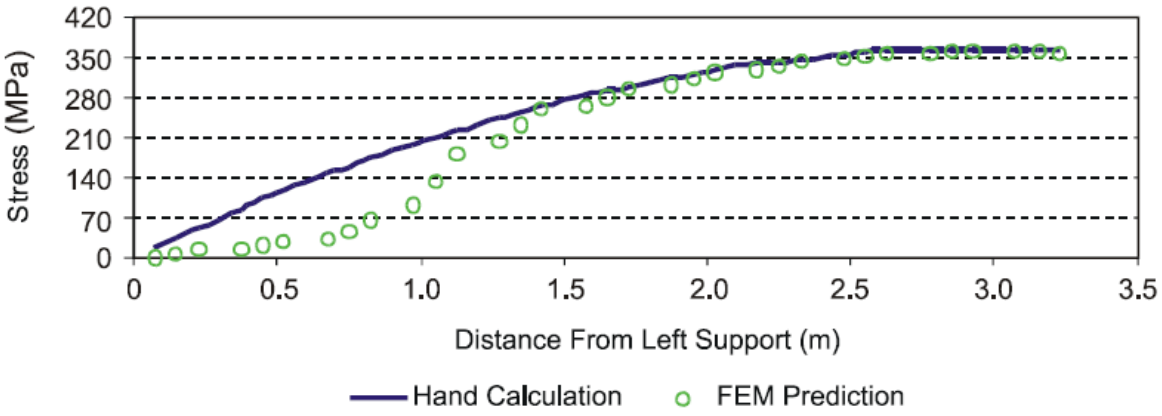


Figure 2.7. Steel Reinforcement Stress Along Beam

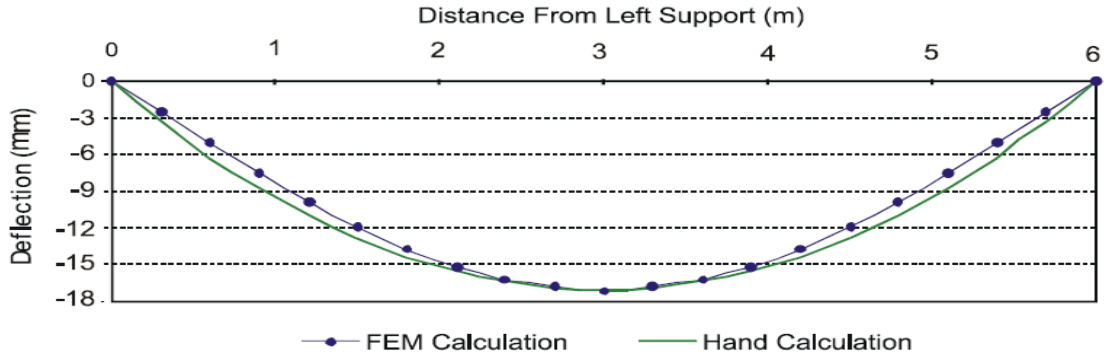

Figure 2.8. Deflection Across Span

experimentally tested previously. The FE model was able to predict the load-deflection behavior and flexural cracking load similar to the test results. Additional models were developed and the results were also analyzed. The conclusions from the report were that ABAQUS has the ability to model concrete and steel, simulate their interaction, apply loads and accurately calculate results and predict behaviors not generally obtained through experimentation. Also, ABAQUS has the ability to predict deflections, strains and stresses of realistic structures (Biggs, Barton, Gomez, Massarelli, & McKeel, 2000).

Another study using ABAQUS was performed to develop the moment-rotation behavior of semi-rigid steel bolted connections (Prabha, Seetharaman, Arul Jayachandran, & Marimuthu, 2007). The beam-to-column connection was modeled with 8-noded solid elements. The elements do not have rotational degrees of freedom; however, they are discretized across the thickness to allow for the effect of bending. Additionally, contact modeling was used between the beam and column, bolts and bolt holes and pre-tensioning in the bolts. The moment-rotation results from the FE model and experimental results are presented in Figure 2.9.

With the validated model in ABAQUS, additional lab testing was able to be avoided and additional FE analysis models were ran. This allowed for a large time and cost saving since there was a need to test up to 34 combinations of connections.

Additional studies have used ABAQUS for 3D FE modeling. A study was conducted involving a bulb-tee deck bridge, which was modeled by finite element analysis and field testing using a loaded end-dump truck was performed (Ma, Chaudhury, Millam, & Hulsey, 2007). After the field testing was finished, the FE model was calibrated and the resulting strain values were similar to the field results.

Although the finite element method does possess disadvantages that may cause inaccurate results, with proper diligence the disadvantages may be overcome. Once the model is validated, future analyses can be completed more cost effectively while providing great detail when compared to lab testing and other analytical models.

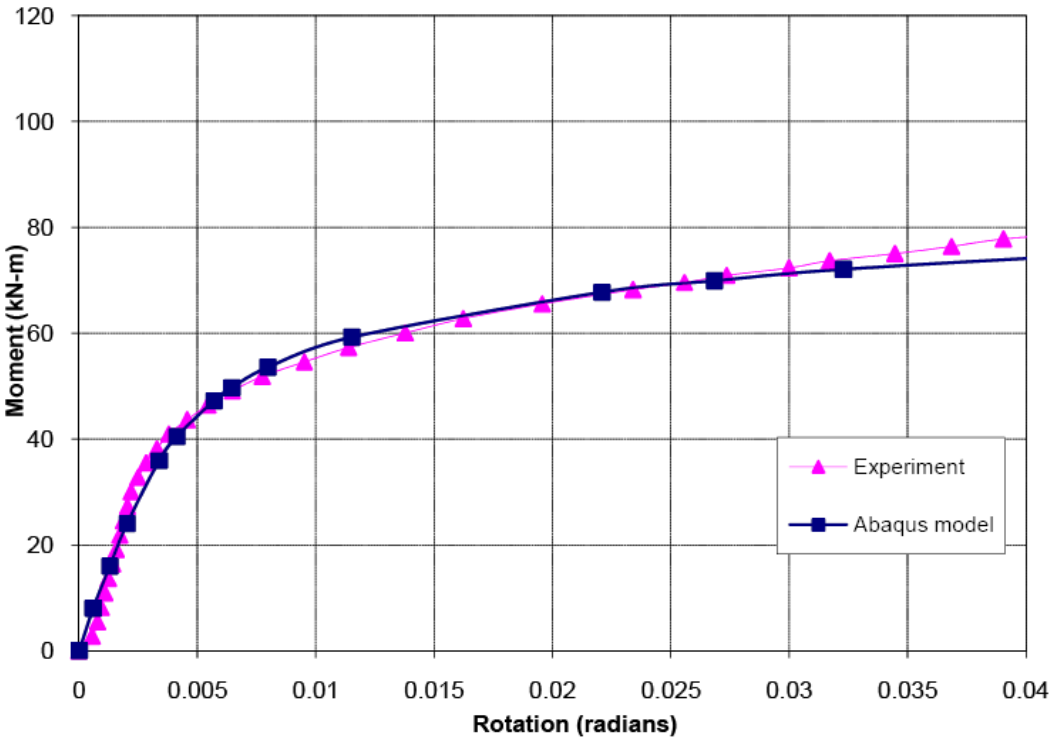


Figure 2.9.Comparison of moment-rotation curves (1 kN-m = .737 kip-ft)

# Chapter 3. PROTOTYPE DESIGN

## 3.1 Introduction

A prototype bridge was designed and used for this research project. The methods of design used were representative of existing inverted-tee cap beam bridges for Caltrans and followed current seismic design practice. The prototype structure was used for the finite element analysis and also, a portion of it was used to establish a large-scale test specimen for laboratory testing under simulated seismic loads. Before the design was undertaken, aspects of the bridge had to be decided, including bent style, number of girders and style of girders. A single-column was chosen and the section was used efficiently to create the maximum load at the column-to-cap-beam interface. A multi-column bent would require a much wider superstructure to develop the maximum demand at the column-cap interface when using the same size column. This would not be feasible for experimental research due to the lab space and cost limitations. A circular column was chosen since it is the preferred cross-section in seismic regions since the moment capacity of this column section is the same in any given earthquake loading direction. The superstructure was considered to have five girders to allow for the maximum width for this bridge. Four girders were considered, but the maximum demand on the column would have been less since the superstructure width is limited by the maximum girder spacing of 8 ft., as allowed by the AASHTO LRFD Bridge Design Specifications 3rd Edition for the live loads of the bridge (AASHTO, 2003). For girders, the California I-girder was chosen, as recommended by Caltrans to closely replicate the existing bridges with inverted-tee bent cap. It was decided that the deepest girder should be chosen to create the greatest demand on the girder-to-cap-beam connection. Successfully showing that the new connection has the capacity to withstand this setup, it would follow that the shallower sections would also have an adequate capacity.

The prototype bridge, presented in Figure 3.1, was designed in accordance to the AASHTO LRFD Bridge Design Specifications 3rd Edition with 2006 Interims and California Amendments

(AASHTO) (AASHTO, 2003), as well as the Caltrans Bridge Design Aid (Caltrans, Bridge Design Aids, 1995) for the design of Inverted-T Cap, Caltrans Bridge Design Specifications (BDS) (Caltrans, Bridge Design Specifications, 2003) and Seismic Design Criteria v. 1.4 (SDC) (Caltrans, Seismic Design Criteria, v. 1.4, 2006). Computer software packages WinRECOL (TRC/Imbsen Software Systems), Xtract (TRC/Imbsen Software Systems) and Conspan (Bentley Systems, Inc., 2008) were used to aid in the design. A design of the column, cap beam, girder dapped end and slab for the prototype was performed and discussed below. The Prototype bridge drawings are given in 0.

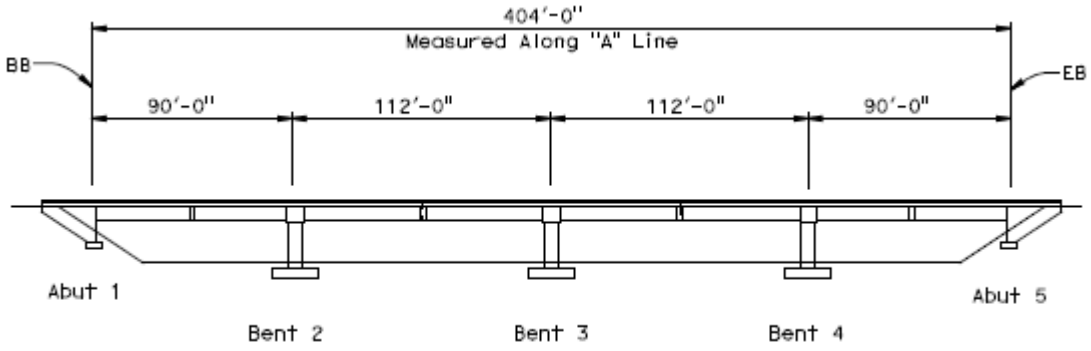


Figure 3.1. Prototype Bridge Elevation View

## 3.2 Material Properties

For the design, the material properties had to be chosen for the concrete, mild steel and prestressing steel. The properties were chosen to represent standard material properties used in previous designs. Listed below are the specified material properties:

Concrete:

Compressive strength of precast girder at the time of stress transfer: $f'_{ci} = 5.5\ ksi$

Compressive strength of precast girder at 28 days: $f'_{c} = 7.0\ ksi$

Compressive strength of deck slab at 28 days: $f'_{c} = 4.0$

Compressive strength of bent cap and substructure at 28 days: $f'_c = 3.6\ ksi$

Density ($\gamma$) = 0.15 kcf

Reinforcing Steel:

Yield strength ($f_y$) = 60 ksi

Modulus of Elasticity ($E_s$) = 29000 ksi

Prestressing Steel:

Type 0.6-in. Low Relaxation strand

Modulus of Elasticity ($E_{ps}$) = 28500 ksi

Prestressing Steel Ultimate Strength ($F_{pu}$) = 270 ksi

Jacking force of the prestressing strands ($F_{jack}$) = $0.75F_{pu}$ = 202.5 ksi

## 3.3 Column Design

The design of the column was completed using the software WinRECOL after the service loads were calculated for the 20 ft.-7 in. tall column with a diameter of 5.5 ft.. The service load was obtained by considering different load combinations considering braking force, wind, superstructure dead load, and two design vehicle loads, HL-93 and P15. The applicable loads were entered into WinRECOL for the design of the column. The required number of reinforcing bars was determined to be 33, #11 bars. From the output, the maximum axial load to be resisted by the column was 2900 kips which corresponded to an axial load ratio of $.23f'_cA_g$. The nominal axial resistance can be calculated using the equation from the AASHTO 5.7.4.4-2, present in Eq. (2.1), where $A_g$ is the gross area of the column, $A_{st}$ is the total area of longitudinal reinforcement in the column, $A_{ps}$ is the area of prestressing steel in the column, and $\varepsilon_{cu}$ is the failure strain of concrete in compression.

$$P_n = 0.85\left(.85f'_c\left(A_g - A_{st} - A_{ps}\right) + f_y A_{st} - A_{ps}\left(f_{pe} - E_p\varepsilon_{cu}\right)\right) \quad (2.1)$$

$$P_n = 0.85\left(.85\left(3.6^{ksi}\right)(3407in^2 - 51.48in^2) + \left(60^{ksi}\right)(51.48in^2)\right)$$

$$= 11354kips$$

The nominal axial load capacity of the column was 11354 kips, which is much larger than the maximum axial load of 2900 kips, therefore the axial load capacity is satisfactory and the additional capacity will be shown to be needed in the combination ratio. Next, the flexural resistance of the column was checked. From WinRECOL, the maximum flexural load was 7297 kip-ft and the chosen longitudinal reinforcement provided a nominal capacity of 8078 kip-ft, which was satisfactory. Next, the shear design of the column was completed for the design shear force of 1065 kips, the resulting longitudinal design shear force from the maximum plastic moment of the column divided by the column length. The BDA Section 8.16.6.2 Eq. 8-51 (3.2) was used for the shear resistance provided from concrete, where $b_w$ is the width of the core section of the concrete and d is the distance from extreme compression fiber to the centroid of the longitudinal reinforcement.

$$\phi V_c = 0.85 * 2\sqrt{f'_c}b_w d \quad (1)$$

$$\phi V_c = 0.85 * 2 * \sqrt{3.6^{ksi}} * 62*49.6 = 314\ kips$$

Therefore, the remainder of the shear resistance must be provided from shear reinforcement. The shear reinforcement needs to be designed for multiple spacings: plastic hinge region, regions requiring shear reinforcement and region of minimum shear reinforcement. The following equations

were used for the respective locations. For the confinement region Eq. 8-62b, presented in Eq. (3.3), from the BDS was used, where $\rho_s$ is the ratio of spiral or hoop reinforcement.

$$\rho_s \geq 0.12 \frac{f'_c}{f_y}\left(.5 + 1.25 \frac{P}{f'_c * A_g}\right) \tag{3.3}$$

For the region outside of the plastic hinge where shear reinforcement was required, Eq 8-53 **Error! Reference source not found.**from Section 8.16.6 of the BDS, shown in Eq. (3.4), was used where $V_s$ is the force to be resisted by steel reinforcement.

$$V_s = \frac{A_v f_y d}{s} \tag{3.4}$$

For the region where the concrete resistance is greater than the design shear force but one-half the concrete resistance is less than the design shear force, the minimum shear reinforcement will be provided according to Eq. 8-63 of the BDS, shown in Eq. (3.5), where $A_v$ is the area of shear reinforcement.

$$A_v = \frac{50 b_w s}{f_y} \tag{3.5}$$

Next, spacing requirements according to section 8.21.1.1 of the CALTRANS BDS was considered. The maximum spacing of the lateral reinforcement shall not exceed:

- 1/5 of the least dimension of the column=1/5*62” = 12.4 inches
- 6 times the nominal diameter of the longitudinal reinforcement:

  = 6*1.41in$^2$ = 8.46 inches

- 8 inches

The maximum spacing allowed shall be 8 inches according to the requirements above. Finally, considering the design shear force of 1065 kips and the concrete contribution of 314 kips, the reinforcement was designed. Using Eq. 5.8.3.3-1 from AASHTO, given in Eq. (3.6), the amount of shear resistance needed from the shear reinforcement was found as followed.

$$V_s = \frac{V_n}{\phi} - V_c \tag{3.6}$$

$$V_s = \frac{1065kips - 314kips}{0.85} = 884kips$$

$$\rho_s = .12\frac{3.6\text{ ksi}}{60\text{ ksi}}\left(.5 + 1.25\frac{1525\ kips}{3.6\text{ ksi} * 23.76ft^2 * 144}\right) = 0.00471$$

$$confinement\ spacing \leq \frac{4A_{sp}}{D'\rho_s} = \frac{4(0.44)}{62\text{ in.} * 0.00471} = 6.02\ inches$$

$$shear\ reinforcement\ spacing \leq \frac{2 * 0.44in^2 * 60\text{ ksi} * 49.6\text{ in.}}{884\ kips} = 2.96\ inches$$

$$minimum\ shear\ reinforcement\ spacing \leq \frac{2 * 0.44\ in^2 * 60\text{ ksi}}{50x62\text{ in.}} = 17.03\ inches$$

However, for the maximum spacing of the shear reinforcement, 8 inches was used according to Article 8.21.1.1 of the BDS. Therefore, instead of the value corresponding to the minimum shear reinforcement calculated above, the maximum spacing of 8 inches was used. The confinement spacing provided above ensures that the plastic hinge will form to adequately dissipate energy while not allowing other inelastic action to occur. In Figure 3.2 the layout of the column reinforcement is shown.

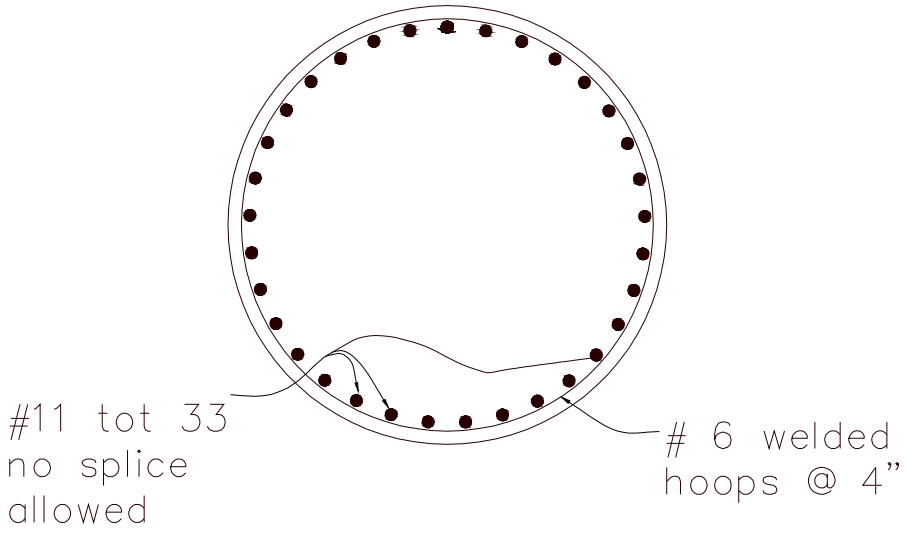


Figure 3.2. Column Reinforcement Layout

## 3.4 Cap Beam

The design of the cap beam considered two load cases as specified by Article 5.6.1 of AASHTO 2003. The first case involved the live and dead loads during the construction process, which the second case involved the dead and live service loads after the diaphragm was cast in place.

### 3.4.1 Construction Loads

First, the loads applied to the inverted-tee section were calculated. During construction the loads on the cap beam will be from the girders, cap beam self-weight, and the weight from the construction equipment. The loads from the interior and exterior girders transmitted to the cap beam were compiled from the self weight, deck and haunch above the girder, intermediate diaphragms and precast components, presented below in Table 3.1. The point load resulting from the deck loads action on exterior girder, $P_{DCe}$, and interior girder, $P_{DCi}$, from both spans is given below.

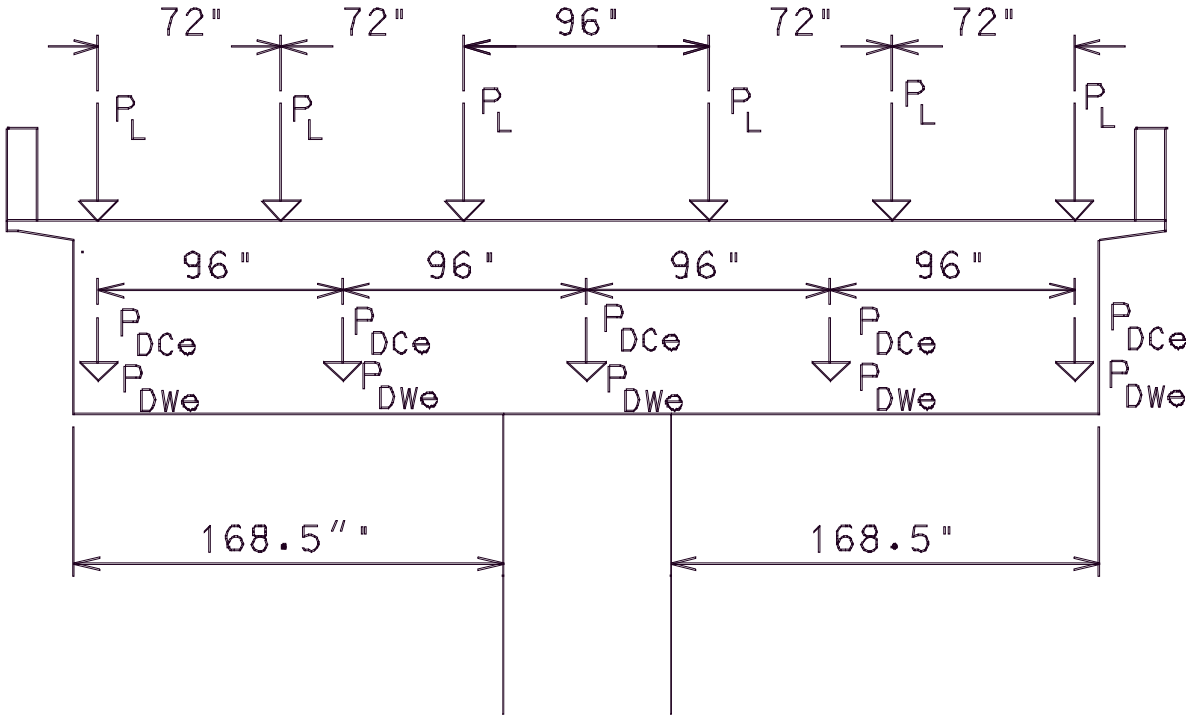


Figure 3.3. Load layout on cap beam

Table 3.1. Loads from deck components on the girders

| | Girder Loads (kip) | |
|---|---|---|
| | Interior | Exterior |
| Self-Weight | 34.8 | 34.8 |
| Deck+Haunch | 41.7 | 39.2 |
| Diaphragm | 2.2 | 1.1 |
| Precast | 5.7 | 3.9 |

$$P_{DCe} = (34.8 + 39.2 + 1.1 + 3.9)(2) = 158\ kips$$

$$P_{DCi} = (34.8 + 41.7 + 2.2 + 5.7)(2) = 169\ kips$$

An additional load needed to be considered from the construction equipment, such as the Bidwell machine. A load of 20 psf was assumed to be exerted on the 20-in. wide overhang in addition to the weight of the machine itself. Therefore, over the 112 ft of the span contributing a load to the cap beam, the construction load, $P_{const}$, is,

$$P_{const} = (0.02)\left(\frac{20 \text{ in.}}{12}\right)(112 \text{ ft.}) + 8 \text{ kips} = 11.7 \text{ kips}$$

Next, the weight of the cap beam, $w_{cb}$, including the weight of the diaphragm, $w_{dia}$, and deck and haunch above the cap beam, $w_{d+h}$, was calculated. The resulting equivalent distributed load ($w$) from the components listed was also calculated.

$$w_{cb} = 44ft^2 * 0.15\frac{kips}{ft^3} = 6.6\frac{kips}{ft}$$

$$w_{dia} = [2.75 \text{ ft.} * 4 \text{ ft.} + 2 \text{ ft.} * 5.5 \text{ ft.}] * 0.15\frac{kips}{ft^3} = 3.3\frac{kips}{ft}$$

$$w_{d+h} = \frac{9.625 \text{ in.}}{12} * 0.15\frac{kips}{ft^3} * (6 \text{ ft.} + 2 \text{ ft.}) = 0.963\frac{kips}{ft}$$

$$w = 6.6\frac{kips}{ft} + .963\frac{kips}{ft} + 3.3\frac{kips}{ft} = 10.9\frac{kips}{ft}$$

Finally, with the loads listed above and shown in Table 3.1, the AASHTO Eq. 3.4.1-1, presented in Eq. (3.7), was used to find the ultimate shear and moment.

$$Q = \sum n_i \gamma_i Q_i \tag{3.7}$$

where Q is the load being calculated, since the structure was designed by conventional design methods, $n_i$ can be taken as 1.0 for all calculations according to AASHTO Articles 1.3.3, 1.3.4, and 1.3.5. The factors for $\gamma_i$, according to AASHTO table 3.4.1-1 and 3.4.1-2, are 1.25 for dead load and 1.75 for live load, assuming the Strength II limit state. The load from the Bidwell machine was also be multiplied by a dynamic load factor that was taken as 1.33. The dynamic load factor is a dynamic load allowance that accounts for the wheel load impact from the moving vehicles.

$$V_u = 1.25 * (158 \text{ kips} + 169 \text{ kips}) + 1.75 * (11.7 \text{ kips})(1.33) + 1.25 * \left(10.9 \frac{\text{kips}}{\text{ft.}}\right)(14.042 \text{ ft.}) = 627\ kips$$

$$M_u = 1.25 * (158 \text{ kips})(13.25 \text{ ft.}) + 1.25 * (169 \text{ kips})(5.25 \text{ ft.}) + 1.25 * \left(10.9 \frac{\text{kips}}{\text{ft.}}\right)\frac{(14.042 \text{ ft.})^2}{2} + 1.75 * (11.7 \text{ kips})(1.33)(13.25 \text{ ft.})$$

$$M_u = 5430 \text{ kip} - \text{ft.}$$

Now the capacity of the cap beam needs to be designed to ensure that it is larger than the ultimate moment calculated above. For the number of reinforcing bars in the cap beam, 22 #11 bundled bars were considered. The depth to the centroid, d, of the tension reinforcing steel from the extreme compression fiber was found as follows.

$$d = 66 \text{ in. } -3 \text{ in.} - 1.375 \text{ in.} - 0.75 \text{ in.} = 60.875 \text{ in.}$$

Then the capacity of the section was calculated using Eq. 5.7.3.2.2-1 from the BDS. This equation was simplified due to the absence of prestressing steel, compression steel and flanges in the section. The reduced equation is shown in Eq. (3.8), in which $A_s$ is the area of longitudinal reinforcing steel and a is the depth of the compression block, presented in Eq. (3.9)**Error! Reference source not found.**,

$$\phi M_n = \phi A_s f_y \left(d - \frac{a}{2}\right) \tag{3.8}$$

where, $a = \frac{A_s f_y}{0.85 f'_c b} = \frac{(34.32\ in^2)(60\ ksi)}{(0.85)(3.6\ ksi)(120\ in)} = 5.61\ in.$ (3.9)

Therefore, $\phi M_n = (0.9)(34.32\ in^2)(60\ ksi)[60.875" - \frac{5.61"}{2}] = 107620\ \text{kip} - \text{in} = 8968\ \text{kip} - \text{ft}.$

As shown above, the capacity significantly exceeds the ultimate moment applied to the section due to the flexural-shear interaction calculated later. Next, the section was checked to ensure the minimum reinforcement required by AASHTO Eq. 5.7.3.3.2, presented in Eq. (3.10), and the check from Article 5.7.3.3.2, shown as Eq. (3.11), were satisfied. The two checks are considered to effectively control the crack width. The amount of tensile reinforcement needs to develop a factored flexural resistance of 8968 kip-ft. above or equal to the lesser of the following values,

$$1.2M_{cr} = 1.2(S_c\ (f_r\ )) \tag{3.10}$$

$$1.2M_{cr} = 1.2 * \left(\frac{105.703ft^4}{3.094ft}\right) * 702\frac{lb}{in^2} * \frac{144in^2}{1ft^2} * \frac{1kip}{1000lb} = 4144\ \text{kip} - \text{ft}$$

$$1.33M_u = 1.33 * 5430\ \text{kip} - \text{ft}. = 7221.0\ \text{kip} - \text{ft}. \tag{3.11}$$

In the above equations, $M_{cr}$ is the cracking moment of the cap beam, $S_c$ is the section modulus cap beam, and $f_r$ is the modulus of rupture of concrete. This condition was satisfied with the provided reinforcement. Next, the spacing of steel, s, was checked to effectively control the crack width. The use of a larger number of closely spaced, smaller bars is more efficient at controlling crack widths than a smaller number of large, widely spaced, bars. The provisions in Article 5.7.3.4 Eq. 5.7.3.4-1 of AASHTO 2003, presented below in Eq. (3.12)**Error! Reference source not found.**, account for this and was checked. In this equation, $\beta_s$ is a ratio of flexural strain at the extreme tension face to the strain at the centroid of the reinforcement layer, $\gamma_e$ is an exposure factor, $f_{ss}$ is the tensile stress in steel reinforcement at the service limit state, and $d_c$ is the cover to the center of the flexural

reinforcement closest to the extreme tension fiber. To calculate $\beta_s$, Eq. (3.13) was used, and for $f_{ss}$, Eq. (3.14) was used; both of these equations were given in Article 5.7.3.4 of AASHTO. For Eq. **Error! Reference source not found.**, the M is the unfactored moment.

$$s \leq \left(\frac{700\gamma_e}{\beta_s f_{ss}} - 2d_c\right) \tag{3.12}$$

$$\beta_s = 1 + \frac{d_c}{.7(h - d_c)} \tag{3.13}$$

$$f_{ss} = \frac{M}{A_s jd} \tag{3.14}$$

Substituting the appropriate values,

$$\beta_s = 1 + \frac{3.75}{.7(66 - 3.75)} = 1.086$$

$$f_{ss} = \frac{4262 * (12)}{34.32 * 0.92 * 60.875} = 26.6\ ksi$$

$$\mathrm{s_{req'd}} = \frac{700 * .75}{1.086 * 26.6ksi} - 2 * 3.75\ in = 10.7\ in.$$

$$s_{provided} = \frac{72 - 2 * 2.5}{10} = 6.7\ in.$$

This completes the flexural design of the cap beam. The reinforcement layout is presented in Figure 3.4; the section was then designed for shear.

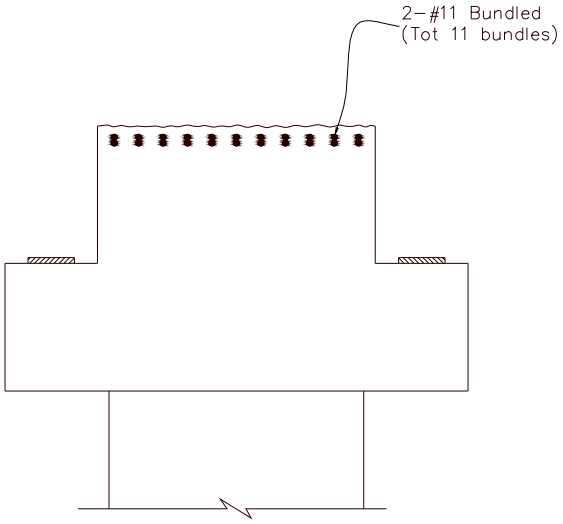


Figure 3.4. Cap Beam Top Flexural Reinforcement

The shear in a concrete member can be resisted in three ways: concrete, shear reinforcement and prestressing. The cap beam has no prestressing, and thus only the shear resistance from the concrete and the shear reinforcement was considered. The shear stress on the section was found by using Article 5.8.2.9 in AASHTO. In that article, Equation 5.8.2.9-1, shown in (3.15), was given for the calculation of the shear stress. Accordingly,

$$v_u = \frac{|V_u - \phi V_p|}{\Phi b_v d_v} \tag{3.15}$$

The AASHTO specification states $d_v$, "Need not be taken to be less than the greater of $0.9d_e$ or .72h", where $d_e$ is the depth from the extreme compression fiber to the tensile reinforcement and $\Phi$ is the shear resistance factor taken as 0.9. Consequently, the shear stress in the beam section is calculated below using Eq. (3.15).

$$v_u = \frac{|627|}{0.9 * 72 * 54.79} = 0.177\ ksi$$

Then, the shear resistance was determined according to AASHTO Article 5.8.3.4. This section presents the following three methods for determining the shear resistance:

1. Simplified Procedure for Nonprestressed Sections (Article 5.8.3.4.1);
2. General Procedure (Article 5.8.3.4.2); and
3. Simplified Procedure for Prestressed and Nonprestressed Sections (5.8.3.4.3)

Article 5.8.3.4.2 was chosen for determining the shear resistance of the cap beam. Assuming the section would contain at least the minimum transverse reinforcement as specified in Article 5.8.2.5, Eq. 5.8.3.4.2-1, shown below in Eq. (3.16), was used to determine the strain at mid-height of the section. The equation can be simplified since no prestressing steel, $A_p$, or axial force, $N_u$, would be present in the cap beam. The value for $\theta$, the angle of inclination of diagonal compressive stresses, was assumed to be 36.4°, by assuming the shear stress-concrete strength ratio is very low, and was verified by Table 5.8.3.4.2.1 after the $\epsilon_x$ was calculated.

$$\epsilon_x = \frac{\frac{M_u}{dv} + 0.5N_u + 0.5|V_u|\cot\theta - \mathrm{A_p f_{po}}}{2\left(E_s A_s + \mathrm{E_p A_p}\right)} \tag{3.16}$$

$$\epsilon_x = \frac{\frac{(5430 * 12)}{54.79} + 0.5 * 627 * cot36.4}{2(29000 * 34.32)} = 811 * 10^{-6}$$

With the value of $\epsilon_x = 811x10^{-6}$ and $\frac{v_u}{f'_c} = 0.049$, Table 5.8.3.4.2.1 of AASHTO gives $\theta = 36.4°$ and $\beta = 2.23$, where $\beta$ is the factor indicating the ability of diagonally cracked concrete to transmit tension and shear. With the resistance of the concrete to shear investigated, the design of the shear reinforcement needed to be completed. Since Article 5.8.3.4.2 was used to determine the effectiveness of the cross section to resist shear, Eq. 5.8.3.3-3, shown below in Eq. (3.17), was used to determine the shear resistance of the concrete cross section as follows,

$$V_c = 0.0316\beta\sqrt{f'_c}b_v d_v \tag{3.17}$$

$$V_c = .00316 * 2.23 * \sqrt{3.6} * 72 * 54.79 = 527.4\ kips$$

With the required nominal shear resistance and the concrete contribution to shear resistance known, the amount of resistance needed from the shear reinforcement was found. Eq. (3.6) was used to solve for $V_s$ as follows:

$$V_s = \frac{627}{0.9} - 527.4 = 169.3\ kips$$

The area of steel and spacing needed to be calculated to ensure that the capacity from the steel reinforcement to resist shear was sufficiently provided. This value was obtained by rearranging equation C5.8.3.3-4 of AASHTO, see Eq. (3.18), to solve for $\frac{A_v}{s_{req'd}}$ as shown in Eq. (3.19).

$$V_s = \frac{A_v f_y d_v \cot\theta}{s} \tag{3.18}$$

$$\frac{A_v}{s}_{req'd} = \frac{V_s}{f_y d_v \cot\theta} \tag{3.19}$$

$$\frac{A_v}{s}_{req'd} = \frac{V_s}{f_y d_v \cot\theta} = \frac{169 * 12}{60 * 54.79 * cot(36.4°)} = 0.46\frac{in^2}{ft}$$

Assuming a #6 shear reinforcement bar at a spacing of .75 ft,

$$\left(\frac{A_v}{s}\right)_{provided} = \frac{6 * 0.44\ in^2}{0.75^{ft}} = 3.52\frac{in^2}{ft}$$

Since the shear reinforcement chosen for the cap beam was greater than the amount required and the shear resistance of the beam section exceeds the nominal shear force. Over the column, the shear reinforcement spacing shall be the maximum spacing ($s_{max}$) allowed by AASHTO Article 5.8.2.7 since the shear shear force will act into the column. Since the shear stress calculated from Eq. (3.15) is less than $0.125f'_c$, Eq. 5.8.2.7-2, reproduced in Eq. (3.20), was used to determine the maximum spacing where $d_v$ is the effective shear depth.

$$s_{max} = 0.4d_v \leq 24.0\ in. \tag{3.20}$$

$$s_{max} = (0.4 * 54.79 \leq 24.0\ in.) = 22\ in.$$

This completes the design of the cap beam under construction loads, and the corresponding reinforcement layout is shown in Figure 3.5.

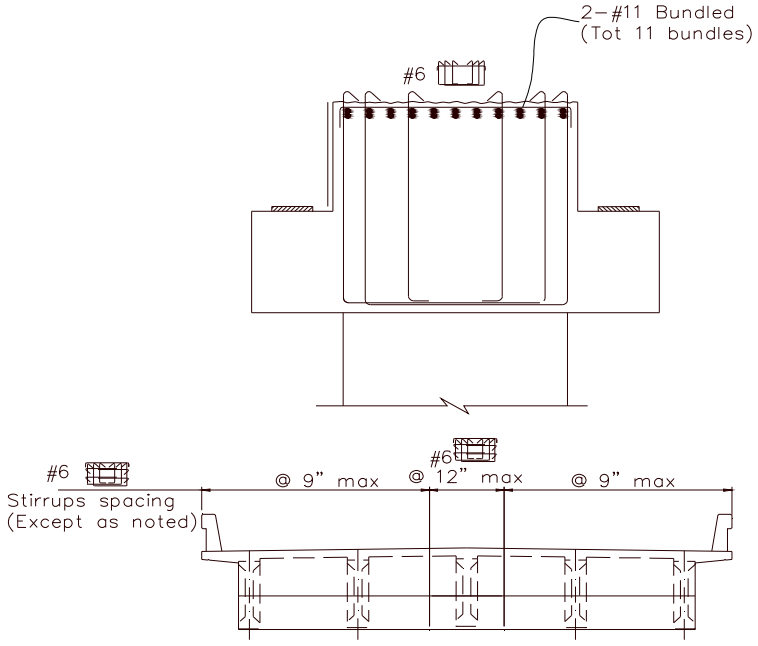


Figure 3.5. Cap Beam Reinforcement designed for Construction Loads

### 3.4.2 Service Loads

The cap beam was then designed for the dead and live service loads after the diaphragm was added. In addition to the loads calculated for the construction phase, the composite weight of the superstructure (DC), superimposed dead load (DW), weight of the barriers ($w_{barr}$ ), weight of formwork ($w_{form}$), and design vehicle load were considered. For the vehicle design loads, the HL-93 and P15 were considered. After a structural analysis, it was concluded that the P15 load governed between the two. All assumed girder loads are presented in Table 3.2 and the remaining loads are presented in Table 3.3. The interior girders include the center and intermediate girders while the exterior girder is listed separately. Another change is the load due to the Bidwell machine is not present because the deck is already present. Accounting for these changes, the resulting cap beam shear and negative moment demands are:

Table 3.2. Assume Girder Loads for the Service Load Desgin

| | Girder Loads (kips) | |
|---|---|---|
| | Interior | Exterior |
| Self-Weight | 34.8 | 34.8 |
| Deck+Haunch | 41.7 | 39.2 |
| Diaphragm | 2.2 | 1.1 |
| Precast | 5.7 | 3.9 |
| DC | 21 | 21 |
| DW | 28.4 | 28.4 |

Table 3.3. Assumed Additional Loads for the Service Load Design

| | |
|---|---|
| $w_{barr}$ | 3.73 kips |
| $w_{form}$ | .28 k/ft |
| P15 | 142 kips |

$$V_u = 1392\ kips$$

$$M_u = 10939 \text{ kip} - \text{ft}$$

First, the flexural capacity of the cap beam was calculated and compared against the demand. Unlike previously, two layers of reinforcement was considered in design. The second layer of 19, #11 bars, is the flexural reinforcement to resist the additional loading which is to be located within the depth of the concrete deck cast in place above the cap beam (see Figure 3.5). The equivalent depth of the two layers is 65.4 in. with a total area of steel is 63.96 in$^2$. The flexural capacity of the section was found using Eq.(3.8).

$$a = \frac{(63.96\ in^2)(60\ ksi)}{(0.85)(3.6\ ksi)(144\ in)} = 8.71\ in.$$

$$\phi M_n = (0.9)(63.96\ in^2)(60\ ksi)\left[65.4 \text{ in.} - \frac{5.61 \text{ in.}}{2}\right] = 210839 \text{ kip} - \text{in}$$

$$= 17570 \text{ kip} - \text{ft}$$

Since the flexural capacity was found to be greater than the ultimate moment demand the beam section was assumed to be sufficiently reinforced. Next the beam section was checked to ensure that the minimum reinforcement required by AASHTO 5.7.3.3.2 was provided. The amount of tensile reinforcement needd to develop a factored flexural resistance of 17570 kip-ft above or equal to the lesser of the following values calculated from Eq. (3.10)**Error! Reference source not found.** and (3.11) previously.

$$1.2M_{cr} = 1.2 * \left(\frac{250.3ft^4}{3.15ft}\right) * 702\frac{lb}{in^2} * \frac{144in^2}{1ft^2} * \frac{1kip}{1000lb} = 9636 \text{ kip} - \text{ft}$$

$$1.33M_u = 1.33 * 10939 \text{ kip} - \text{ft} = 14549 \text{ kip} - \text{ft}$$

This condition was found to be satisfied with the provided reinforcement. Next, the spacing of steel needs to be checked to effectively control the crack width. The provisions in Article 5.7.3.4 of AASHTO need to be satisfied for this check. Eq. (3.12)**Error! Reference source not found.** from above was used to calculate the following,

$$s \leq \left(\frac{700 * 0.75}{1.0488 * 26.1ksi} - 2 * 2.5\ in. = 14.2\ in.\right)$$

The maximum spacing provided was 9 in., which was less than the maximum spacing permitted of 14.2 in., the reinforcement layout is presented in Figure 3.6. Then, the shear capacity design was performed as required by Article 5.8.2.9 in AASHTO and Eq. (3.15). The shear stress acting on the section as,

$$v_u = \frac{|1392|}{0.9 * 144 * 58.86} = 0.182\ ksi$$

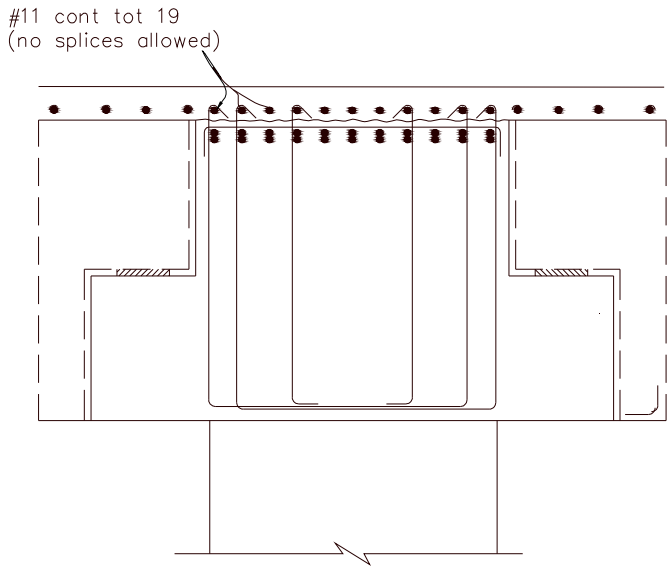


Figure 3.6. Cap Beam Flexural Reinforcement under Service Loads

Next, the shear resistance of the section was calculated according to AASHTO article 5.8.3.4.2. Using Eq. (3.16), the strain at mid-height of the section was calculated.

$$\epsilon_x = \frac{\frac{(10939 * 12)}{58.86} + 0.5 * 1392 * cot\ 36.4}{2(29000 * 63.96)} = 856x10^{-6}$$

With the value of $\epsilon_x = 856x10^{-6}$ and $\frac{v_u}{f'_c} = 0.049$, Table 5.8.3.4.2.1 of AASHTO gives $\theta = 36.4°$ and $\beta = 2.23$. The check of the $\theta$ value is complete and next the design of shear reinforcement needed to be completed. Since article 5.8.3.4.2 was used to determine the shear resistance, Eq. (3.17) is used to determine the shear resistance of the concrete cross section as follows:

$$V_c = 0.0316\beta\sqrt{f'_c}b_v d_v = .0316 * 2.23 * \sqrt{3.6} * 144 * 58.86 = 1133\ kips$$

With the required nominal shear resistance and the concrete contribution to shear resistance known, the amount of resistance needed from the shear reinforcement was found. For this calculation, Eq. (3.6) was used as follows:

$$V_s = \frac{1392}{0.9} - 1133 = 414\ kips$$

The area of shear reinforcement per spacing was then calculated. To find this value, Eq. (3.19) was used and compared to the reinforcement provided.

$$\frac{A_v}{s}_{req'd} = \frac{414 * 12}{60 * 54.79 * cot(36.4°)} = 0.46\frac{in^2}{ft}$$

$$\frac{A_v}{s}_{provided} = \frac{6 * 0.44in^2}{.75^{ft}} = 3.52\frac{in^2}{ft}$$

Therefore, the shear reinforcement provided is greater than the amount required, the check is satisfied.

Next, the flexure-shear interaction was checked. The longitudinal reinforcement would experience greater force due to shear in the cross section. In general, as the shear crack angle decreases and $V_c$ increases, the tension force in the longitudinal reinforcement would be greater for a given shear force. To account for this, Eq. 5.8.3.5-1 of AASHTO Article 5.8.3.5 was used. Eq. 5.8.3.5-1 will determine if the chosen longitudinal reinforcement would be sufficient for the flexural-shear interaction. Since no prestressing or axial force is present in the cap beam, a simplified form of this equation as shown in Eq. (3.21) was used. Accordingly,

$$A_s f_y \geq \frac{|M_u|}{d_v \phi_f} + \left(\left|\frac{V_u}{\phi_v}\right| - .5V_s\right)\cot\theta \tag{3.21}$$

$$\left((63.96 * 60) = 3838^{kips}\right) \geq \left(\frac{|10939*12|}{58.86x0.90} + \left(\left|\frac{1392}{0.9}\right| - .5(1405)\right)\cot 36.4\right) = 3623 \text{ kips}$$

Since this condition is satisfied and that the provided longitudinal reinforcement is only 6% greater than that required for the loading conditions; the reinforcement quantity was not adjusted. This completes the design of the cap beam under service loads. The final reinforcement layout of the cap beam is presented in Figure 3.7.

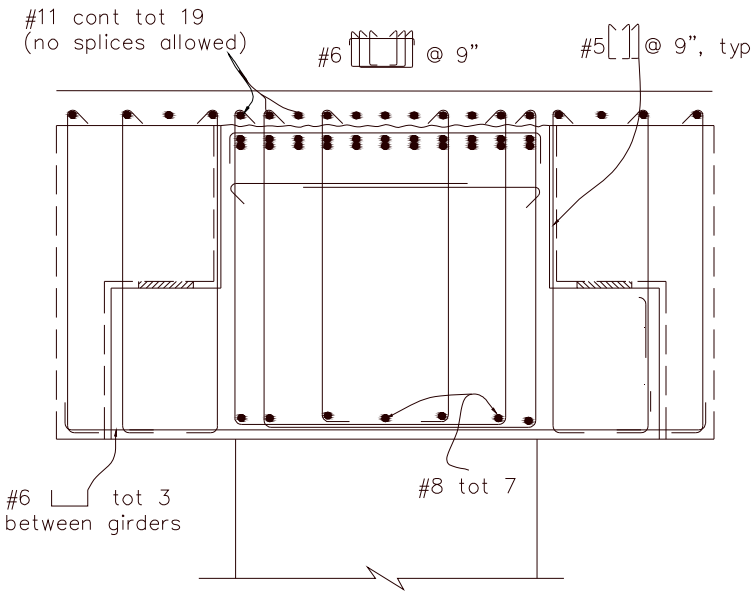


Figure 3.7. Cap Beam Reinforcement under Service Load Conditions

### 3.4.3 Torsional Demand on the Cap Beam

Finally, the torsional capacity of the cap beam was calculated to ensure that it would be greater than that induced by the column seismic moment. From XTRACT, the overstrength moment of the column ($\phi M_n$) was found to be 17,662 kip-ft when the moment was extrapolated to the centerline of the superstructure. Current design practice considers 40% of the overstrength moment to be applied as a torsional moment on the cap beam. Therefore, the resulting torsional moment on the cap beam was 7,065 kip-ft. Eq. (3.22), from Eq. 5.8.2.1-4 of AASHTO, was used to determine the torsional capacity of the cap beam.

$$T_{cr} = 0.125x\sqrt{f'_c}\frac{{A_{cap}}^2}{p_c} \tag{3.22}$$

$$T_{cr} = 0.125\sqrt{3600}\frac{(10890in^2)^2}{439.25\text{ in.}} = 64033kip - in = 5336\ kip - ft$$

According to Article 5.8.2.1, if one-quarter of the capacity is greater than the applied torsional moment, then the shear capacity of the section would be affected. Hence,

$$0.25\phi T_{cr} = 0.25 * 0.9 * 5336\text{ kip} - \text{ft} = 1200.6\ kip - ft < T_u = 7065\ kip - ft$$

Since one-quarter of the torsional capacity of the cap beam is less than the applied torsion, the torsion needed to be considered as it would reduce the shear capacity of the cap beam. The ultimate shear acting on the cap beam from the dead load was only 538 kips. The equivalent shear force acting on the cap beam from Eq. 5.8.2.1-6, shown in Eq. (3.23) of AASHTO was calculated. The shear resistance from the concrete was 1133 kips, as calculated during the cap beam design under service loads.

$$V_u = \sqrt{{V_u}^2 + \left(\frac{\cdot 9p_h T_u}{2A_o}\right)^2} \tag{3.23}$$

$$V_u = \sqrt{(538^{kips})^2 + \left[\frac{(0.9)(278\text{ in.})(7065\ in^2)(12)}{(2)(4104\text{ in}^2)}\right]^2} = 2640\ kips$$

During the cap beam shear design, multiple shear reinforcing bars were placed in the section and the capacity was calculated to ensure the equivalent shear force was resisted. Within the cap beam, six-legged #6 bars and six-legged #5 bars were provided at a spacing of 9 in. The resistance provided was calculated with an assumed crack inclination angle of 36.4°.

$$V_s = \frac{[(0.44)(6) + (0.31)(6)](58.86\text{ in.})(60\text{ in.})}{(9)\tan(36.4°)} = 2395\text{ kips}$$

Then the shear resistance provided was calculated using Eq. 5.8.3.3-1, presented in Eq. (3.24), of AASHTO and compared to the ultimate shear force.

$$\phi V_n = \phi\left(V_c + V_s + V_p\right) \tag{3.24}$$

$$\phi V_n = (1.0)(1133 \text{ kips} + 2395 \text{ kips}) = 3528\ kips > V_u = 2640\ kips$$

This check ensured that the cap torsion would be satisfactorily resisted through the reinforcement provided in the cap beam to resist shear demand.

## 3.5 Inverted Tee Ledge Design

To ensure satisfactory performance of the cap beam, the ledges of the inverted-tee were also designed. For the ledge design, the loads transmitted from the girders to the cap beam were considered along with the load transmitted from the diaphragm to the cap beam between the girders. Since the ledge on each side of the cap beam, which supports the girder loads, extends significantly wider than the column, the design should ensure that the loads will be satisfactorily transferred to the column. For this purpose, the design steps detailed in the BDA are followed.

First, the loads were calculated at the points where the girders would rest on the cap beam along with the area between the girders where the diaphragm would transmit a load to the cap beam. The loads applied to the ledge from the girders were resulting from design vehicle loads, dead load and the additional dead loads detailed previously in Table 3.2 and Table 3.3. For each section, the applied shear load, $V_u$, was found as:

Interior Girders:

$$V_u = (1.25)(84.4 \text{ kips}) + (1.25)(49.4 \text{ kips})\left(\frac{49 \text{ in.}}{96 \text{ in.}}\right) + (1.35)(206.7 \text{ kips})\left(\frac{49 \text{ in.}}{96\text{in.}}\right)$$

$$V_u = 280 \text{ kips}$$

Exterior Girders:

$$V_u = (1.25)(79 \text{ kips}) + (1.25)(49.4 \text{ kips})\left(\frac{2*31\text{in.}}{78 \text{ in.}+31 \text{ in.}}\right) + (1.35)(206.7 \text{ kips})\left(\frac{2*31\text{in.}}{31 \text{ in.}+78 \text{ in.}}\right)$$

$$V_u = 280 \text{ kips}$$

Between Girders:

$$V_u = (1.25)(49.4 \text{ kips})\left(\frac{47 \text{ in.}}{96 \text{ in.}}\right) + (1.35)(206.7 \text{ kips})\left(\frac{47 \text{ in.}}{96 \text{ in.}}\right) = 167 \; kips$$

Next, the horizontal shear, $N_{uc}$, values was calculated according to the BDA. For the same sections, the design values were calculated as per Eq. (3.25):

$$N_{uc} = 0.2 * V_u \tag{3.25}$$

Interior Girders:

$$N_{uc} = 0.2 * (280 \text{ kips}) = 56 \; kips$$

Exterior Girders:

$$N_{uc} = 0.2 * (280 \text{ kips}) = 56 \; kips$$

Between Girders:

$$N_{uc} = 0.2 * (167 \text{ kips}) = 33.4\ kips$$

Then the capacity of the area below the bearing surfaces was checked to ensure that the demand would not exceed the capacity. First, the flange needs to be checked for the ratio of the bearing point, $a_v$, to depth, $d$, of the flange, according to BDS 8.16.6.8.1, as follows in Eq. (3.26) and Figure 3.8,

$$\frac{a_v}{d} < 1.0 \tag{3.26}$$

$$\left(\frac{12 \text{ in.}}{31 \text{ in.}} = 0.39\right) < 1.0$$

This check is satisfied and the flange dimensions were thus adequate. The punching strength of the girders were then calculated. To calculate the effective area for the punching strength, the BDA was used for define the appropriate dimensions. The seat width considered for the interior girders, $b_{int}$, is the width of the bearing pad, w, plus the depth of the corbel, d. For the exterior girders, the seat width, $b_{ext}$, is the width of the bearing pad plus one-half the depth of the corbel plus the edge distance to the end of the cap, x, which should not exceed one-half the depth according to the BDS. The seat width for the area between the girders, $b_{between}$, is the girder spacing minus the bearing pad width minus the depth of the section. Figure 3.8 shows the effective widths for the interior and exterior girders, and the remaining distance between the girders is used for the between girder width.

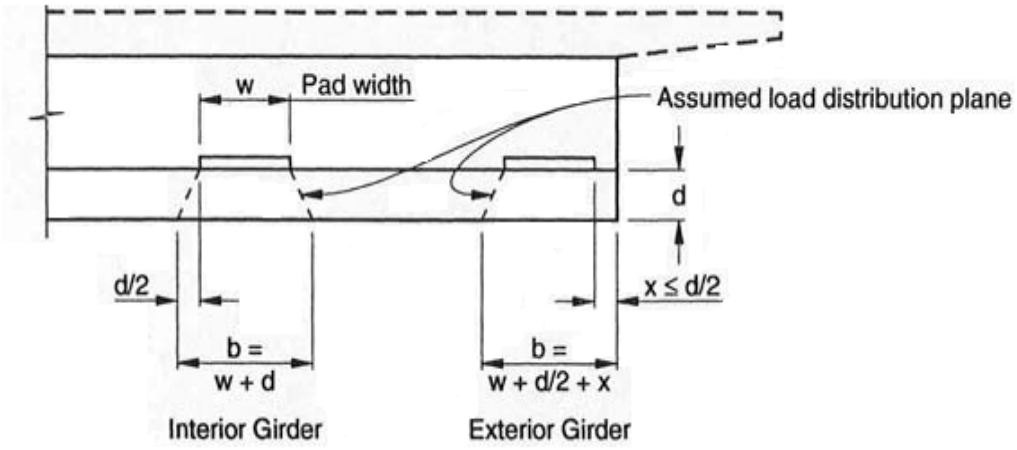


Figure 3.8. Distribution Plane Layout (Caltrans, Bridge Design Specifications, 2003)

Accordingly,

$$b_{int} = \mathrm{w_{int}} = 18\text{ in.} + 31\text{ in.} = 49\text{ in.}$$

$$b_{ext} = \mathrm{w_{ext}} = 18\text{ in.} + \frac{1}{2}(31\text{ in.}) = 33.5\text{ in.}$$

$$b_{between} = \mathrm{w_{between}} = 96\text{ in.} - 18\text{ in.} - 31\text{ in.} = 47\text{ in.}$$

As per BDS 8.16.6.6.2, the shear strength of the concrete shall not be taken greater than the value determined from that presented in Eq. (3.27),

$$\phi V_n = \phi 4\sqrt{f'_c} b_o d \tag{3.27}$$

$$b_o = 2(L + x + \frac{d}{2}) + w_{int/ext} \tag{3.28}$$

where $b_o$ is the length of the perimeter which the load acts on, presented in Eq. (3.28), L is the bearing pad length, and x is the edge distance. Therefore, the shear strength under the interior girders was calculated to be:

$$\phi V_n = (0.90)(4)\sqrt{3600}\left(2\left(12\text{ in.}+6\text{ in.}+{}^{31\text{ in.}}/_{2}\right)+49\text{ in.}\right)(31\text{ in.}) = 777\ kips$$

$$> (V_u \cong 280\ kips)$$

Similarly, for the exterior girders:

$$\phi V_n = (0.90)(4)\sqrt{3600}\left(\left(12\text{ in.}+6\text{ in.}+{}^{31\text{ in.}}/_{2}\right)+33.5\text{ in.}\right)(31\text{ in.}) = 448\ kips >$$

$$(V_u \cong 280\ kips)$$

According to the BDA, the next step in the design was to calculate the primary tension reinforcement needed to resist the loads on the ledge. The tension reinforcement needs to simultaneously resist shear ($V_u$), moment ($V_u a_v + N_{uc}(h-d)$) and tensile forces ($N_{uc}$) acting on the corbel, which are shown in Figure 3.9 from the BDA.

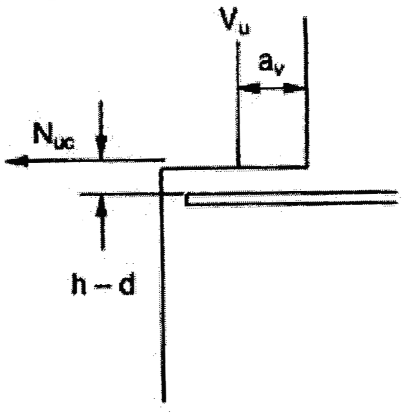


Figure 3.9. Forces to be resisted by primary tension reinforcement

The shear design was performed in accordance with Article 8.16.6.4 of the BDA and Eq. (3.29). However, for normal weight concrete, the shear strength shall not be greater than $0.2f'_c b_w d$ nor $0.8b_w d$ from BDS 8.16.6.8.3, which are presented below in Eq. (3.30) and (3.31).

$$V_n = \frac{V_u}{\phi} \tag{3.29}$$

$$V_n = \frac{280}{0.9} = 312\ kips$$

$$V_n \leq 0.2f'_c b_w d \tag{3.30}$$

$$V_n \leq (0.2(31\text{ in.} * 49\text{ in.})(3.6\text{ ksi}) = 1094\ kips)$$

$$V_n \leq 0.8b_w d \tag{3.31}$$

$$V_n \leq (0.8(31\text{ in.} * 49\text{ in.}) = 1215\ kips)$$

Since nominal shear strength was less than the two supper limits suggested in Article 8.16.6.8.3 of the BDS, the equations in Article 8.16.6.4 of the BDS were used to determine the area of needed steel reinforcement in the ledge. The value for coefficient of friction for Eq. 8-56 of the BDS, presented in Eq. (3.32), can be found in Article 8.16.6.4.4c, of the BDS. The required area, $A_{vf}$, of steel for the interior girder ledge is:

$$A_{vf} = \frac{V_n}{f_y \mu} \tag{3.32}$$

$$A_{vf} = \frac{312kips}{(60\text{ ksi})1.4} = 3.71\ in^2$$

Next, the shear load at the exterior girder was designed. The same articles were used for this design as before, including Eqs. (3.29)-(3.32). Therefore,

$$V_n = \frac{280}{0.9} = 312\ kips$$

$$V_n \leq (.2(31\text{ in.} * 33.5\text{ in.})(3.6\text{ ksi}) = 747\ kips)$$

$$V_n \leq (.8(31\text{ in.} * 33.5\text{ in.}) = 830\ kips)$$

The nominal shear was less than the two calculated values from Article 8.16.6.8.3 of the BDS. Next, the area of steel required for the exterior girder:

$$A_{vf} = \frac{312kips}{(60)1.4} = 3.71\ in.^2$$

Finally, the area between the girders:

$$V_n = \frac{V_u}{\phi} = \frac{167\text{ kips}}{0.9} = 185.6\ kips$$

$$A_{vf} = \frac{V_n}{f_y \mu} = \frac{185.6\ kips}{(60\text{ ksi})1.4} = 2.21\ in.^2$$

Then the reinforcement to resist the moment was designed. The moment to be resisted was calculated from Article 8.16.6.8.3 of the BDS, presented below in Eq. (3.33). The procedure to follow for this design is given in BDS section 8.16.3. For each of the three locations, the resulting

moment needs to be determined then the area of steel required to resist that value was determined from Eq. (3.34).

$$\mathrm{M_u = V_u a_v + N_{uc}(h - d)} \tag{3.33}$$

$$M_u \leq \phi A_f f_y \left(d - \frac{A_f f_y}{1.7 f'_c b}\right) \tag{3.34}$$

For the interior girder region,

$$M_u = 280 \text{ kips}(12 \text{ in.}) + 56 \text{ kips}(33 \text{ in.} - 31 \text{ in.}) = 3472 kip - in.$$
$$= 289.3\ kip - ft.$$

$$3472 kip - in. = (0.9) A_f (60 \text{ ksi}) \left(31 \text{ in.} - \frac{A_f (60 \text{ ksi})}{1.7(3.6 \text{ kips})(49 \text{ in.})}\right)$$

$$\Longrightarrow A_f = 2.102\ in.^2$$

For the exterior girder region,

$$M_u = 280 \text{ kips } (12 \text{ in.}) + 56 \text{ kips}(33 \text{ in.} - 31 \text{in.}) = 3472 kip - in.$$
$$= 289.3 kip - ft.$$

$$3472 kip - in. = (0.9) A_f (60 \text{ ksi}) \left(31 \text{ in.} - \frac{A_f (60 \text{ ksi})}{1.7(3.6 \text{ ksi})(33.5 \text{ in.})}\right)$$

$$\Longrightarrow A_f = 2.116 in^{.2}$$

For the region between the girders,

$$M_u = 167 \text{ kips}(12 \text{ in.}) = 2004kip - in. = 167kip - ft.$$

$$2004kip - in. = (0.9)A_f(60 \text{ ksi})\left(31 \text{ in.} - \frac{A_f(60 \text{ ksi})}{1.7(3.6 \text{ ksi})(47 \text{ in.})}\right)$$

$$\Longrightarrow A_f = 2.102in.^2$$

The third primary tension reinforcement that was designed for was the reinforcement resisting the tensile forces. The force, $N_{uc}$, shown above in Figure 3.9 was also considered in this design calculation. The area of steel required, $A_n$, to resist the force $N_{uc}$ was determined using Article 8.16.6.8.3d, presented in Eq. (3.35), as follows,

$$N_{uc} \leq \phi A_n f_y$$

$$A_n = \frac{N_{uc}}{0.9f_y} \tag{3.35}$$

Therefore, using the values for $N_{uc}$ listed previously, the area of steel required for each of the three design sections are,

Interior Girder,

$$A_n = \frac{56 \text{ kips}}{(0.9)(60 \text{ ksi})} = 1.037 \ in.^2$$

Exterior Girder,

$$A_n = \frac{56 \text{ kips}}{(0.9)(60 \text{ ksi})} = 1.037 \ in.^2$$

Between Girders,

$$A_n = \frac{0 \text{ kips}}{(0.9)(60 \text{ ksi})} = 0\ in.^2$$

After the values of tension steel required to resist shear ($V_u$), moment ($V_u a_v + N_{uc}(h-d)$)and tensile forces ($N_{uc}$) acting on the corbel separately were designed the amount of steel required to resist the forces simultaneously was determined. According to Articles 8.16.6.8.3e and 8.16.6.8.5 of the BDS, the area of steel provided, $A_s$, needs to be greater than the three values presented in Eq. (3.36),

$$A_s \geq \begin{cases} {}^{2}/_{3}\, A_{vf} + A_n \\ A_f + A_n \\ 0.04\left({}^{f'_c}/_{f_y}\right) bd \end{cases} \tag{3.36}$$

Therefore, using Eq. (3.36), for each design section the area of steel required was,

Interior Girder,

$$A_s \geq \begin{cases} {}^{2}/_{3}\,(3.704\ in.^2) + 1.037\ in.^2 = 3.51\ in.^2 \\ 2.102\ in.^2 + 1.037\ in.^2 = 3.14\ in.^2 \\ .04\left({}^{3.6 \text{ ksi}}/_{60 \text{ ksi}}\right)(49 \text{ in.})(31 \text{ in.}) = 3.65\ in.^2 \end{cases}$$

$$A_s \geq 3.65\ in.^2 \Longrightarrow 4 - \#8 \text{ @ } 9\text{in.} \Longrightarrow A_s = 4(0.79\ in.^2)\left(\frac{12 \text{ in.}}{9 \text{ in.}}\right) = 4.21\ in.^2$$

Exterior Girder,

$$A_s \geq \begin{cases} {}^{2}/_{3}\,(3.704\ in.^2) + 1.037\ in.^2 = 3.51\ in.^2 \\ 2.116\ in.^2 + 1.037\ in.^2 = 3.153\ in.^2 \\ .04\left({}^{3.6 \text{ ksi}}/_{60 \text{ ksi}}\right)(33.5 \text{ in.})(31 \text{ in.}) = 2.5\ in.^2 \end{cases}$$

$$A_s \geq 3.51\ in.^2 \Longrightarrow 5 - \#8\ @12\ \text{in.} \Longrightarrow A_s = 5(0.79\ in.^2) = 3.95\ in.^2$$

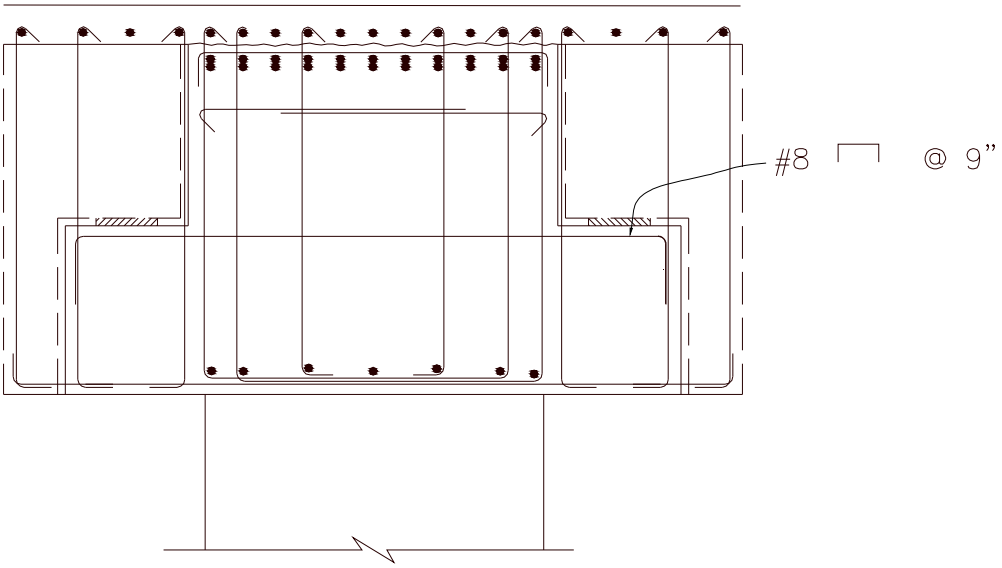


Figure 3.10. Primary tension reinforcement for the interior girders

Between Girders,

$$A_s \geq \begin{cases} {}^{2}/_{3}\,(2.21\ in.^2) + 0\ in.^2 = 1.473\ in.^2 \\ 1.207\ in.^2 + 0\ in.^2 = 1.207\ in.^2 \\ 0.04\left({}^{3.6\ \text{ksi}}/_{60\ \text{ksi}}\right)(47\ \text{in.})(31\ \text{in.}) = 3.5\ in.^2 \end{cases}$$

$$A_s \geq 3.5 in^2 \Longrightarrow 4 - \#8\ @\ 9\text{in.} \Longrightarrow A_s = 4(0.79 in.^2)(\frac{12\ \text{in.}}{9\ \text{in.}}) = 4.21\ in.^2$$

Figure 3.10 shows the primary tension reinforcement for the interior girder only, the other two sections will change size and spacing accordingly. Next, the secondary tension reinforcement required was designed. The steel required was obtained from the equation described in Article

8.16.6.8.4 of the BDS and presented in Eq. (3.37). The steel should be placed parallel to $A_s$ with the total area greater than $.5(A_s - A_n)$. According to the BDS, the steel "shall be distributed uniformly within two-thirds of the effective depth adjacent to $A_s$." Therefore, for the three sections, the required steel is,

$$A_h \geq 0.5(A_s - A_n) \tag{3.37}$$

Interior Girder,

$$A_h \geq .5(4.21\ in.^2 - 1.037\ in.^2) = 1.59\ in.^2$$

$$\Longrightarrow use\ 2 - double\ legged\ \#6 = A_h = 1.76\ in^2$$

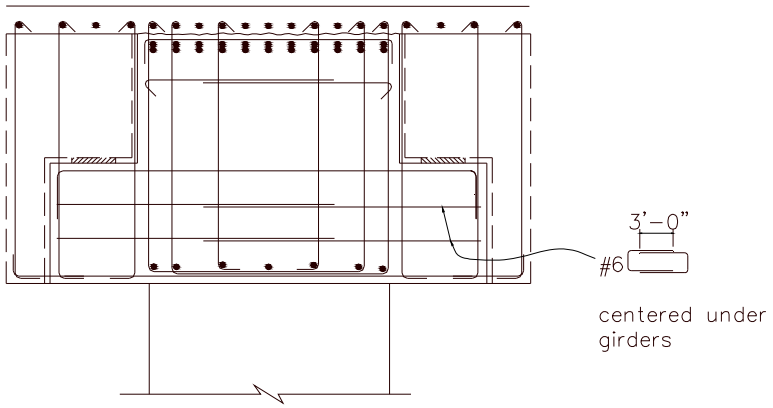


Figure 3.11. Secondary tension reinforcement for the interior girders

Exterior Girder,

$$A_h \geq 0.5(3.95\ in.^2 - 1.037\ in.^2) = 1.46\ in.^2$$

$$\Longrightarrow use\ 2 - double\ legged\ \#6 = A_h = 1.76\ in.^2$$

Between Girders,

$$A_h \geq .5(4.21\ in.^2) = 2.11\ in.^2 \Longrightarrow use\ 6 -\ \#6 = A_h = 2.64\ in.^2$$

Figure 3.11 shows the secondary tension reinforcement for the interior girders, the other two sections will change size and spacing accordingly. Next, according to the BDA, the longitudinal corbel distribution reinforcement ($A'_s$) was designed. The bars should be centered under the exterior bearing pads. The minimum area should be one-half of the primary tension reinforcement, as presented in Eq. (3.38). The steel should be uniformly spaced and extend a distance "d" beyond the seat width. For the exterior girders, the steel required is:

$$(A'_s)_{min} = 0.5A_s \tag{3.38}$$

$$(A'_s)_{min} = 0.5(3.95\ in.^2) = 1.98\ in.^2 \Longrightarrow 5 - \#6 = 2.2\ in.^2$$

For the other locations, use a minimum of 3-#5 reinforcing bars.

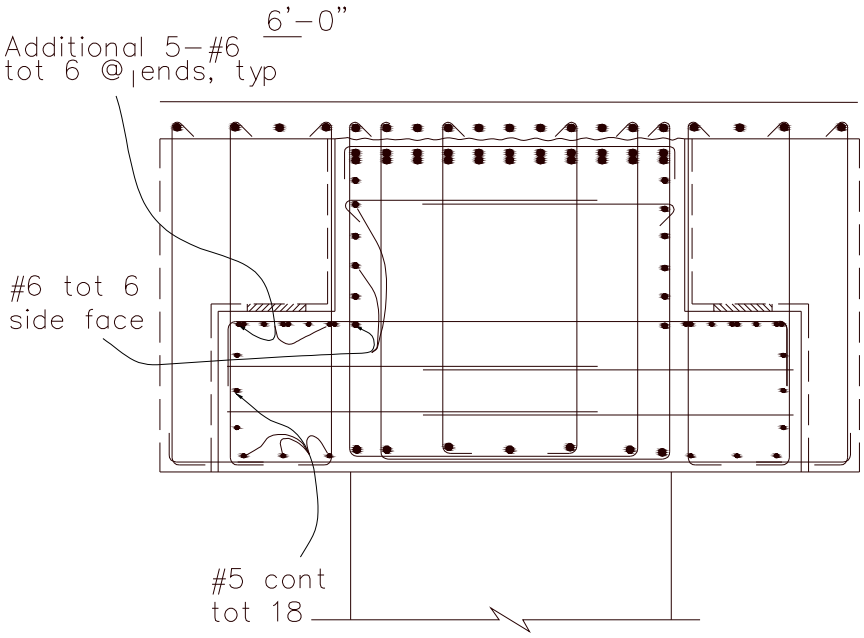


Figure 3.12. Longitudinal corbel reinforcement at the exterior girder

The longitudinal corbel distribution reinforcement at the exterior girder is shown in Figure 3.12 with the additional side reinforcement required. Next, the cap beam was designed for the diagonal tension reinforcement, $(A_v)_{req'd}$, presented in Eq. (3.39). The girders apply loads onto the ledge that may cause diagonal cracks from the location where the ledge and stem meet. The diagonal reinforcement spans the crack opening and the shear can be carried through these reinforcing bars, as shown below in Figure 3.13.

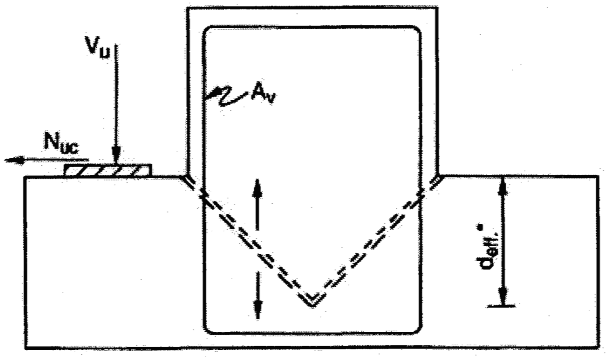


Figure 3.13. Corbel diagonal cracking and tension reinforcement (Caltrans, Bridge Design Aids, 1995)

Article 8.16.6.2.3 of the BDS was used to design the required reinforcing. Eq. 8-52from the BDS, presented below in Eq. (3.40), was used to calculate the force resisted by the concrete, where $b_w$ are the seat widths calculated previously.

$$(A_v)_{req'd} = \frac{V_s}{f_y} \tag{3.39}$$

$$V_c = 2\left(1 + \frac{N_u}{500A_g}\right)\sqrt{f'_c}\, b_w d_{eff} \tag{3.40}$$

The remainder of the shear force was resisted by the steel being designed. The cracking was assumed to be at a forty-five degree angle so the value of $d_{eff}$ cannot be greater than one-half the width of the stem of the cap beam. The value for $N_u$ was taken as the shear from the girder, negative when in tension. Once the force needing to be resisted by reinforcing steel was determined, the contributing resistance from the cap beam reinforcement was checked to determine if it was adequate to be used for the diagonal cracking reinforcement. Therefore, for the three sections the steel check is presented below.

Interior Girder,

$$V_c = 2\left(1 + \frac{280 \text{ kips}}{0.5(49 \text{ in.}*31\text{in.})}\right)\frac{\sqrt{3600 \text{ ksi}}(49\text{in.})(31\text{in.})}{1000} = 115 \text{ kips}$$

$$V_{s,req'd} = \frac{V_u}{\phi} - V_c = \frac{280 \text{ kips}}{0.9} - 115 \text{ kips} = 196 \text{ kips}$$

To check the contribution of the cap beam shear reinforcement provided from previous design steps, it was assumed only two legs of the reinforcement are effective. Within the distance $b_{int}$ there were already five sets of #6 bars. The area of steel required was calculated and the area of steel provided from previous design was calculated and compare to check if additional reinforcement was required.

$$(A_v)_{req,d} = \frac{V_{s,req'd}}{f_y} = \frac{196 \text{ kips}}{60 \text{ ksi}} = 3.27\ in.^2$$

$$(A_v)_{provided} = 5\ sets\ of\ 2\ legged - \#6 = 4.4\ in.^2$$

The provided reinforcement was sufficient to act as the diagonal cracking reinforcement.

Exterior Girder,

$$V_c = 2\left(1 + \frac{280 \text{ kips}}{0.5(33.5 \text{ in.}*31 \text{ in.})}\right)\frac{\sqrt{3600 \text{ ksi}}(33.5 \text{ in.})(31 \text{ in.})}{1000} = 57.4 \text{ kips}$$

$$V_{s,req'd} = \frac{V_u}{\phi} - V_c = \frac{280 \text{ kips}}{0.9} - 57.4 \text{ kips} = 254 \text{ kips}$$

Similar to the interior girder region the provided cap beam shear reinforcement provided from previous design steps was checked to see if that did satisfy the area of steel required, it was assumed

only two legs of the reinforcement are effective. Within the distance $b_{int}$ there were four sets of #6 bars.

$$(A_v)_{req'd} = \frac{V_{s,req'd}}{f_y} = \frac{254 \text{ kips}}{60 \text{ ksi}} = 4.23\ in.^2$$

$$(A_v)_{provided} = 4\ sets\ of\ 2\ legged - \#6 = 3.52\ in.^2$$

The provided reinforcement was not sufficient to act as the tension reinforcement, additional steel was designed to satisfy the requirement. According to the BDA, when using diagonal bars, the effective area is taken by adjusting according to the angle of the bar. Additional bars were placed at a 45 degree angle from vertical, so the additional steel required was,

$$(V_s)_{req'd} = 254 \text{ kips} - (3.52\ in.^2)(60 \text{ ksi}) = 42.8 \text{ kips}$$

$$(A_v)_{req'd} = \frac{V_{s,req'd}}{f_y} = \frac{42.8 \text{ kips}}{60 \text{ ksi}} = 0.72\ in.^2 \Longrightarrow 4 - \#6@45° = 4(0.44)\cos(45°)$$

$$= 1.25\ in.^2$$

For the exterior girder region, an additional 4-#6 reinforcing bars placed at a 45 degree angle was required for the diagonal cracking design as shown in Figure 3.14.

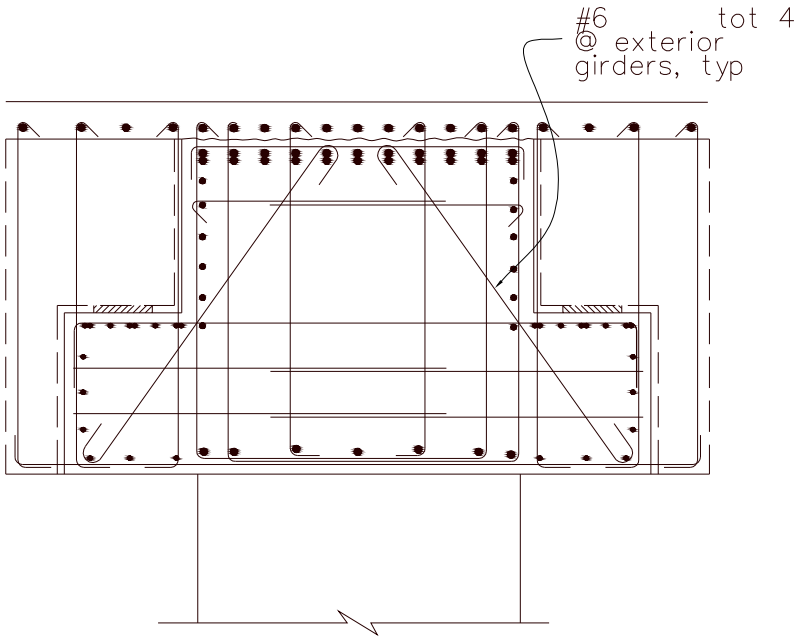


Figure 3.14. Corbel diagonal cracking reinforcement

Between Girders:

$$V_c = 2\left(1 + \frac{-167 \text{ kips}}{0.5(47 \text{ in.} * 31 \text{ in.})}\right)\frac{\sqrt{3600 \text{ ksi}}(47 \text{ in.})(31 \text{ in.})}{1000} = 135 \text{ kips}$$

$$V_{s,req'd} = \frac{V_u}{\phi} - V_c = \frac{167 \text{ kips}}{0.9} - 135 \text{ kips} = 51 \text{ kips}$$

Similar to the previous two regions, the assumption of only 2 legs effective was used. Within the distance $b_{between}$ there were five sets of #6 bars.

$$(A_v)_{req'd} = \frac{V_{s,req'd}}{f_y} = \frac{51 \text{ kips}}{60 \text{ ksi}} = 0.85 \ in.^2$$

$$(A_v)_{provided} = 5 \ sets \ of \ 2 \ legged - \#6 = 4.4 \ in.^2$$

From the described calculations, only the region under the exterior girder requires any additional diagonal steel. The rest of the sections satisfy the check by the contribution of the existing shear reinforcement present. The existing shear reinforcement was utilized in this design step because the loads being designed for were accounted for in the previous shear design of the cap beam and that these were not additional loads on the cap beam.

The final step in the cap beam ledge design was the calculation of the development length ($l_{hb}$) for the #8 ledge bars. From Article 8.29.2 of the BDS, the basic development length for a hooked bar with the yield strength equal to 60,000 psi shall be taken as:

$$l_{hb} = \frac{38d_b}{\sqrt{f'_c(ksi)}} = \frac{1200d_b}{\sqrt{f'_c(psi)}} \tag{3.41}$$

where $d_b$ is the bar diameter. However, since the side cover is greater than 2½ inches, the development length can be multiplied by 0.7 according to Article 8.29.3.2 of the BDS. Therefore, the development required was:

$$l_{dh} = \frac{38(1\text{ in.})}{\sqrt{3.6(ksi)}} = 20.03\text{ in.} * (0.7) = 14\text{ in.}$$

Based on the above estimate, the #8 bar was provided with 16 in. of development length, which completes the cap beam ledge design and the cap beam design.

## 3.6 Dapped End Beam

The shear resistance of the concrete section needs to be checked; the same procedures used previously in designing the cap beam will be used. From Article 5.8.3.4.2 of AASHTO, the strain can be determined and then by checking Table 5.8.3.4.2-1 of AASHTO, the appropriate angle of inclination and shear stress ratio can be determined with iteration. First, the actual shear stress ratio

was determined. The shear stress ratio is given below and the values for $d_v$, the effective shear depth, and $b_v$, the effective web width, can be determined from Article 5.8.2.9 of AASHTO.

$$d_v = 0.9(66\text{ in.} - 5\text{ in.}) = 54.9\text{ in.} \approx 55\text{ in.}$$

$$b_v = 19\text{ in.} \Longrightarrow width\ of\ the\ block\ end\ of\ the\ girder$$

$$V_u = 1.25DL = 1.25 * 84.4\ kips = 106\ kips$$

$$v_u = \frac{|V_u - \phi V_p|}{\Phi b_v d_v} = \frac{106\text{ kips}}{55"x19"} = 0.101ksi$$

$$\frac{v_u}{f'_c} = \frac{0.101ksi}{5.5ksi} = 0.0184$$

Given the value for the actual shear stress ratio, the midsection strain was calculated by assuming an angle of inclination for the cracks. Once the midsection strain was calculated, the strain value and the shear stress ratio was used to check if the assumed angle of inclination was correct. The previously presented Eqs. (3.15) and (3.16) were used. However, the girder prestressing in the section did provide a force, $V_p$, to resist the shear force present. The moment used for the strain calculation was taken between the $V_u$ and center of gravity of the vertical ties. For the angle of inclination, 33.7° was assumed.

$$V_p = (0.6 * 270\ ksi)(6 * 0.217\text{ in}^2)\left(\frac{24\text{ in.}}{30\text{ in.}}\right)\sin(5.836°) = 17\ kips$$

$$N_u = 0.2 * V_u = 0.2 * 84.4\ kips = 21\ kips$$

$$M_u = 106\text{ kips} * 18.5\text{ in.} = 1961\ kip - in.$$

$$d_v = 66 \text{ in.-}2 \text{ in.-}3.5 \text{ in.} = 60.5 \text{ in.}$$

$$\epsilon_x = \frac{\frac{1961 \text{ kip} - \text{in.}}{60.5 \text{ in.}} + .5(21 \text{ kips}) + .5|106 \text{ kips} - 17 \text{ kips}| \cot(33.7°)}{2\left((29000\ ksi)(3.472\ in.^2)\right)}$$

$$\epsilon_x = 554 * 10^{-6}$$

Next, by consulting Table 5.8.3.4.2-1 in AASHTO, the angle of inclination listed for a shear stress ratio of 0.0184 and a midsection strain of 554x10$^{-6}$ was 33.7°, which was assumed. Therefore, the section was adequate to be used in designing the shear resistance.

## 3.7 Dapped End Reinforcement

A strut-and-tie design was completed to efficiently design the dapped end reinforcement. For the strut-and-tie analysis the nodes were placed at the location of the bearing pad support, locations of point loads and other suitable locations where struts and/or ties cross. The layout of the model chosen for analysis is shown below in **Error! Reference source not found.**. The point loads applied at nodes B and E were equivalent to the sum of the distributed force within the contributory area of the node. The distributed force was equal to the reaction at node A, which was $V_u$, distributed evenly over the half the length of the cap beam. presents the resultant values for the struts and ties for the model shown. In addition to the loads considered above, the additional dead load and live load acting on the span was checked to ensure proper transfer of these loads from the girders to the diaphragm with appropriate engagement of the dapped end.

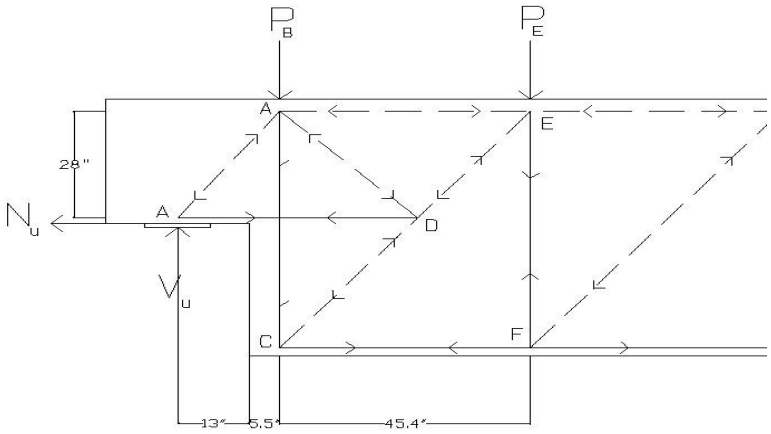


Figure 3.15. Diagram showing the Strut and Tie model used for detailing the Dapped End of girders

Table 3.4. Forces in Struts and Ties in the model shown

| Strut/Tie | Force (kips) |
|---|---|
| $C_{AB}$ | 127 |
| $T_{AD}$ | 91 |
| $C_{BD}$ | 74.4 |
| $T_{BC}$ | 158 |
| $C_{BE}$ | 21.1 |
| $C_{CD}$ | 197.6 |
| $T_{CF}$ | 118.6 |
| $C_{DE}$ | 127.4 |
| $T_{EF}$ | 97.9 |

First, the amount of force required to be transferred was calculated, and then the value of force transferred through shear friction from girder to diaphragm was calculated. The remainder of the force not able to be transferred by shear friction was assumed to transfer through the dapped end.

$$V_u = (1.25)(49.4 \text{ kips}) + (1.35)(206.7 \text{ kips}) = 341 \text{ kips}$$

Now the shear transfer through shear friction must be calculated. The steel acting in the shear transfer include the three 1-in. dowel bars connecting each side of the girder to the diaphragm along with four, #11 bars placed transversely in the deck. The shear force provided from the steel is:

$$\phi V_{sf} = (0.9)[(1.0)(4 * 1.56 \text{ in.}^2)(60 \text{ ksi}) + 3(9.6 \text{ kips})] = 363 \text{ kips}$$

The shear resistance provided from the steel was greater than the shear demand estimated on the section, and therefore, the dapped end was considered not to need to provide any additional shear transfer.

With the forces estimated from the strut and tie analysis, adequate reinforcement was designed to resist all forces. Steel reinforcement was needed to resist the tension forces from nodes A-D, B-C and C-F. Using 60 grade steel, the area of reinforcement required for each of these ties is given below.

Tie AD,

$$A_s = \frac{T_u}{\phi f_y} = \frac{91 \text{ kips}}{(0.9)(60 \text{ ksi})} = 1.69 \text{ in.}^2$$

Tie CF,

$$A_s = \frac{T_u}{\phi f_y} = \frac{118.6 \text{ kips}}{(0.9)(60 \text{ ksi})} = 2.20 \text{ in.}^2$$

Tie AD,

$$A_s = \frac{T_u}{\phi f_y} = \frac{158 \text{ kips}}{(0.9)(60 \text{ ksi})} = 2.93 \text{ in.}^2$$

For Tie AD, in addition to the steel provided by the dapped end reinforcement, an additional steel amount was provided to resist the bursting stresses expected in this region from the prestressing strands. From the CONSPAN analysis, the amount of reinforcement needed to control bursting stresses was 1.93 $in^2$. Therefore, the area of steel required in the dapped end region at tie AD was estimated as follows,

Tie AD,

$$A_s = 2.93in^2 + 1.93in^2 = 4.86\ in^2$$

To provide adequate reinforcement to resist the tie forces, for #7 bars were used and detailed as shown in Figure 3.16. In addition to the #7 bars, four #5 hoops were provided at the anchorage region of the prestressing strands to aid in resisting the bursting stresses.

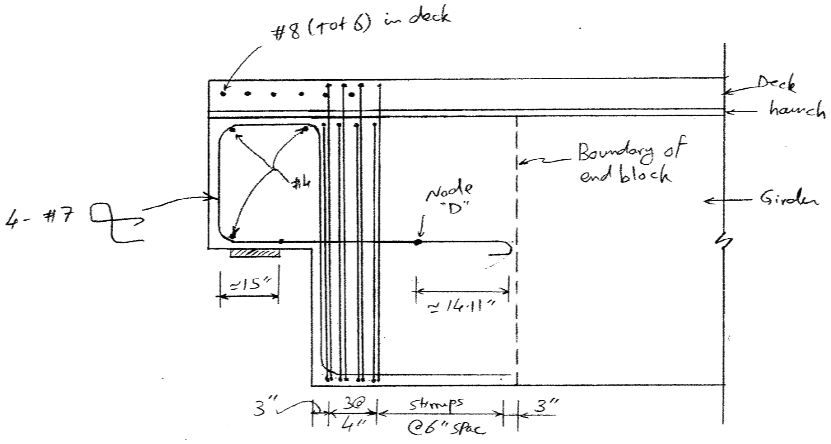


Figure 3.16. Dapped End Region Reinforcement Layout

## 3.8 Top Deck Reinforcement

Additional bars were provided over the cap beam for each girder to resist the negative moment acting at that location. From the CONSPAN output, the negative moment over the exterior and interior girders was 3661 kip-ft and 3516 kip-ft, respectively. Adequate negative moment

reinforcement was then designed to resist the greater value, 3661 kip-ft. The process for the design was similar to that which was used for designing the flexural reinforcement of the cap beam, and Eqs. (3.8) and (3.9) were used for this purpose. The girders are spaced at 8-foot intervals and the compressive strength of the concrete was assumed to be 3.6 ksi. To determine the required deck steel, Eq. (3.8) was solved for $A_s$. Hence,

$$3661 \text{ kip} - \text{ft.}\left(\frac{12 \text{ in.}}{1 \text{ ft.}}\right) = 0.9A_s(60 \text{ ksi})\left(71.7 \text{ in.} - \frac{\frac{A_s(60 \text{ ksi})}{0.85(3.6\text{ksi})(96 \text{ in.})}}{2}\right)$$

$$\Longrightarrow A_s = 11.53 \text{ in.}^2$$

To provide the required amount of steel, ten #10 reinforcing bars were provided per girder location. The development length of the reinforcing bars was then calculated. From Section 8.25.1 of the BDS, the development length required for the negative moment reinforcement was determined from the following equation:

$$l_d = \frac{0.04A_b f_y}{\sqrt{f'_c}} = \frac{0.04 * 1.27 \text{ in.}^2 * 60000 \text{ psi}}{\sqrt{3600psi}} = 50.8 \text{ in.} = 4.23 \text{ ft.}$$

The above designed reinforcement was terminated in two separate locations: point of 50% of the moment capacity and point of zero negative moment. According to the CONSPAN output, the location of moment equal to 50% of the resisting moment capacity was at 13.5 feet from the centerline of the cap beam. By adding the development length of the bars to that distance, a length of 17.73 feet was obtained, and thus a length of 18 feet was used. A further calculation should be performed to ensure that proper capacity is provided. Therefore, at the location the reinforcing bars are fully developed, 13.77 feet from the cap beam centerline, the moment demand due to the applied

loading was found to be 1884 k-ft, from CONSPAN. The provided moment capacity, assuming five #10 bars are effective to account for, was:

$$\phi M_n = (0.9)(5 * 1.27 \text{ in}^2)(60 \text{ ksi})\left(71.7 \text{ in.} - \frac{\frac{(5 * 1.27 \text{ in.}^2)(60 \text{ ksi})}{0.85(3.6 \text{ ksi})(96 \text{ in.})}}{2}\right)\frac{1 \text{ ft.}}{12 \text{ in.}}$$

$$= 2030 \text{ kip} - \text{ft.} > 1884 \; kip - ft.$$

Finally, the location to terminate the remainder of the bars was determined. An assumption that the bars would continue a distance equal to twice the length of the terminated bars was made. Therefore, the bars would extend 36 feet from the centerline of the cap beam before terminating them. The development length for these bars is the same as above so the moment at a distance 31.77 feet from the centerline was checked to ensure that the negative moment at this location was zero. From the CONSPAN output, there was zero negative moment at that location, and thus the reinforcement was terminated as shown in Figure 3.17.

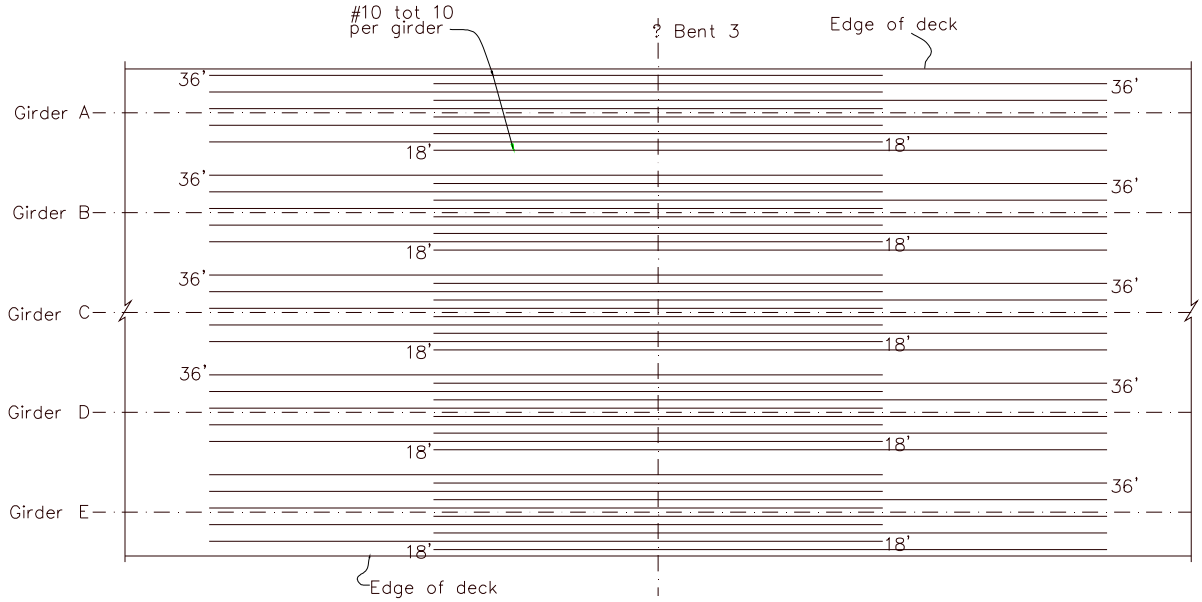


Figure 3.17. Additional Deck Reinforcement

### 3.9 Column-Bent Cap Joint Shear

The joint was detailed adequately to resist all possible shear forces from the superstructure and column for the column overstrength flexural capacity this process ensured the force can be transferred effectively between the two components. The SDC details the steps required to ensure that the joint would be designed properly. The first step was to check the principal stresses in the joint to ensure they are less than the allowable, according to Article 7.4.2 of the SDC, and they are listed below in Eqs. (3.42)-(3.42) where $p_c$ is principal compression and $p_t$ is principal tension.

$$p_c \leq 0.25 * f'_c \tag{3.42}$$

$$p_t \leq 12 * f'_t \tag{3.43}$$

To find the principal stresses the joint shear stress, vertical normal joint stress and horizontal normal joint stress were all required before proceeding on to the principal stress calculation. The values for the stress were obtained by using Eq. 7.10 in Article 7.4.2.1 and Eq. 7.13 to 7.17 in Article 7.4.4.1 of the SDC presented below in Eqs. (3.44)-(3.49).

$$B_{cap} = D_c + 2\,(ft) \tag{3.44}$$

$$v_{jv} = \frac{T_c}{A_{jv}} \tag{3.45}$$

$$A_{jv} = l_{ac} * B_{cap} \tag{3.46}$$

$$f_v = \frac{P_c}{A_{jh}} \tag{3.47}$$

$$A_{jh} = (D_c + D_s) * B_{cap} \tag{3.48}$$

$$f_h = \frac{P_b}{B_{cap} * D_s} \tag{3.49}$$

where $v_{jv}$ is the vertical joint shear stress, $T_c$ is column tensile force at the overstrength moment, $A_{jv}$ is the effective vertical joint area, $l_{ac}$ is the length the column longitudinal reinforcement is embedded into the cap, $B_{cap}$ is the bent cap width, $f_v$ is the vertical stress acting on the joint, $P_c$ is the column axial force, $A_{jh}$ is the effective horizontal joint area, $D_c$ is the cross-sectional dimension of the column in the direction of bending, and $D_s$ is the depth of the superstructure at the bent cap. With the equations available, the joint stresses were calculated.

$$B_{cap} = 5.5 \text{ ft.} + 2 \text{ ft.} = 7.5 \text{ ft.} = 90 \text{ in.}$$

$$A_{jv} = 59 \text{ in.} * 90 \text{ in.} = 5310 \text{ in}^2$$

$$v_{jv} = \frac{3032 \text{ kips}}{5310 \text{ in.}^2} = 0.571 \text{ ksi} = 571 \text{ psi}$$

$$A_{jh} = (5.5 \text{ ft.} + 6.3 \text{ ft.}) * 7.5 \text{ ft.} = 88.5 \text{ ft.}^2 = 12746.3 \text{ in.}^2$$

$$f_v = \frac{1547 \text{ kips}}{12746.3 \text{ in.}^2} = -0.121 \text{ ksi} = -121 \text{ psi}$$

In the above calculations, positive stress is a tensile stress and negative stress is a compressive stress. Next the principal stresses were calculated from Eq. 7.12 of the SDC, given below in Eq. (3.50), as follows,

$$p = \frac{f_h + f_v}{2} \pm \sqrt{\left(\frac{f_h - f_v}{2}\right)^2 + {v_{jv}}^2} \tag{3.50}$$

$$p_c = \frac{-121}{2} - \sqrt{\left(\frac{121}{2}\right)^2 + 571^2} = |-635 \text{ psi}| < 0.25(3600 \text{ psi}) = 900 \text{ psi}$$

$$p_t = \frac{-121}{2} + \sqrt{\left(\frac{121}{2}\right)^2 + 571^2} = 514 \text{ psi} < 12\sqrt{(3600 \text{ psi})} = 720 \text{ psi}$$

The stresses in the section are less than the allowable limits. The section was then checked for required reinforcement. First, a check was performed to see if the minimum reinforcement could be provided or if a more detailed reinforcement design based on a force transfer model was required. In Article 7.4.4.2 of the SDC, if the principal tensile stress does not exceed $3.5\sqrt{f'_c}$ only the minimum joint shear reinforcement is required. The corresponding stress limit is 210 psi, which was less than the principal tensile stress. Therefore, section 7.4.4.3 must be considered in the reinforcement design. The joint was then designed for vertical stirrups, horizontal stirrups, horizontal side reinforcement and j-dowel bars. For the vertical stirrups (${A_s}^{jv}$), Eq. 7.19 was be used as presented in Eq. (3.51), where $A_{st}$ is the total area of longitudinal bars being anchored from the column.

$${A_s}^{jv} = 0.2 * A_{st} \tag{3.51}$$

$$\mathrm{A_s^{jv}} = 0.2 * (33 * 1.56 \text{ in.}^2) = 10.296 \text{ in.}^2$$

According to the SDC, existing stirrups in the cap beam can be considered for the vertical stirrups. Within the column six 4-legged #6 bars and eight 6-legged #9 bars were provided from previous design. The total area of steel provided was 31.68 in.$^2$ and thus no additional vertical stirrups were needed. Next, the area of horizontal stirrups ($A_s{}^{jh}$) were detailed. From Eq. 7.20 of the SDC, shown below in Eq. (3.52), the required area of steel was calculated.

$$A_s{}^{jh} = 0.1 * A_{st} \tag{3.52}$$

$$A_s{}^{jh} = 0.1 * (33 * 1.56\ \text{in}^2) = 5.15\ \text{in}^2$$

Within the joint region, from the previous cap beam design, there were 14 sets of double legged #6 bars in the horizontal direction. The area provided was 12.32 in.$^2$, and therefore, no additional reinforcement was provided. Third, area of horizontal side reinforcement ($A_s{}^{sf}$) was detailed. From Eq. 7.21 of the SDC, presented in Eq. (3.52), the area of steel required is the greater of the two values that are proportional to the area of cap beam flexural steel ($A_{cap}$) as given below.

$$A_s{}^{sf} \geq \begin{cases} 0.1 * A_{cap}{}^{top} \\ 0.1 * A_{cap}{}^{bot} \end{cases} \tag{3.52}$$

$$A_s{}^{sf} \geq \begin{cases} 0.1 * (41 * 1.56\ \text{in}^2) = 6.4\ \text{in}^2 \\ 0.1 * (0) = 0 \end{cases}$$

The area of top flexural reinforcement controlled for the calculation and the required amount of steel is 6.4 in$^2$. In the cross section, there already existed two #8 and twelve #6 bars. The total area of steel provided was 6.86 in.$^2$, which was greater than the area required. According to the SDC, the bars must be spaced less than 12 in. along the side of the cap beam. The existing steel already had been placed at spacing less than 12 in. Therefore, the reinforcement spacing was satisfactory. The

next reinforcement designed was J-dowels according to Article 7.4.4.3d of the SDC. The required amount of steel ($A_s{}^{j-bar}$) was found from Eq. 7.22, provided below in Eq. (3.54), and was based on the area of column longitudinal reinforcement, $A_{st}$,

$$A_s{}^{j-bar} = 0.08 * A_{st} \tag{3.54}$$

$$A_s{}^{j-bar} = 0.08 * 51.48 \text{ in}^2 = 4.12 \text{ in}^2$$

However, since there ws a large amount of additional vertical stirrups, some of the vertical legs can be considered as J-dowels. Therefore, the amount of required vertical stirrups, $A_s{}^{jv}$, and the amount of J-dowel reinforcement, $A_s{}^{j-bar}$, must be less than the provided steel in the section. The amount of steel provided is 31.68 in.$^2$ and the combined amount of steel required is 14.41 in.$^2$ requiring no additional steel for J-dowels. Finally, the transverse reinforcement ratio in the joint must exceed the value calculated in Eq. 7.23 of the SDC, reproduced in Eq. (3.55). The transverse reinforcement in the column may be extended into the cap beam to meet the requirement. The following ratio was obtained for the joint region:

$$\rho_s = 0.4 * \frac{A_{st}}{l^2{}_{ac}} \tag{3.55}$$

$$\rho_s = 0.4 * \frac{51.48\ in.^2}{(59 \text{ in.})^2} = 0.00592$$

The longitudinal bars were extended as close as possible to the top flexural reinforcement of the cap beam. The provided confinement reinforcement was #6 hoops at 4 in. spacing with a 2 in. clear cover. Eq. (3.56) provides the equation used to calculate ratio of the reinforcement provided, $\rho_s$,

where $A_b$ is the reinforcement bar area, D' is the diameter of the confined concrete core and s is the spacing of the reinforcement.

$$\rho_s = \frac{4A_b}{D's} \tag{3.56}$$

$$\rho_s = \frac{4(0.44 \text{ in.}^2)}{(61.25 \text{ in.})(4 \text{ in.})} = 0.00718$$

The provided reinforcement ratio was greater than the required and that completed the detailing for the column-bent cap joint shear.

The prototype structure designed in this chapter was similar to many bridges designed in the recent times in the state of California. The structure was detailed for flexure and shear of the cap beam and column, and adequate force transfer through the joints and connections.

# Chapter 4. DETAILS OF TEST UNIT

## 4.1 Introduction

In Chapter 3, the design calculations for the prototype bridge chosen for investigating the seismic behavior of inverted tee bent cap supporting precast girders were presented. For a large-scale laboratory test investigation, a half-scale model was developed based on the prototype bridge. A summary of the dimensions and reinforcement details of the test unit are provided in this chapter. In addition, an analysis was performed to ensure that the loading of the test unit would accurately replicate the moment and shear forces expected in the prototype bridge in the critical regions. A summary of that analysis is also provided together with an equivalent hold down force required on the test unit to ensure comparable gravity load effects on the prototype and test structures. The test unit drawings are provided in Appendix B.

As mentioned previously, it was decided, based on economy and space considerations of the Powell structural laboratory at USCD that the test unit would be scaled to 50% of the length of the Prototype. The dimensions and forces were scaled according to the 0.5 dimension scale factor to ensure that the stresses and strains in the test unit would be similar to the stresses and strains in the prototype bridge. In order to maintain compatibility between the stresses and strains experienced in the test unit to those in the prototype, scale factors presented below in Table 4.1 were used in establishing and analyzing the test unit.

Table 4.1. Scale Factors for the Model Unit

| Parameter | Scale Factor |
|---|---|
| Length | 0.5 |
| Area | 0.25 |
| Stress | 1 |
| Force | 0.25 |
| Moment | 0.125 |
| Uniform Load | 0.5 |
| Displacement | 0.5 |

This chapter follows the same sequence as the previous chapter presenting the design of the prototype structure. The values from the prototype structure were scaled according to scale factors in Table 4.1. Many of the values scaled down directly; however, certain reinforcement sizes could not be easily scalable, and thus reinforcement ratios were calculated to provide evidence that the test unit reinforcement was accurately quantified .

## 4.2 Material Properties

The material properties assumed for the test unit were the same as those taken for the prototype bridge design. This assumption ensures that stress-strain behavior of materials is the same between the two structures and stresses and strains in the test unit are comparable to those in the prototype bridge.

## 4.3 Cap Beam Design

In accordance with the above discussion, the cap beam dimensions in the test unit were established using the model scale factors given Table 4.1. The final values are provided in Table 4.2.

Table 4.2. Dimensions of the inverted-tee cap beam in the test unit

| | Prototype Structure | Test Unit |
|---|---|---|
| Length | 33 ft. 6 in. | 16 ft. 9 in. |
| Height | 5 ft. 6 in. | 2 ft. 9 in. |
| Width (without diaphragm) | 12 ft. | 6 ft. |
| Width (with diaphragm) | 10 ft. | 5 ft. |
| Stem Width | 6 ft. | 3 ft. |
| Ledge Width (each side) | 2 ft. | 1 ft. |
| Diaphragm Width (each side) | 2 ft. | 1 ft. |

### 4.3.1 Construction Loads

The reinforcement in the cap beam designed for construction load was scaled using the area scale factor for the reinforcing bars and the length scale factor for the spacing. The values for the reinforcement details are given in Table 4.3. It was not possible to directly scale down the flexural steel bar sizes due to the lack of a bar one-quarter in area to a #11 bar. However, the following calculation shows that the steel ratio of the flexural reinforcement on the top of the cap beam was similar in the prototype and test structures.

$$\left(\frac{A_v}{s}\right)_{proto,scaled} = \frac{A_v}{4} x \frac{2}{s} = \frac{22x1.56in^2}{4} x \frac{2}{6.7in} = 2.56 \frac{in^2}{in}$$

$$\left(\frac{A_v}{s}\right)_{test\ unit} = \frac{20x0.44in^2}{3.72in} = 2.37 \frac{in^2}{in}$$

The ratio of reinforcement in the test unit was slightly smaller than that which would be obtained by directly scaling down the prototype reinforcement. However, when consulting the prototype design calculation in Section 3.4.1 the flexural reinforcement provided exceeded the required amount significantly, confirming that provided steel reinforcement in the test unit was sufficient.

Table 4.3. Cap Beam reinforcement under construction loads

| | | Prototype Structure | Test Unit |
|---|---|---|---|
| Flexural Steel | Quantity | 22-#11 bars | 20-#6 bars |
| | Spacing | 6.7 in. | 3.72 in. |
| Shear | Quantity | 6-#6 bars | 6-#3 bars |
| | Spacing | 9 in. | 4.5 in. |

### 4.3.2 Service Loads

The values for the additional reinforcement needed to resist the service loads are given below. Similar to the construction load reinforcement, the scale factors were used. If the scaling didn't result in exact bar sizes, then the steel ratio was maintained. Under service loads, no additional shear reinforcement was required. The values for the flexural reinforcement are given in Table 4.4 and calculated below.

$$\left(\frac{A_v}{s}\right)_{proto,scaled} = \frac{A_v}{4} * \frac{2}{s} = \frac{19x1.56in^2}{4} x \frac{2}{9\,in.} = 1.65\frac{in^2}{in}$$

$$\left(\frac{A_v}{s}\right)_{test\ unit} = \frac{17x0.44in^2}{4.33in} = 1.73\frac{in^2}{in}$$

Table 4.4. Additional Cap Beam Reinforcement to resist the Service Loads

| | | Prototype Structure | Test Unit |
|---|---|---|---|
| Flexural Steel | quantity | 19-#11 | 17-#6 |
| | spacing | 9" | 4.33" |

The flexural reinforcement in the test unit slightly exceeded the prototype structure values; however, it was small and the difference was disregarded.

## 4.4 Inverted Tee Ledge Design

The design on the ledge for the prototype cap was performed in Section 3.4 and the necessary reinforcement was detailed. The reinforcement was scaled down to the correct dimensions and spacing for the test unit. The new values are given in Table 4.5. The values of $A_s$ for the interior girder and between girders are detailed below, as they needed to be adjusted from the exact scaled value.

$$\left(\frac{A_s}{s}\right)_{proto,scaled} = \frac{A_v}{4} * \frac{2}{s} = \frac{.79in^2}{4} x \frac{2}{9in} = 0.0439 \frac{in^2}{in}$$

$$\left(\frac{A_s}{s}\right)_{test\ unit} = \frac{.22in^2}{4.5in} = 0.049 \frac{in^2}{in}$$

The difference in the ratio was minimal and therefore the above reinforcement was retained. For the $A'_s$ at the same locations, the ratios are given below.

$$(A'_s)_{proto,scaled} = \frac{A_v}{4} = \frac{0.31in^2}{4} = 0.0775in^2$$

$$(A'_s)_{test\ unit} = 50.27mm^2\ x\ \left(\frac{1in^2}{645.16mm^2}\right) = 0.0779\ in^2$$

For the $A'_s$ values, the spacing was not included, because the same number of bars were located underneath the girders and the girder dimension was halved. Therefore, the reinforcement spacing was also halved.

Table 4.5.Additional Ledge Reinforcement in the Inverted-Tee bent cap

| | | | $A_s$ | $A_h$ | $A'_s$ | $A_v$ |
|---|---|---|---|---|---|---|
| Interior Girders | Prototype | Size | #8 | 4- #6 bars | 3-#5 bars | 0 |
| | | Spacing | 9 in. | under girder | per ledge | 0 |
| | Test Unit | Size | #4 | 4- #3 bars | 3-D8 bars | 0 |
| | | Spacing | 4.5 in. | under girder | per ledge | 0 |
| Exterior Girders | Prototype | Size | 5-#8 bars | 4-#6 bars | 5- #6 bars | 4- #6 bars |
| | | Spacing | under each girder | under each girder | per ledge | at girder |
| | Test Unit | Size | 5-#4 bars | 4- #3 bars | 5- #3 bars | 4- #3 bars |
| | | Spacing | under each girder | under each girder | per ledge | at girder |
| Between Girders | Prototype | Size | #8 | 6- #6 bars | 3-#5 bars | 0 |
| | | Spacing | 9 in. | between girders | per ledge | 0 |
| | Test Unit | Size | #4 | 6- #3 bars | 3-D8 bars | 0 |
| | | Spacing | 4.5 in. | between girders | per ledge | 0 |

The final step for the ledge design was to ensure that the development length of the #4 ledge bars will be adequate in the test unit.

$$l_d = \frac{38(0.5\ in.)}{\sqrt{3.6(ksi)}} = 10.01\ in.*(0.7)=7 \text{ inches}$$

Since the bar was embedded by 8 inches, and the above calculation only required 7 inches of development length, the design of the #4 bars was adequate, which completes the scaling of the cap beam.

## 4.5 Dapped End Beam Reinforcement

The dapped end required special reinforcement, which was designed using a strut-and-tie model presented in Section 3.5. For the test unit, the #7 bars could not be directly scaled due to there not being a type of rebar one-quarter of the size. Therefore, the ratio of the area of reinforcement provided from the prototype-to-test unit is detailed below. The spacing was not considered because the steel was located within the girder width, which had been scaled down properly.

$$(A_{de})_{proto,scaled} = \frac{A_v}{4} = \frac{4*0.60in^2}{4} = 0.60in^2$$

$$(A_{de})_{test\ unit} = 3 * 0.22in^2 = 0.66in^2$$

The difference in the steel ratios was 10%. However, the dapped ends in both structures were designed in such a manner that a failure mechanism would not develop and the actual demand in the test unit is to be monitored during test. Therefore, the overdesign was considered acceptable. That was the extent of the scaling for the dapped end region. The results are presented in Table 4.6.

Table 4.6. Dapped End Reinforcement

| | | Prototype Structure | Test Unit |
|---|---|---|---|
| Dapped End Reinforcement | Quantity | 4 | 3 |
| | Size | #7 | #4 |

## 4.6 Column Design

In this section, both the reinforcement and dimensions of the column are scaled appropriately. The values for the dimensions are given below in Table 4.7.

Table 4.7. Column Dimensions

| | Prototype Structure | Test Unit |
|---|---|---|
| Height | 20 ft. 8 in. | 10 ft. 4 in. |
| Diameter | 5 ft. 6 in. | 2 ft. 9 in. |

In Table 4.8 the column reinforcement is presented. The scaling of the longitudinal reinforcement in the column is detailed below.

$$(\rho_l)_{proto,scaled} = \frac{A_s}{A_c} = \frac{33*1.56in^2}{\pi(33in)^2} = 0.0150$$

$$(\rho_l)_{test\ unit} = \frac{30*0.44in^2}{\pi(16.5in)^2} = 0.0154$$

Table 4.8. Comparison of Column Reinforcement Details

| | | Prototype Structure | Test Unit |
|---|---|---|---|
| Flexural | Quantity | 33-#11 bars | 30-#6 bars |
| | Spacing | 1.36 in. | 1.03 in. |
| Shear | Size | #6 | #3 |
| | Spacing | 4 in. | 2 in. |

## 4.7 Top Deck Reinforcement

As designed in Section 3.7, additional reinforcement was required over the cap beam to resist the negative moment that would be induced over the section. In consideration with the prototype details, the reinforcement is placed over the cap beam and girders only. First, the dimensions of the slab in the Test Unit are presented in Table 4.9. Next, the reinforcement quantities, lengths, and offsets are presented in Table 4.10. Similar to the prototype structure, the reinforcement was staggered over the cap beam to allow the bars to terminate at the point of 50% negative moment.

Table 4.9. Comparison of Deck Dimensions

| | Prototype Structure | Test Unit |
|---|---|---|
| Height | 8 in. | 4 in. |
| Width | 39 ft. | 19 ft 6 in. |
| Haunch | 2 in. | 1 in. |

Table 4.10. Comparison of Top Deck reinforcement

| | Prototype Structure | Test Unit |
|---|---|---|
| quantity | 10- #10 bars | 10- #5 bars |
| spacing | per girder | per girder |
| bar length | 54 ft. | 27 ft. |
| offset | 18 ft. | 9 ft. |

## 4.8 Column-Bent Cap Joint

The joint detailing required no additional reinforcement to be scaled. As stated in Section 3.8, the reinforcement provided from the previous design considerations was considered adequate to sufficiently transfer forces through the joint of the test unit, which completes the design of the test unit.

## 4.9 Test Unit Hold-Down Force

In order to accurately subject the test unit to the same type of loading that was assumed for the prototype structure, it was necessary to apply a vertical hold-down force on each side of the cap. The discrepancy between the forces experienced in the test unit and prototype was shear due to the fact that the test unit consisted of a half span on each side of the cap and that it was modeled at 50% scale. Additionally, loads that were applied to the prototype, such as the future wearing surface and barriers, were not applied to the test unit. The forces were compared at two different stages, the initial stage where the spans act as simply supported spans and the final stage where the deck is hardened and the spans act as continuous spans. Therefore, without compensating for these dissimilarities, the gravity effects and resulting forces as well as the behavior experienced by the test unit would not adequately compare to the prototype structure, as demonstrated in Figure 4.2 and Figure 4.3. The moment and shear diagrams presented in these figures are for the center girder with the locations of the girder bearing points indicated by the dashed lines.

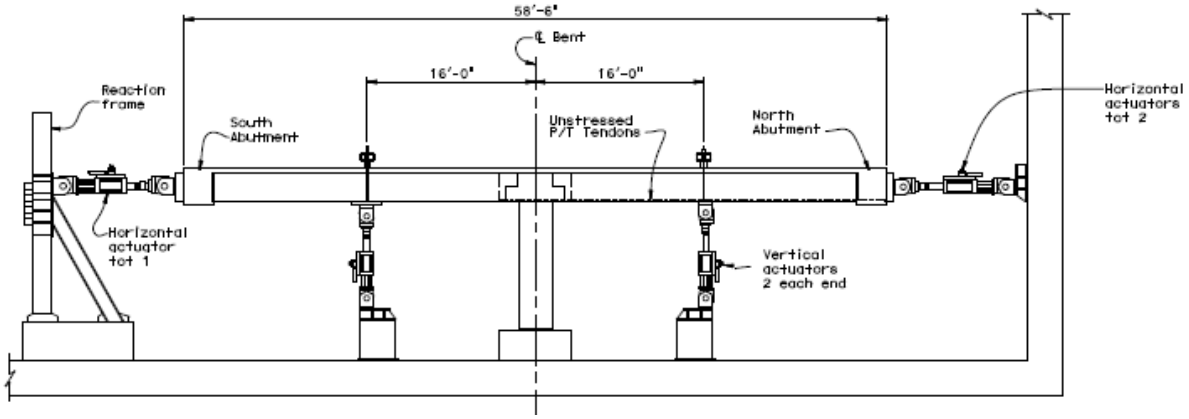


Figure 4.1. Setup used for lateral load testing of the test unit

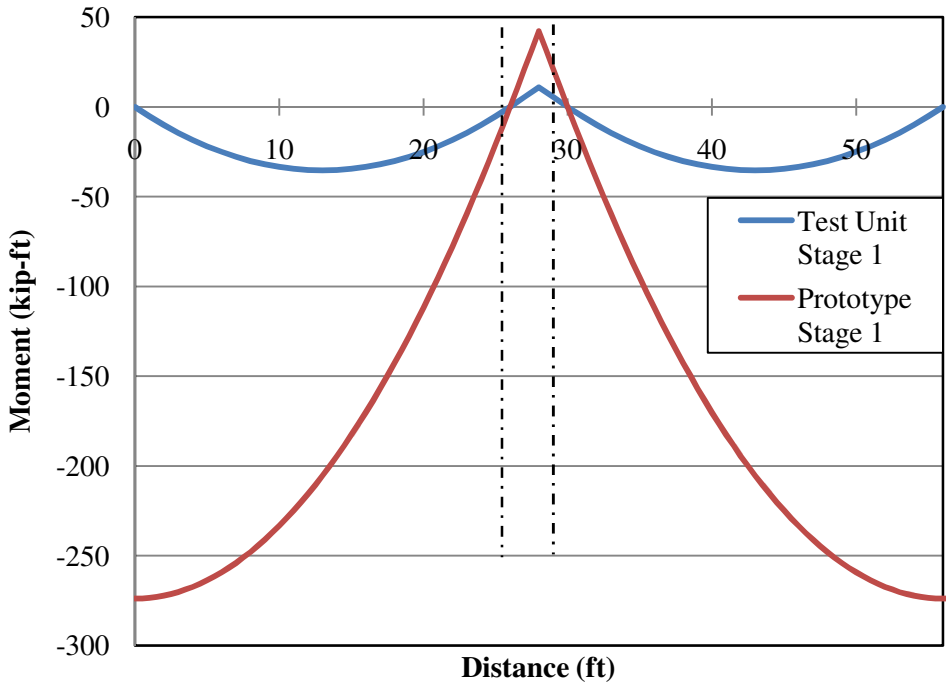


Figure 4.2. Comparison of bending moments for stage 1 loading at the test unit scale

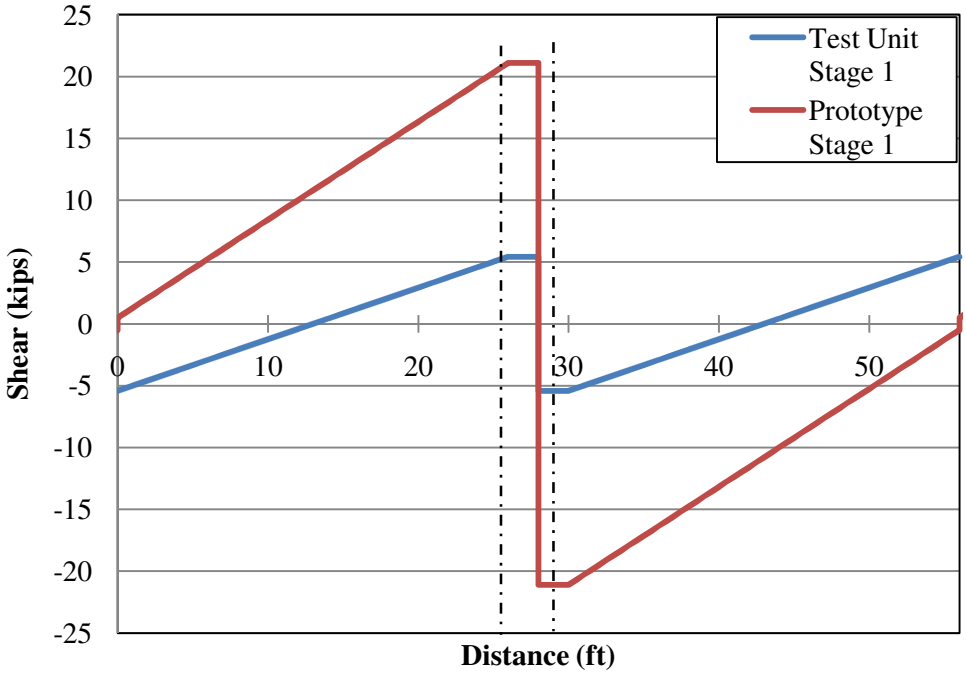


Figure 4.3. Comparison of shear for stage 1 loading at the test unit scale

To ensure the shear forces were comparable between the test unit and prototype, vertical actuators were included in the test setup at a distance of 16 feet from the center of the column along the span, as seen in Figure 4.1. This distance was selected based on the anchor-hole layout on the floor of the test laboratory at UCSD. A structural analysis (Snyder, 2010) of the superstructure indicated that, in order to provide shear and moment agreement within the connection, a hold-down force of 34.6 kips per girder (173 kips total on each span) needed to be applied during after erecting the girders but before placing the deck concrete. At this stage, which is referred to as Stage 1, the girders were simply supported. The moment and shear profiles for Stage 1 after applying the hold-down forces are presented in Figure 4.4 and Figure 4.5 respectively.

Once the superstructure was made continuous through hardening of the deck, an additional hold-down force of 12.37 kips per girder (61.9 kips total on each span) was applied in order to

provide a final agreement between the shear and moments experienced between the test unit and prototype structure. Figure 4.6 and Figure 4.7 below show the comparison of the moment and shear diagrams after the hold-down for this stage is applied, which is referred to as Stage 2.

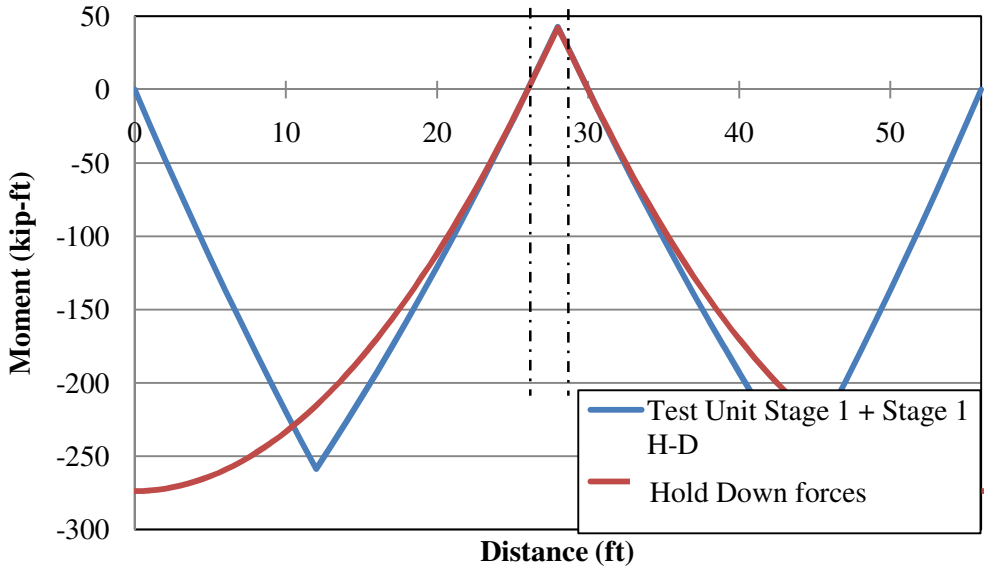


Figure 4.4. Comparison of bending moments for stage 1 loading and hold down force at the test unit scale

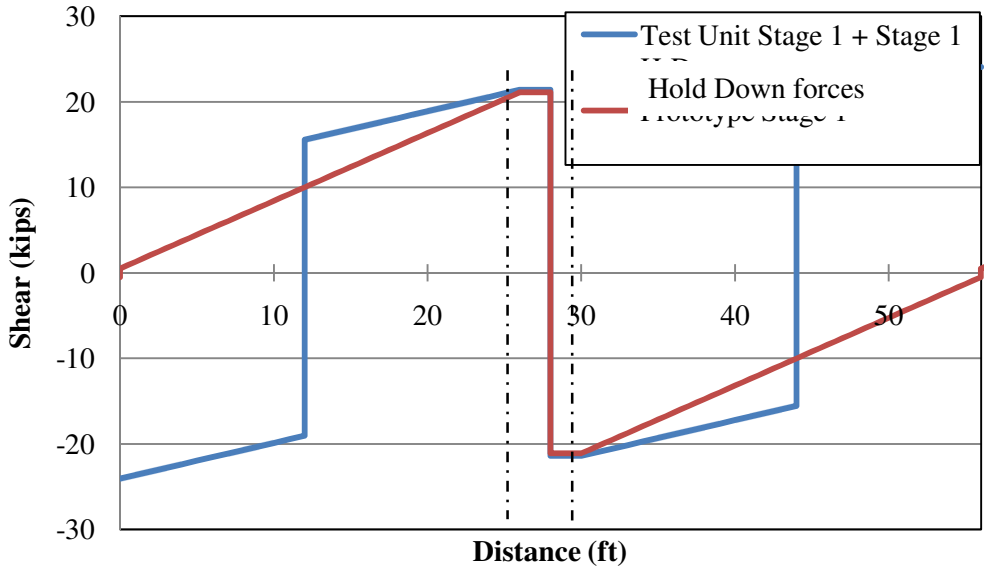


Figure 4.5. Comparison of shear for stage 1 loading and hold down force at the test unit scale

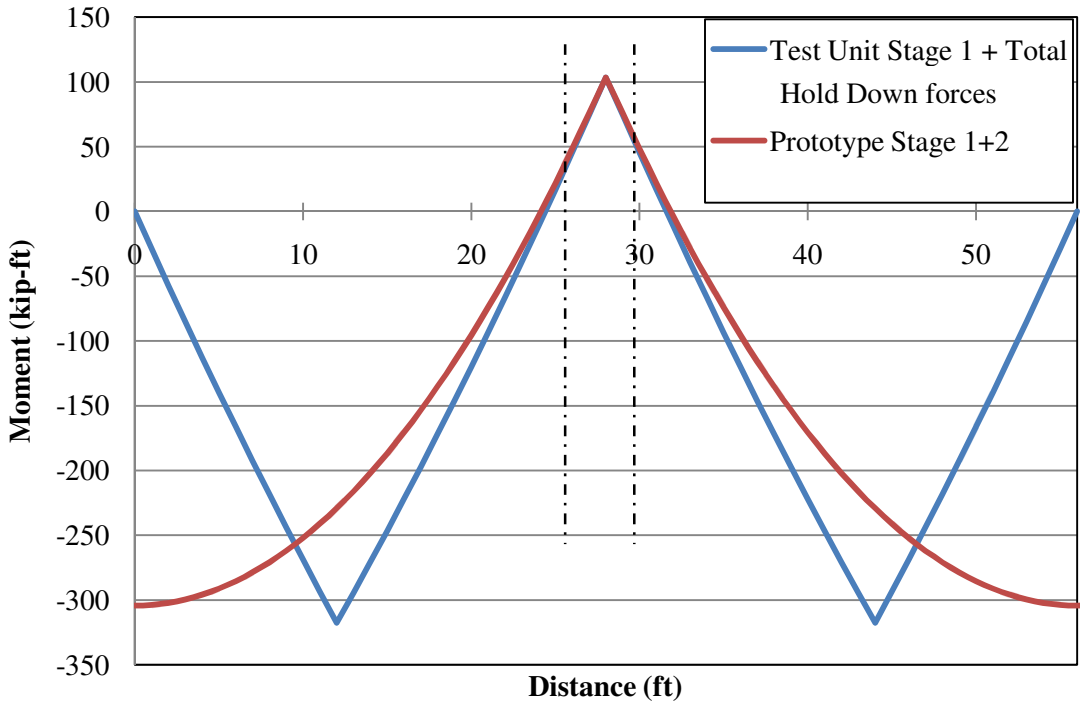


Figure 4.6. Comparison of bending moments after stage 2 loading and hold down force at the test unit scale

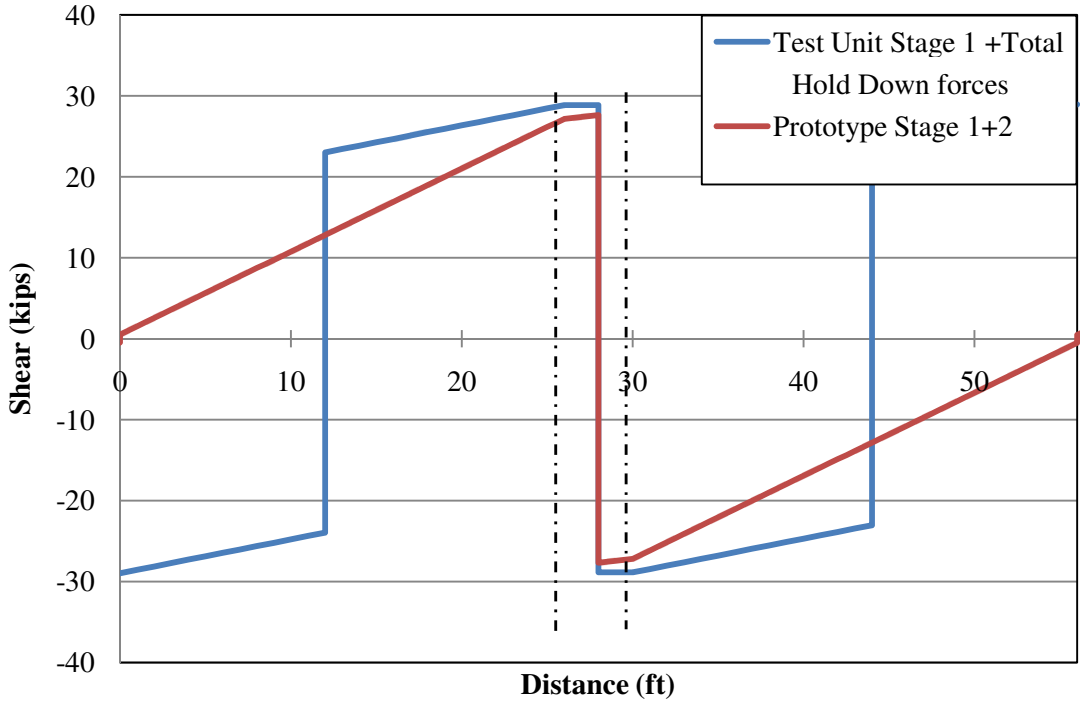

Figure 4.7. Comparison of shear after stage 2 loading and hold down force at the test unit scale

At each stage during construction and testing, the forces being compared differed in magnitude along parts of the span. However, the test unit, during each comparison, exhibited an equal or greater force at the girder to cap beam connection region than the prototype. Therefore, the results and conclusions drawn from the test unit could be applied to the prototype with a high degree of confidence. The final moment and shear diagrams, including the maximum seismic load, are presented below in Figure 4.8 and Figure 4.9.

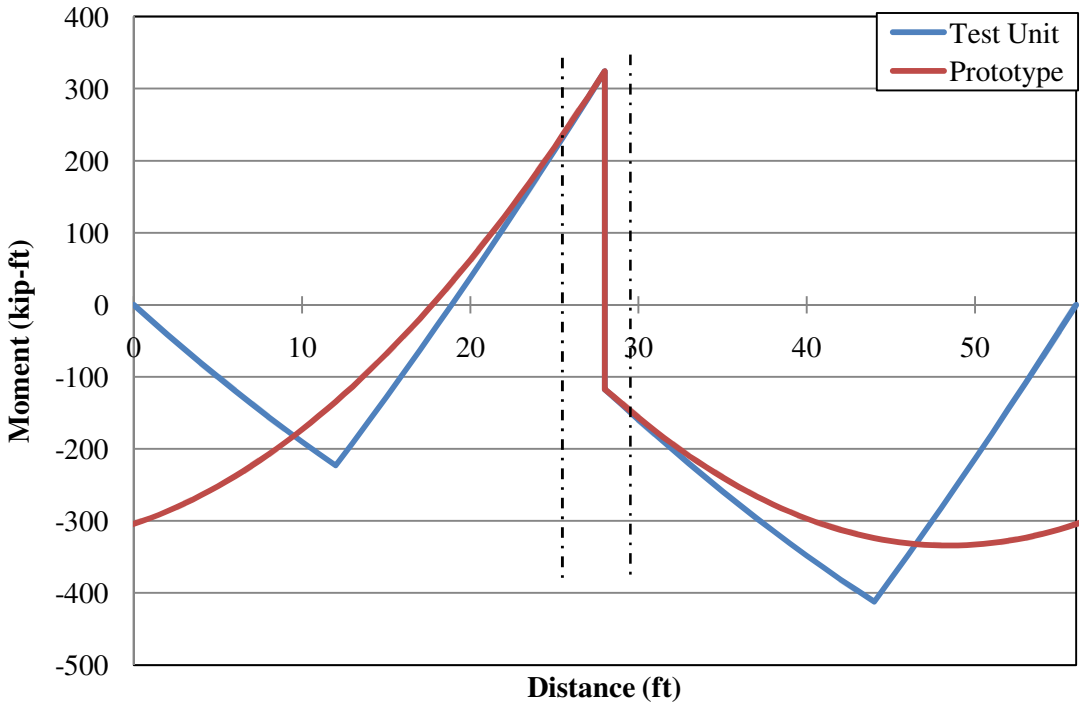


Figure 4.8. Comparison of combined dead load and seismic bending moment at the test unit scale

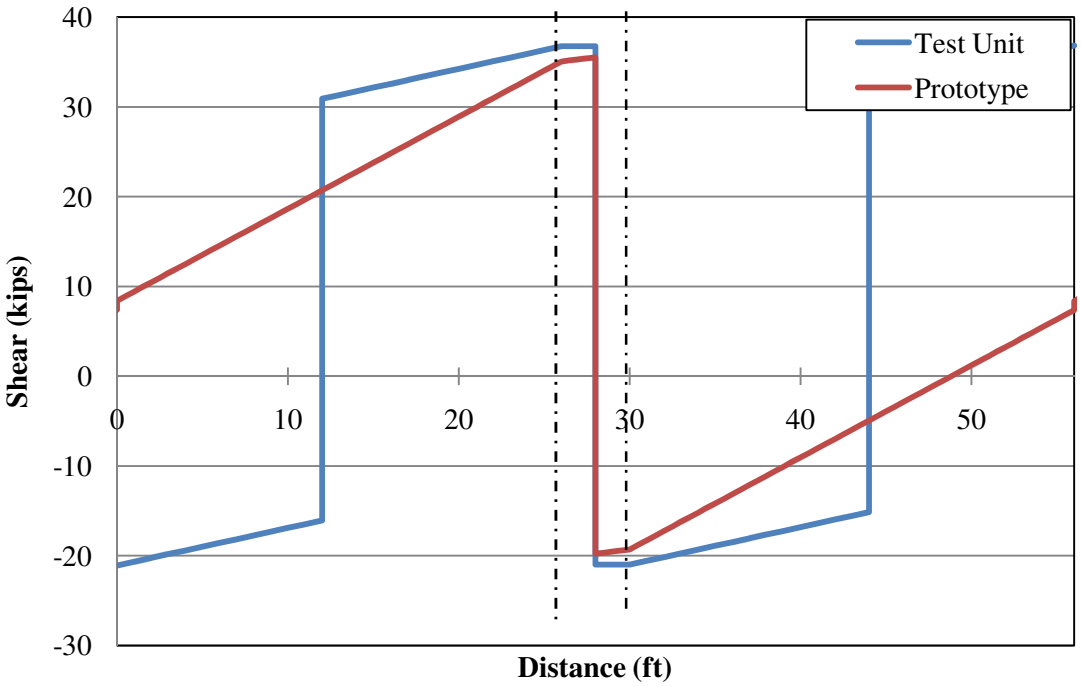


Figure 4.9. Comparison of combined dead load and seismic shear at the test unit scale

# Chapter 5. FINITE ELEMENT MODEL DEVELOPMENT

## 5.1 Introduction

This chapter describes the details of finite element model developed for the prototype structure and the test unit, which included the cap beam, diaphragms, girders, slab and reinforcing bars. ABAQUS v6.8 (Dassault Systemes Simulia Corporation, 2008), a commercial finite element package, was used for the analysis. Two element types were primarily used in the development of the model: C3D8R and T3D2. The C3D8R element is the continuum three dimensional 8-noded solid element, commonly known as the "brick" element. Each of these nodes has three degrees of freedom, allowing translation in the x-, y- and z-direction. The elements do not have rotational degrees of freedom; however, this limitation can be overcome. One approach is to use the incompatible mode of

the element which internally adds deformation modes that allow the element to overcome parasitic shear effects, creating a better bending behavior. Another alternative to overcome the bending problem is to discretize sufficiently over the thickness of the object to consider the effect of bending. For the model, the concept of discretizing sufficiently through the thickness of the object was used. The other element used extensively was the T3D2, which is a three dimension 2-node truss element. This element only resists forces in the axial direction, which is similar to the action of a reinforcing bar.

## 5.2 Material Model

The concrete material model was of great importance during the model development process. In ABAQUS, there are three different models that can be used for defining concrete material behavior: brittle cracking, smeared cracking and damaged plasticity. Each model has been developed for distinct purposes with many differences between them. The brittle cracking model assumes that the concrete compressive response remains linearly elastic while the tension is the cause of failure (Dassault Systemes Simulia Corporation, 2008), which is controlled by a specified tensile strength value that is user defined. The smeared cracking model was developed for use during loading in a monotonic manner with a low confining stress. This allows the concrete to experience either compressive crushing or tensile cracking. Large cracks are not tracked in the specimen modeled. However, once the stress exceeds the cracking strength, the material stiffness is reduced to account for the softening behavior. A drawback of this model is the mesh size; a fine mesh will lead to narrow crack bands (Hillerborg, Modeer, & Petersson). Also, after compressive crushing occurred in an element, the unloading stiffness is softened when compared to the original stiffness. This is not captured by the model as the post-cracking stiffness is assumed to be constant in the model regardless of the magnitude of inelastic strain. In comparison, the tensile stiffness is reduced after cracking, but as unloading occurs, the stiffness always allows for the tensile response to exhibit no residual

displacement. The stress-strain responses in compression and tension are provided in Figure 5.1 for the smeared cracking model.


a) Tensile response b) Compressive response

Figure 5.1. Stress-strain behavior of the smeared cracking model in ABAQUS

The third model is the damaged plasticity model and is the most complex of the three models. This model is suitable for modeling a concrete member subjected to either monotonic or cyclic loading, with low confining pressures. This material model is a compilation of many attempts to create an effective model to capture the true behavior of concrete (Lee & Fenves, 1998). Originally, concrete models were developed to capture the effects of crushing and cracking with one damage variable for all the damage states (Lubliner, Oliver, Oller, & Onate, 1989). This was ineffective as the responses in each damage state are significantly different. The damaged plasticity model incorporates two damage variables, one for compression and one for tension, to model the stiffness degradation during the inelastic action of concrete. With damage variables for each response, the concrete stiffness can accurately be modeled during inelastic action in each state, if calibrated properly. The damage variables also allow for the stiffness to continuously undergo degradation depending on the extent of inelastic action that occurs in the member. The unconfined concrete properties are defined by providing the stresses at various elastic and inelastic strains. For the elastic portion of the concrete curve, an elastic option is defined with a Young's Modulus and a Poisson's

Ratio. Once the concrete strain exceeds the elastic strain limit, the damage variables are activated and any response at higher stress incorporates the effects. The general response of the concrete is presented in Figure 5.2. The model also has the ability to incorporate the confining effects of reinforcing steel; validation of this capacity will be presented in Chapter 6. For modeling of the inverted-tee bridge, the damaged plastic model was chosen. Additional inputs such as dilation angle, eccentricity, uniaxial to biaxial stress ratio, stress variant and viscosity parameter are required to completely define the damage plasticity model of concrete. The suggested default values from ABAQUS were used and listed in Table C.1 in 0. The material properties used in the model are also given in Table C.1 in 0.

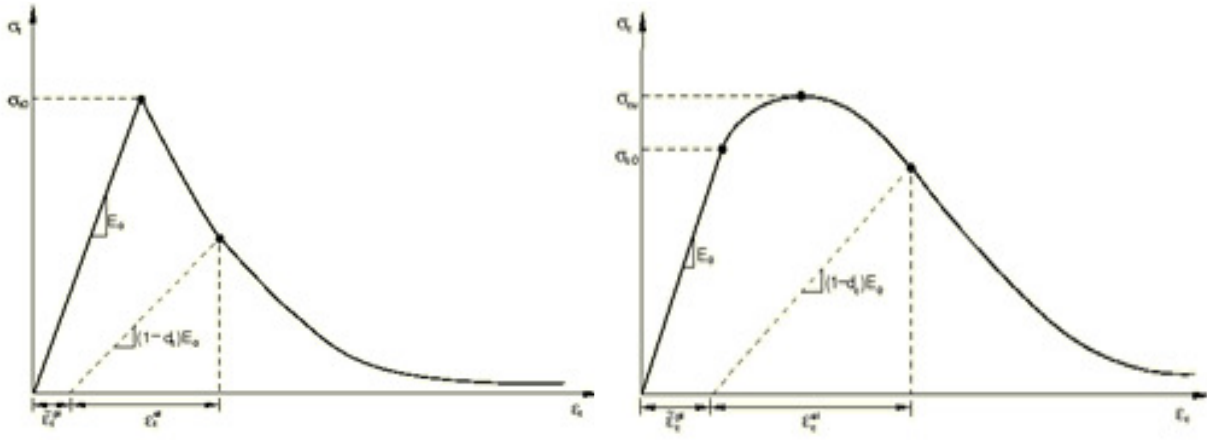

a) Tensile response b) Compressive response

Figure 5.2. Concrete stress-strain behavior according to the Damaged Plasticity Model in ABAQUS

For the steel elements, a general elastic-plastic model was used. Both the prestressing steel and mild reinforcing steel were modeled accordingly. Similar to concrete, the elastic portion of the response is defined by providing a Young's Modulus and Poisson's Ratio. However, for the post-yielding response, a separate plastic model was used. For the analysis, five points were defined to capture the strain hardening effect of the mild reinforcement steel. Once the material experiences a plastic strain, the original stiffness is used for unloading, causing a residual strain at zero stress. For

the prestressing, three points were defined to replicate the actual behavior including yielding and fracture. The values used for the concrete model are given in Table C.2 in 0.

## 5.3 Contact and Constraint Modeling

Representing the contact between the different components in the model was an important aspect to accurately capture response of the moment-rotation characteristics of the cap-beam-and-girder interface model. With the bridge under consideration having precast girders set in place, followed by embedment of reinforcing bars, multiple contact assignments and embedding commands were needed. Contact assignments were applied at the cap-beam-to-diaphragm interfaces, diaphragm-to-girder interfaces, and cap-beam-to-slab interfaces. Additional interactions were used for embedding the reinforcement. For the contact assignments, the surface-to-surface option was chosen with the contact properties including a friction tangential behavior and a "hard" contact normal behavior. The concrete-to-concrete friction coefficient was taken as 0.6 as specified by the ACI 318-05 code (ACI Committee 318, 2005) specifies for concrete poured against existing components where the edges would be smooth. The value for the friction coefficient was chosen since the pieces were not expected to slide much since the pieces were held into place with reinforcing bars but to actually open and close gaps. The "hard" contact normal behavior does not resist any pressure when a gap is opened but as soon as the gap is closed the compressive stress is transmitted from one surface to the other, which is illustrated in Figure 5.3. The contact between the cap beam and slab was modeled with a tie command. By using the tie command, the nodes on the edge of the deck were tied to the nodes on the edge of the cap beam intersecting the deck. In doing this, the nodes on the deck were eliminated and the nodes of the cap beam were used in replacement. Therefore, the deflections at each point on the overlapping faces of the cap beam and deck were the same. This approach was used because the reinforcement between the deck and slab were considered to be effective in not allowing the deck to slip with respect to the reinforcing bars and subsequently

separate, as that was not within the scope of the project. For the all the reinforcement modeled in the analysis the embedding command was used in ABAQUS to model the interaction. The embedding ties the nodes of the embedded element to the nodes of the master element that it is embedded within. By using this method, a perfect bond is assumed between the reinforcement and surrounding concrete.

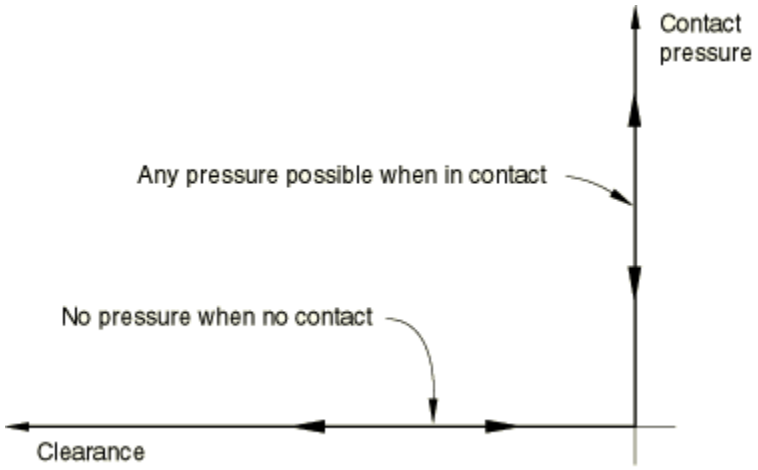


Figure 5.3. "Hard" contact behavior assumed in ABAQUS

In the new connection modeling, the unstressed strands were initially coupled to the girder, diaphragm and deck beam using the coupling command. This command is intended to use the coupled displacements of the master node, the girder, as the displacement for the slave node, the prestressing strand. At the girder ends, the strand was pinned to the girder end and was not able displace relative to the girder. However, along the girder and at the connection interface the longitudinal direction degree-of-freedom was released to allow the strand to slip since it was initially considered to be unbonded. Another coupling command was used at the cap face where a rotational boundary condition was applied. The coupling command was needed due to the lack of rotational degrees-of-freedom within the elements of the cap beam. A reference point was used as the master

node and then the cap cross-section and the portion of the deck directly above the stem of the cap were all constrained as slave nodes, seen in Figure 5.4.

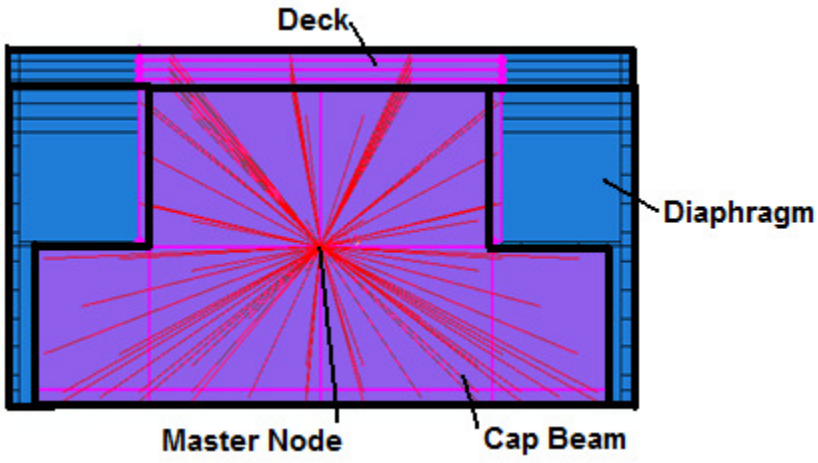


Figure 5.4. Cap Beam pivot constraint achieved through the use of the coupling command

## 5.4 Boundary Conditions

The proper boundary conditions were of significant importance to ensure that the modeling was completed as accurately as possible to the true behavior. In Chapter 7, a comparison of different boundary condition combinations will be discussed. In this section, a general discussion of the boundary condition will be presented.

For the analysis, the cap beam was pinned through the center of area of the cap beam and allowed to pivot. The girder ends were restrained with a z-symmetry boundary condition. This boundary condition allows for displacement in the transverse and longitudinal direction of the bridge but restrained movement of the girder ends in the vertical direction. The boundary condition was applied at the same height as the boundary condition on the cap beam. Also, only the girder ends were restrained, not the length of the end diaphragm.

Additionally, for the single girder model, the edges of the slab in the longitudinal direction were restrained with a z-axis symmetry condition, allowing the edges to deflect vertically and longitudinally but restraining the movement in the transverse direction. This condition was chosen since the slab has been sliced for a single-girder model. For a full bridge, the slab will not be able to freely move in the transverse direction for the middle and intermediate girders and this constraint will properly model this aspect.

Also, for the multiple girder models, the middle girder had to be restrained along the longitudinal cross-section for symmetry purposes. To do this, a z-axis symmetry condition was applied. The behavior of the boundary condition has been discussed above.

Additional boundary conditions were analyzed, but were not common to the model for every analysis and the effects will be discussed in the following chapter.

## 5.5 Modeling of Components

The modeling of different components will be discussed below and additional details will be included. The dimensions and material descriptions are provided on the structure details in 0.

### 5.5.1 Cap Beam

The cap beam was modeled according to the structural drawings. On the cap beam, the bearing pads were included monolithically to the ledges. However, the area of the bearing pads was modeled with a material property corresponding to the bearing materials. The rest of the cap beam was modeled with the damage plasticity model with a concrete strength of 4.5 ksi, which is the expected material strength of the concrete in the field. Figure 5.5 shows the cap beam model that was created using solid elements were used for the modeling of the cap beam. The same element type was used for the bearing pads.

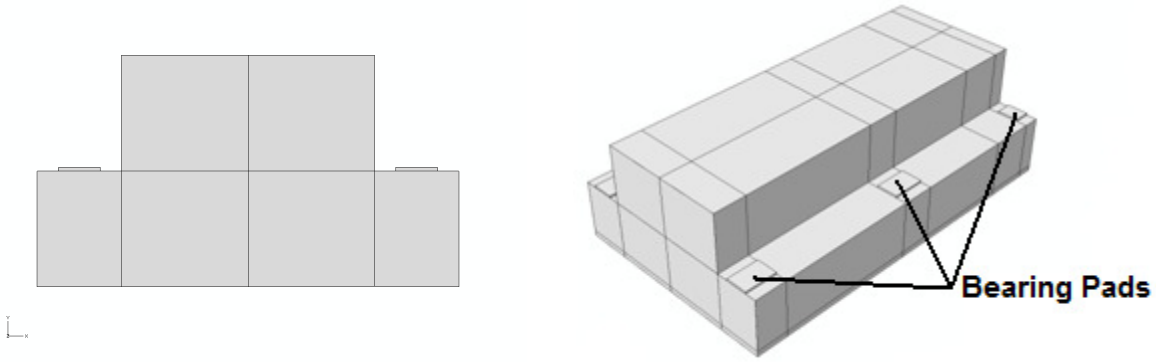


a) End view of Cap Beam b) Angled view of Cap Beam

Figure 5.5.Views of modeled Cap Beam

### 5.5.2 Cap Beam Diaphragm

The diaphragm is cast around the cap beam after the girders are placed, which was modeled as one piece for each side of the cap beam. A solid L-shaped piece was made using sold elements and the areas where the bearing pads and girders would be located had to be cut out of the solid piece, as seen in Figure 5.6.

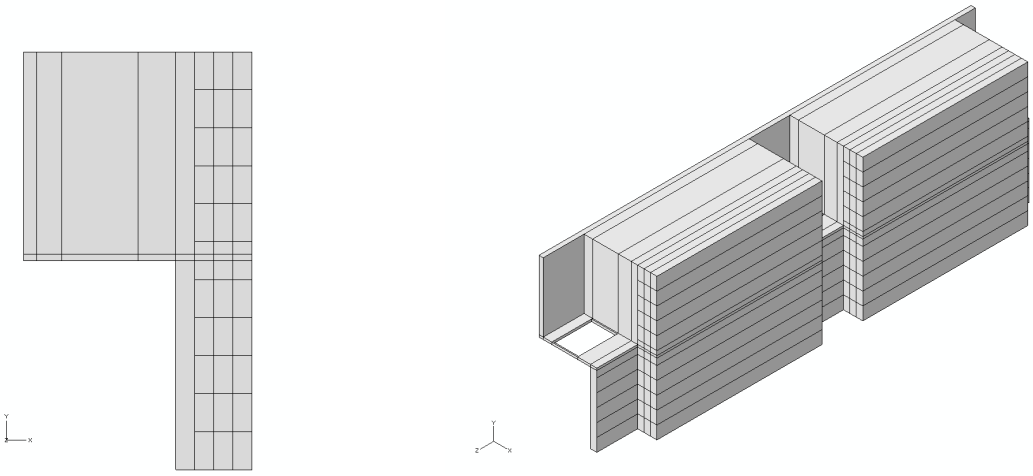

a) End view of Diaphragm b) Angled view of Diaphragm

Figure 5.6. Views of modeled Diaphragm

### 5.5.3 Girders and Slab

The precast girders and the in-situ slab were modeled monolithically since the interaction between the two members was not anticipated due to the exposed vertical girder reinforcement is embedded into the deck. A solid, rectangular block was modeled, to be formed into the girders and deck, and extended the length corresponding to the mid-span to mid-span distance. Next the outlines of the girder and slab were drawn and the remaining volume was removed from the block. Then the cap beam cross section was removed from the girders. Finally, the volume was partitioned to allow section to be meshed using solid elements. The model of the girder and slab can be seen in Figure 5.7. Similar to the cap beam and bearing pads, the slab and the girders were modeled with their respective material properties. Concrete in both of members was modeled using the damaged plasticity model unconfined concrete strength of 7 ksi for girders and 4.5 ksi for the slab.

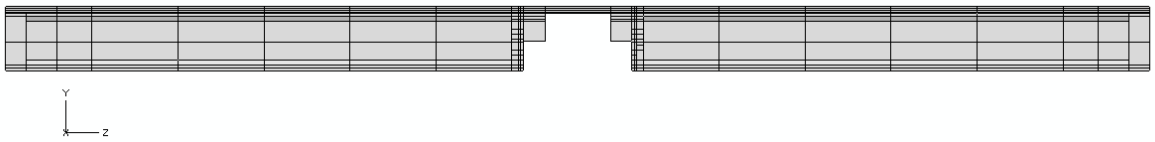

a) Side view of girders and deck

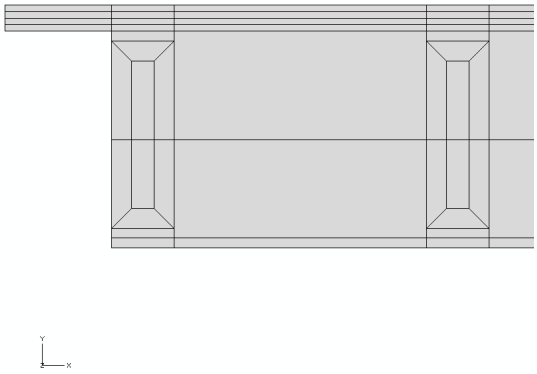

b) End view of girders and deck

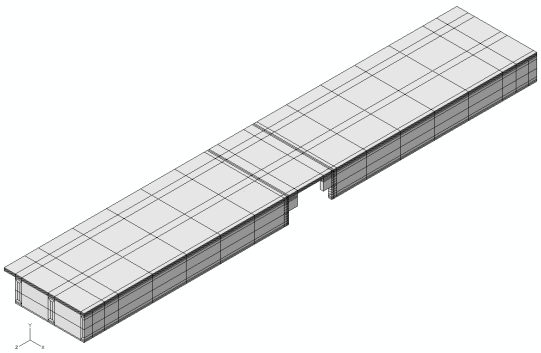

c) Angled view of girders and deck

Figure 5.7. Views of the modeled girders and slab of model

### 5.5.4 Reinforcing Bars and Prestressing Strands

In the test unit and prototype structure there are multiple different sizes and lengths of reinforcing bars, but the modeling technique for each is the same. For the reinforcing bars, a wire part was used to draw the length of the bar. Then the mesh was applied and the elements were manually switched from beam elements to truss elements. To accurately model the bar sizes, the truss section was used and the bar area size was defined along with by choosing the appropriate material property. The section was then applied to the part and the reinforcing bar was then modeled. The differences in the bars were the length of the wire element and the area defined in the section module. For the prestressing strands, the truss elements were also used when the strands were embedded. The same method, as for the reinforcing bars, was followed to define the cross-section being used. The unstressed strands used in the connection were also modeled similarly; the only difference was that the wire was partitioned with breaks in the wire at each point where a coupling was being defined to allow for the prestressing strand to deform similarly to the girder.

The reinforcing bars placed transversely through the girders and cast into the diaphragms were modeled using spring elements in ABAQUS. The springs were used due to time constraints when performing analysis with three-dimensional solid elements representing the reinforcing bars caused excessive analysis times. Twenty springs were defined on each face of the girders to replace the three reinforcing bars connecting the girders to diaphragms For the capacity of the springs, the shear capacity of the reinforcing bars was calculated and considered to not slip or allow any displacement until the capacity was reached. Once the capacity was reached, the capacity from the reinforcing bars was kept constant because the model would not converge if the value was lessened in the ABAQUS.

# Chapter 6. ANALYSIS VALIDATION AND RESULTS

## 6.1 Introduction

In this chapter the analysis undertaken to capture the response of the existing connection and develop the new connection will be discussed. The current connection detail was modeled and analyzed to understand the behavior of the current cap-beam-to-girder connection region. To capture the response a single girder model at the prototype scale was developed. Once that was completed then a multiple girder model at the prototype scale was developed and the behavior in the connection region was studied. This process was also completed at the test unit scale which was then compared to a grillage model analysis concurrently being completed (Snyder, 2010). Once the current behavior was captured then a new connection detail was developed and placed in the same models to allow for the difference in performance to be captured. The following sections will provide greater detail in this process.

## 6.2 Material Model Validation

To validate the concrete model chosen in ABAQUS, a series of concrete cylinders were tested in the Iowa State Structures Laboratory using a uniaxial MTS machine. To obtain strain values, the cylinders were cast with steel rods placed in them at a spacing of approximately 1.5 inches on which DCDT gauges were attached. The stress was obtained by recording the applied force and dividing by the cross-sectional area of the cylinder. The cylinders were three-inch by six-inch with 4 ksi concrete with varying confinement. Initially, two unconfined cylinders were tested to develop the actual strength of the concrete. Next, cylinders with confinement ratios of either 0.7% or 1.2% were tested. The confinement ratios of 0.7% and 1.2% were chosen since these values correspond to a typical low confinement and high confinement sample, respectively.

For validation of the concrete model, a cylinder of the same dimensions was modeled in ABAQUS and compressed in the same manner; one face of the cylinder was restrained from displacing axially while the other face was displaced. The stress and strain of an element, the same height as the gauge length of the DCDT used in the lab test, in the center of the cylinder was monitored and recorded. To model the confinement, the resulting pressure from the confining steel was applied to the side surface of the cylinders along the perimeter. The resulting pressure was determined by using Eq. 6.1, where $K_e$ is the an effective factor depending on type of confinement reinforcement, $A_{sp}$ is the area of confinement reinforcement, $f_y$ is the expected yield strength of the confinement steel, D′ is the diameter of the core concrete and s is the spacing of the confinement reinforcement.

$$f_l = K_e * \frac{4A_{sp}f_y}{D's} \qquad \text{Eq 6.1}$$

Initially, the unconfined properties obtained from the testing were defined in ABAQUS and a confining pressure was applied to the sides of the cylinder. Once the analysis was completed, it was noted that the response of the confined cylinders in ABAQUS did not match well with the test results. The results from ABAQUS over predicted the response with higher strengths. To overcome the deficiency, the unconfined curve was then altered by lowering the stress values, mainly after yielding, to obtain better results between the confined specimens. Presented in Figure 6.1 and Figure 6.2 the comparison between the ABAQUS results and test data for the two different confinement ratios tested under monotonic loading conditions. With the results matching adequately, the unconfined properties were used in the models that were developed for the prototype structure and test unit. For concrete with different $f'_c$ then tested, the values of the material properties will be scaled based on the ratio of the ultimate compressive stress.

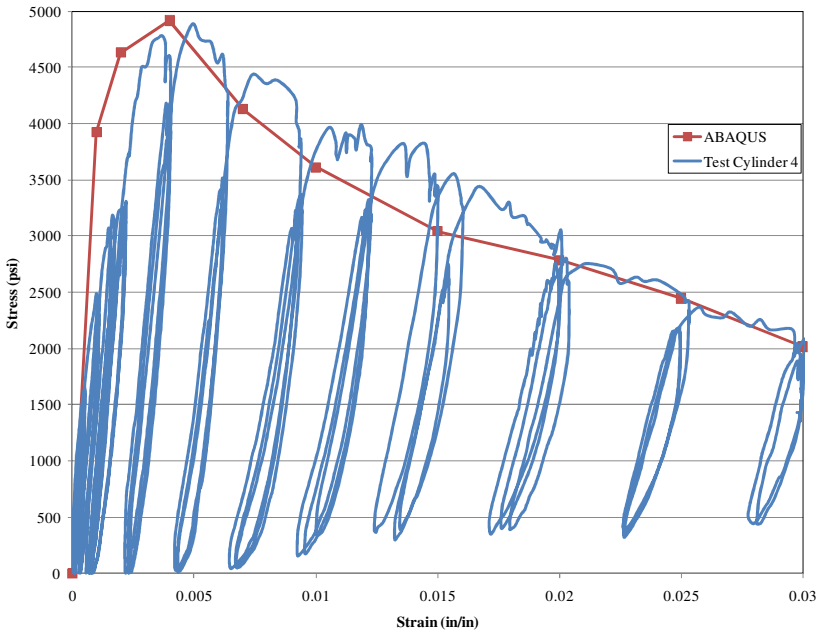


Figure 6.1. Comparison of results for a high confinement concrete cylinder

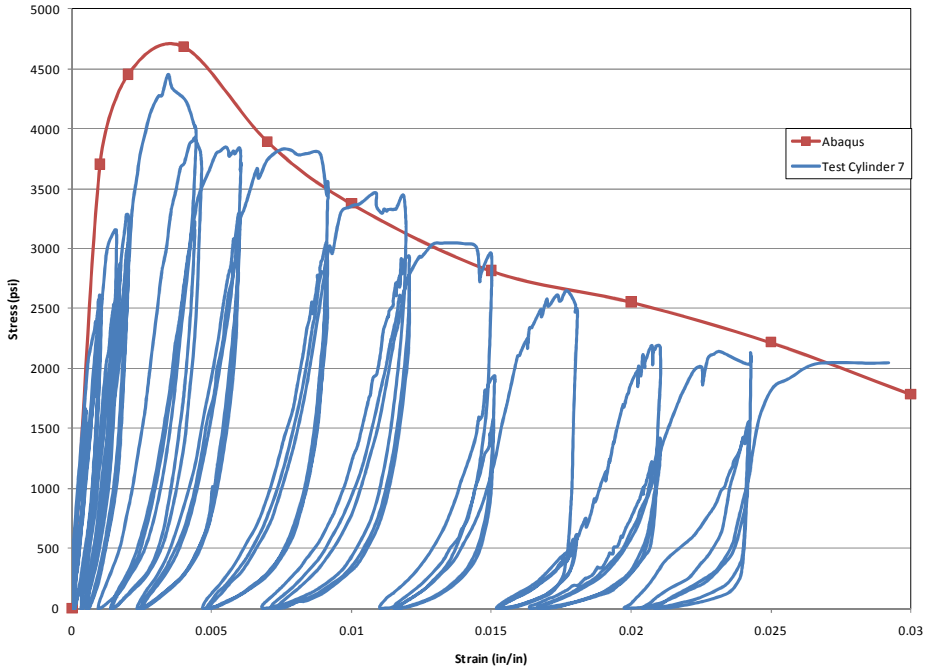


Figure 6.2. Comparison of results for a low confinement concrete cylinder

## 6.3 Prototype Structure

### 6.3.1 Single Girder Model

The prototype structure was first analyzed to obtain information regarding the performance of the connection used in practice today and the impact on the bridge structure. This connection is currently used in design with little verification of its true performance under seismic loading. One main objective of the prototype analysis was to investigate whether the current connection has the moment transfer capacity to create a plastic hinge at the top of the column. Initially, during the prototype analysis, the girder lengths on each side of the cap in the analysis model were two different lengths with the forces applied by a rotation of the cap beam. The girder lengths were taken as the distance from the cap beam to the zero moment point on the moment profile obtained from the grillage analysis. The lengths were taken in order to replicate the moment and shear profile as closely as possible. However, convergence problems relating to the concrete models experiencing instability after concrete cracking led to simplifying the model and to overcome the problems in the smaller test unit model discussed later in the chapter.

The cap rotation was removed and the girder end was displaced vertically. In this loading condition, only the shorter of the two sides was analyzed by applying displacements in both the positive and negative direction in multiple analysis runs, shown below in Figure 6.3 and Figure 6.4. The slab was fixed at the location where the slab extends over the cap beam. The force required to displace the girder end was recorded. The results for the prototype analysis were given by plotting the moment as a function of girder end displacement. The moment was found by multiplying the force required to displace the girder ends by the distance from the connection to the girder ends.

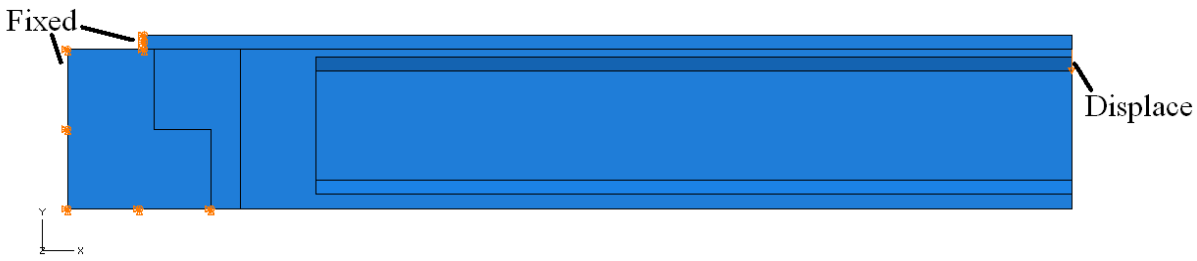


Figure 6.3. Singe girder prototype boundary conditions

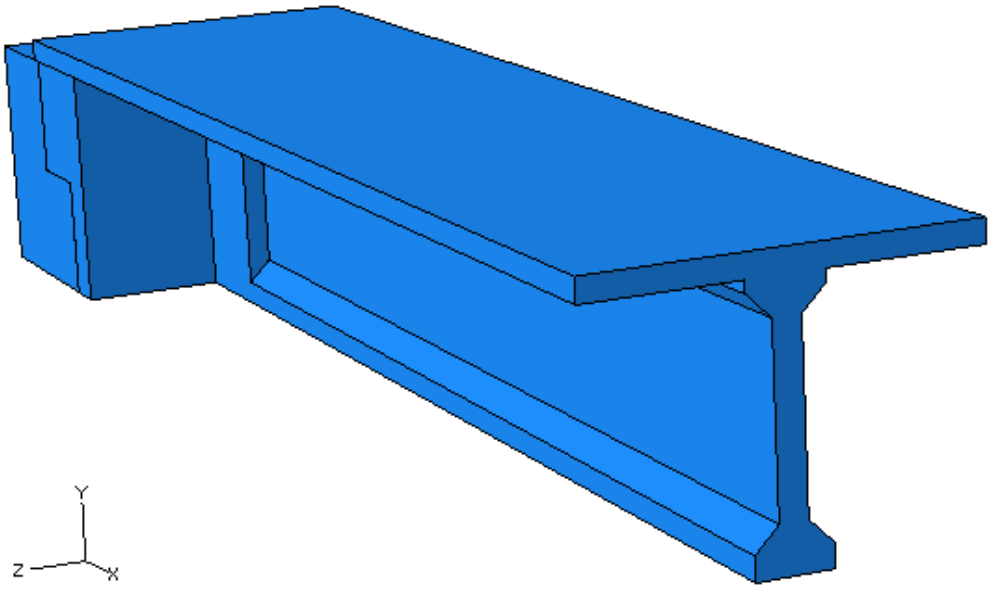


Figure 6.4. Single girder prototype model

As discussed in section 5.5.4 the girder-to-diaphragm reinforcing bars were modeled with 20 springs on each face of the girder. The capacity of the springs was equal to the shear capacity of the reinforcing bars.

### 6.3.2 Single Girder Analysis Results

The results from the single girder analysis are presented in Figure 6.5 and Figure 6.6 to observe the adequacy of the connection region for developing a plastic hinge in the column. The

negative moment connection, shown in Figure 6.5, will exceed the capacity required for the plastic hinge to form, denoted by the line at 3150 kips responding to the amount of overstrength moment of the column, $M_{co}$,to be resisted by the negative moment connection. The overstrength values were obtained from the combined dead load and seismic moment profile resulting from the grillage model (Snyder, 2010). At the point where the required capacity is exceeded, the girder-to-diaphragm connection remained elastic and thus it would be sufficient to resist future loads.

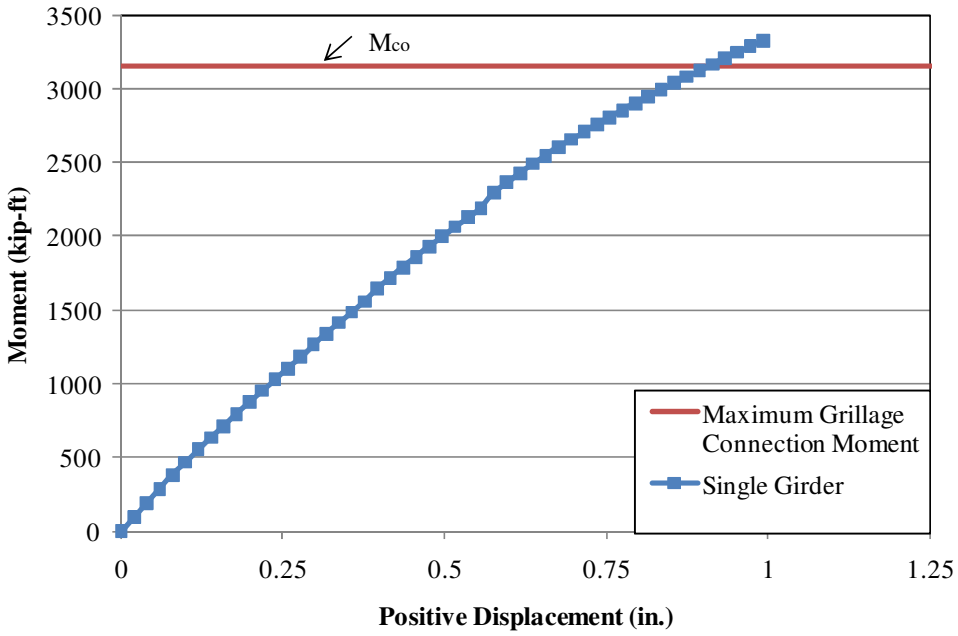


Figure 6.5. The negative moment vs. the girder end displacement response obtained for the single girder analysis at the prototype scale

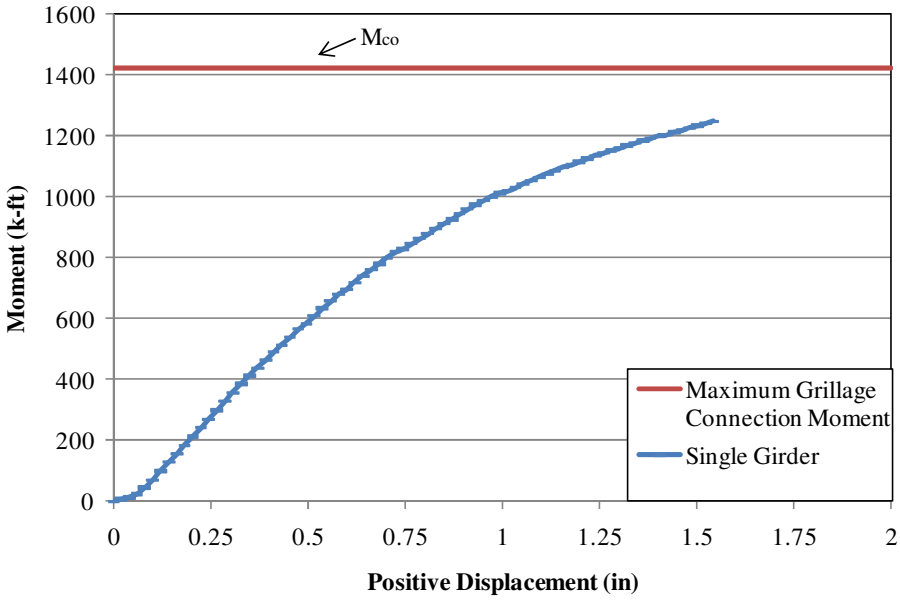


Figure 6.6. The positive moment vs. the girder end displacement response obtained for the single girder analysis at the prototype scale

However, the response of the positive moment connection was different. Through the point of nonconvergence, the connection springs had already yielded and the moment capacity of the cap-beam-to-girder connection had not yet exceeded the demand established from the column overstrength capacity of 1425 kip-ft, which was obtained in the same manner as the negative moment capacity requirement. Note that yielding of the reinforcing springs in combination with cracking in the slab resulted in progressive change in stiffness as seen in Figure 6.6.

A concern that was raised from the analysis technique was the effect of redistribution of the moment experienced in the connections was not able to be captured by the simplified single girder model. To resolve that, the test unit modeling was performed with the redistribution effects as an initial objective to be completed.

### 6.3.3 Multi Girder Model

Two-and-one-half girders from the prototype structure were then modeled with the cap beam fixed along the height. The diaphragms were restrained in the longitudinal direction at the cap beam to girder interface. The capacity of the model was measured and compared to the single girder model. In the multi-girder model, girder-to-diaphragm connections were modeled by using the springs and spring properties described in section 5.5.4 on both side faces of the intermediate girder, while only one face of the middle and exterior girder included a connection. The middle girder was modeled as one-half due to symmetry, which allowed for only one of the connections to be modeled. Figure 6.7 shows the end view of the 2 ½ girder layout, in which the middle girder is on the right, shown as ½ a girder.

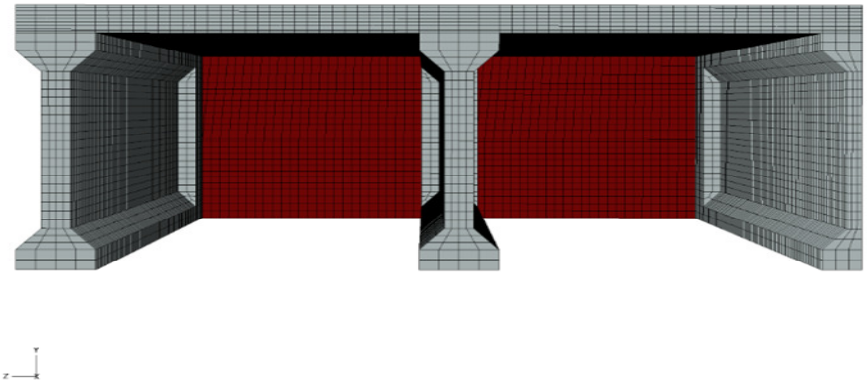

Figure 6.7. Multi girder prototype layout end view as modeled in ABAQUS

### 6.3.4 Multiple Girder Analysis

The result from the negative displacement analysis is shown in Figure 6.8. The moment created from displacing the girder ends in the negative direction appears to be 2.5 times the moment created from the single girder model by comparing moments at a displacement of 0.45 in., which is where the two analysis results begin to diverge, where the single girder model resisted 2000 kip-ft and the 2 ½ girder model resisted 5000 kip-ft. The capacity was consistent with the additional

compressive force resulting from the girders pressing against the cap beam and not the resistance of the girder-to-diaphragm connection. Therefore, the initial stiffness of the single girder and 2 ½ girder model were similar once the one girder model stiffness was scaled up by a factor of 2.5. One mechanisms of failure was captured in the analysis, the reinforcing bars yielding in the slab. The first reinforcing bar located in the concrete deck began to yield when 0.55 in. of displacement was imposed at the girder ends and the concrete at the girder-to-cap beam interface reached a strain of 0.0005 in./in. at that displacement. At the maximum displacement, the concrete strain was 0.0016 in./in. Also, the girder-to-diaphragm connection did not affect the force vs. displacement response significantly. The springs representing the girder-to-diaphragm reinforcing bars yielded at a negative displacement of 1 in., but the resistance from the girder pressing against the cap beam did not allow the girder end to rotate. However, the capacity at 1 in. of displacement was less than expected if established by multiplying the single girder model response by a factor of 2.5. The drop in resistance from the springs was believed to be the factor for this. In the 2 ½ girder model, the springs on each girder-to-diaphragm face begin yielding at different displacements, causing the stiffness to drop.

The result from the positive direction displacement analysis is shown in Figure 6.9. For the stiffness comparison, the single girder response was multiplied by 2.5, similar to the negative displacement analysis. The stiffness of the 2.5 girder model was slightly higher than the single girder model. The failure mechanisms for the system were the girder-to-diaphragm connection yielding along with the slab cracking in tension.

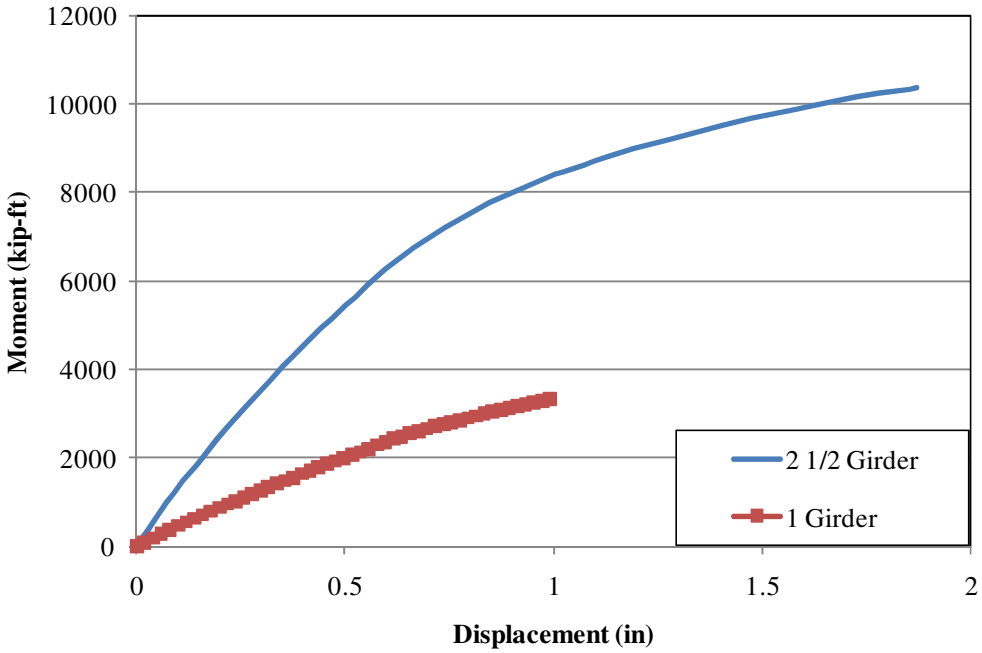


Figure 6.8. Cap-beam-to-girder connection moment vs. negative displacement of the single girder and 2 ½ girder prototype structure models

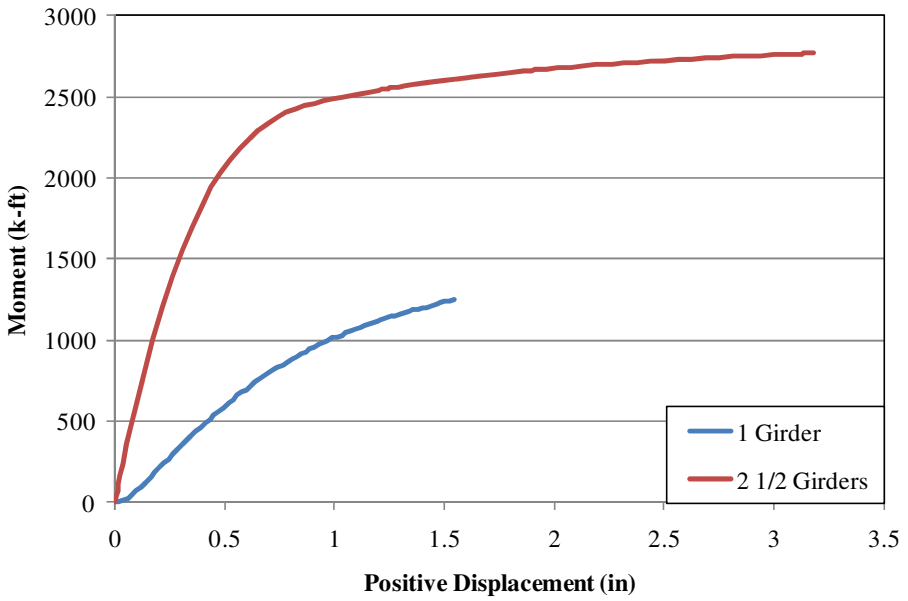

Figure 6.9. Cap-beam-to-girder connection moment vs. positive displacement of the single girder and 2 ½ girder prototype structure models

## 6.4 Test Unit

### 6.4.1 Comparison to Prototype

Initially the test unit was compared to the prototype to ensure the scaled model would result in accurate data when compared to the prototype. The test unit originally was scaled based on the dimensions used for the prototype, because the test unit details were not available at the time. The boundary conditions of both models were the same and the scaling was 50%. The results of the two analyses are shown below in Figure 6.10 for the negative displacement and Figure 6.11 for the positive displacement. The prototype values were scaled down to the test unit magnitude by dividing the force by four and the displacements by two. As can be seen, the initial stiffness matches until yielding. Further comparisons were unable to be performed because of the convergence problems in the prototype model. The Test Unit model was much smaller in number of elements and nodes and after developing the model which resulted in convergence problems were easier to overcome. Due to that, the test unit analysis was able to be completed to a higher displacement.

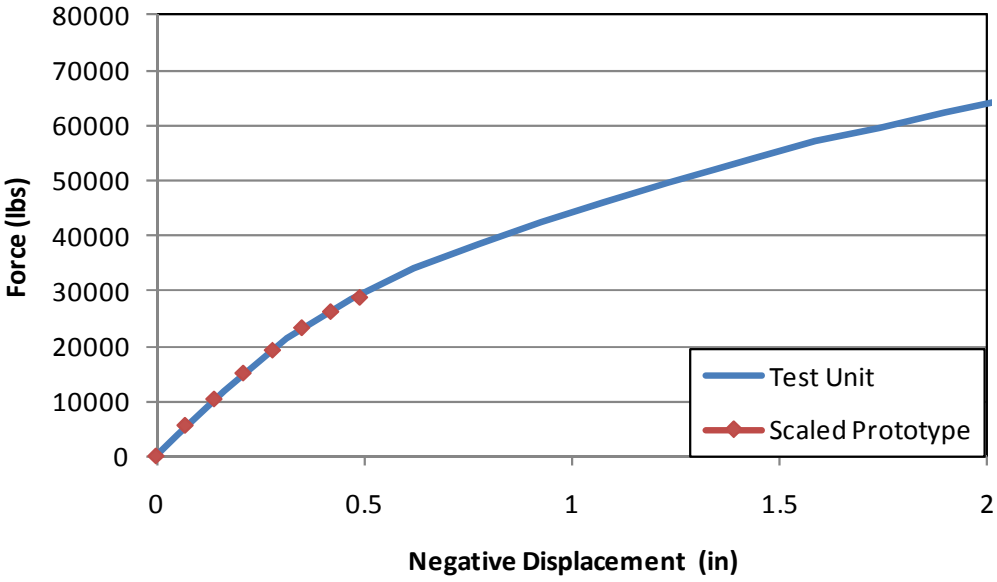


Figure 6.10. Girder end force vs. girder end negative displacement comparison for the prototype and test unit

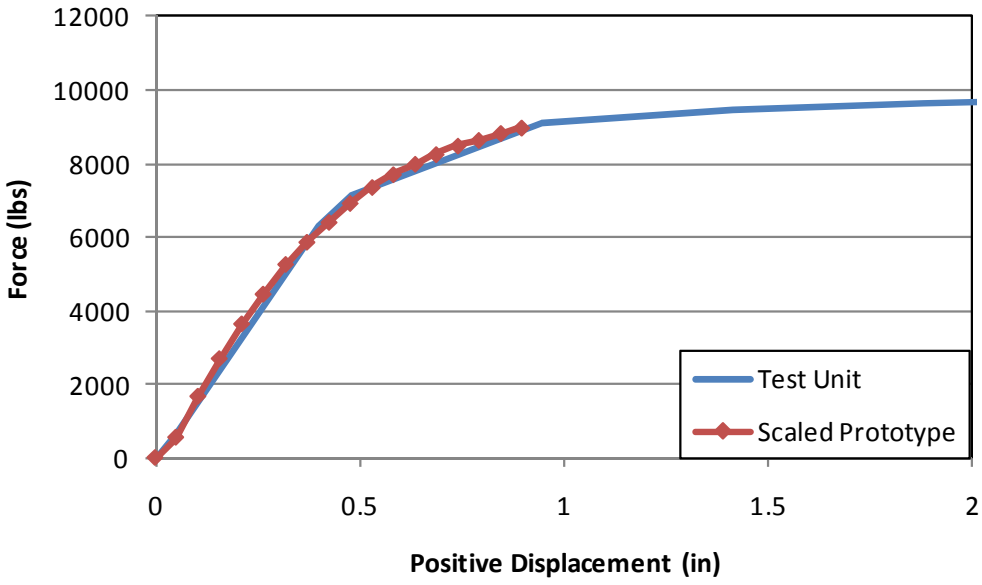


Figure 6.11. Girder end force vs. girder end positive displacement comparison for the prototype and test unit

### 6.4.2 Analysis Results

The main purpose of analyzing the response of one-girder on the test unit was to develop the moment-rotation behavior of the girder-to-diaphragm-to-cap-beam connection. The properties were inputted into a grillage model for the analysis of the bridge system to be developed in a companion study. The positive moment connection was expected to degrade as the system is subjected to seismic loading. The forces acting on the bridge deck will be transferred from the superstructure to the cap beam. Through the analysis three components were observed to contribute in developing the moment resistance of the connection: cap-beam-to-diaphragm reinforcing bars, girder-to-diaphragm reinforcing bars and the concrete slab capacity. The two sets of reinforcing bars previously mentioned are shown in Figure 6.12 and the modeling technique used in this case is discussed after presenting this figure. In the following analysis the overall behavior of the single girder model is presented and used to develop the connection properties for the moment-rotation spring in the grillage model.

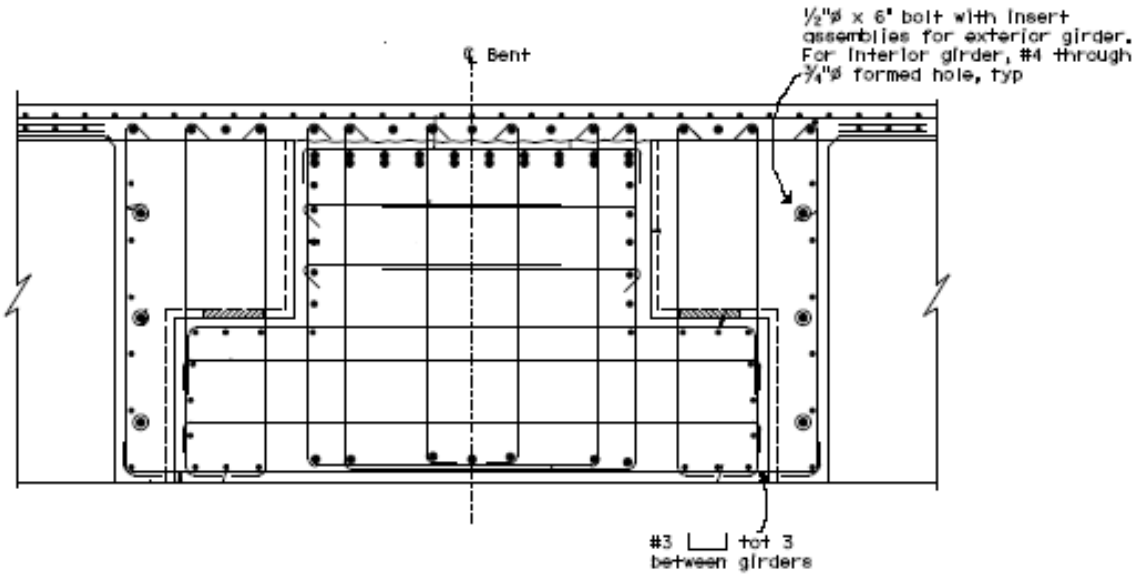


Figure 6.12. Connection details of reinforcing bars connecting the girders to the diaphragm and cap beam

For the girder-to-diaphragm connection at exterior girders, ½ in.-diameter bolts are placed on the interior face of the girders and cast into the diaphragm, instead of using the reinforcing bars. These reinforcing bars have been replaced with springs, as described in Chapter 5, for the girder reinforcing bar connection. The cap-beam-to-diaphragm reinforcing bars were modeled with wire elements, as described in Chapter 5. Once either the reinforcing bars or springs yield, the connection degrades and its future behavior is likely to be affected.

To develop the moment-rotation characteristics of the cap-beam-to-girder region, a single girder layout from the test unit was considered. The actual girder length of 27 ft. 8 in. was used since the test unit details were available at this stage. The width of the deck section modeled was 4 ft., which was the girder spacing of the test unit, as shown in Figure 6.13. The width was modeled from 2 ft. each side of the girder centerline to capture the additional stiffness and moment capacity of the concrete slab. The cap beam cross-section was rotated at both end faces by a rotation of 0.03 rad. to simulate the effects of the column deflecting and causing the cap beam to rotate. The cap rotation required to develop the moment needed to form the plastic hinge in the column was found to be only .0037 rad. from an analysis completed by the grillage model (Snyder, 2010). However, the model was subjected to larger cap beam rotation to capture the full behavior of the connection. Once the analysis was completed, the girder end force and rotations of the cap beam were recorded.

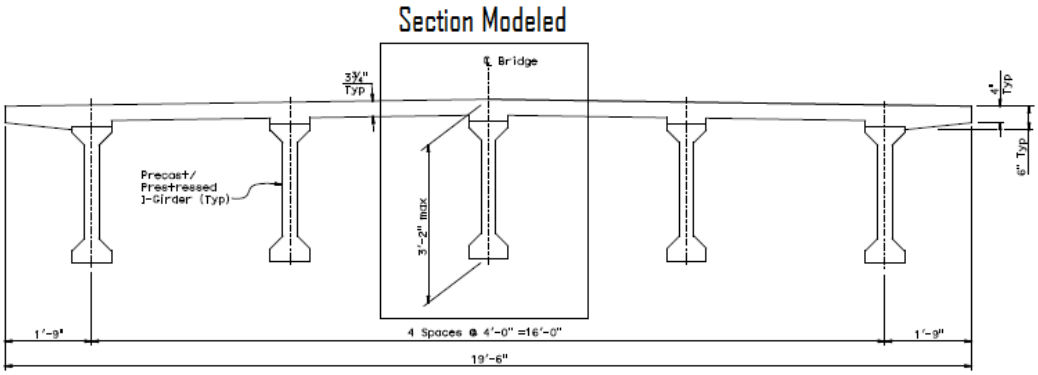


Figure 6.13. Region chosen for the single girder section model of the test unit in ABAQUS

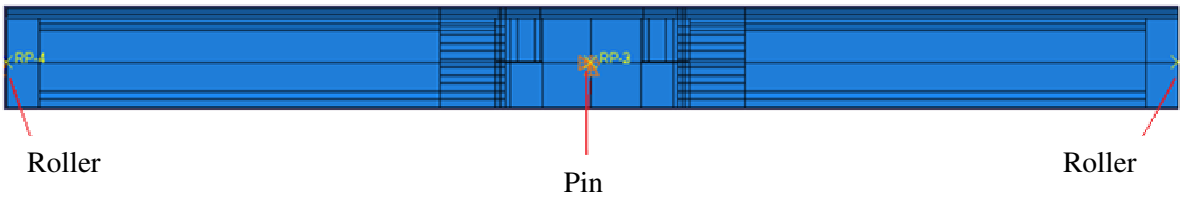


Figure 6.14. Boundary conditions used for the single girder model of the test unit

The resulting end reaction recorded at the girder ends and the moment at the connection is presented in Figure 6.15. The girder-to-cap-beam connection on the positive moment side of the cap beam had a moment capacity of 162 kip-ft with a girder end reaction of 6126 lbs. For the negative moment side, the girder-to-cap-beam connection has a moment capacity of 1220 kip-ft with a girder end reaction of -46021 lbs.

Further inspection of the model at the rotation causing development of the flexural plastic hinge capacity at the column ends (i.e., at 0.0037 rad.) was performed to understand the condition of the connections. On the negative moment side, the girder end reaction response shown in Figure 6.16 confirms that the girder-to-diaphragm connection was fully effective at the end of the analysis, at 0.03 rad. The initial change in slope at 0.00336 rad. was the rotation at which the deck slab experienced cracking under tension. The deck flexural cracking occurred over the girder-to-diaphragm connection since the compression force causing the moment couple was provided from the girder pressing against the face of the cap beam. The diaphragm-to-cap-beam reinforcing bars also remained elastic throughout the duration of the analysis. The transfer of forces from the girder to the cap beam happened by the girders pressing against the cap beam and not the connection from the girder to the diaphragm. The moment transfer was limited due to the girder ends starting to crack in compression as the pressed against the cap beam. The location on the girder of concrete crushing is shown in black with the diaphragm removed in Figure 6.17.

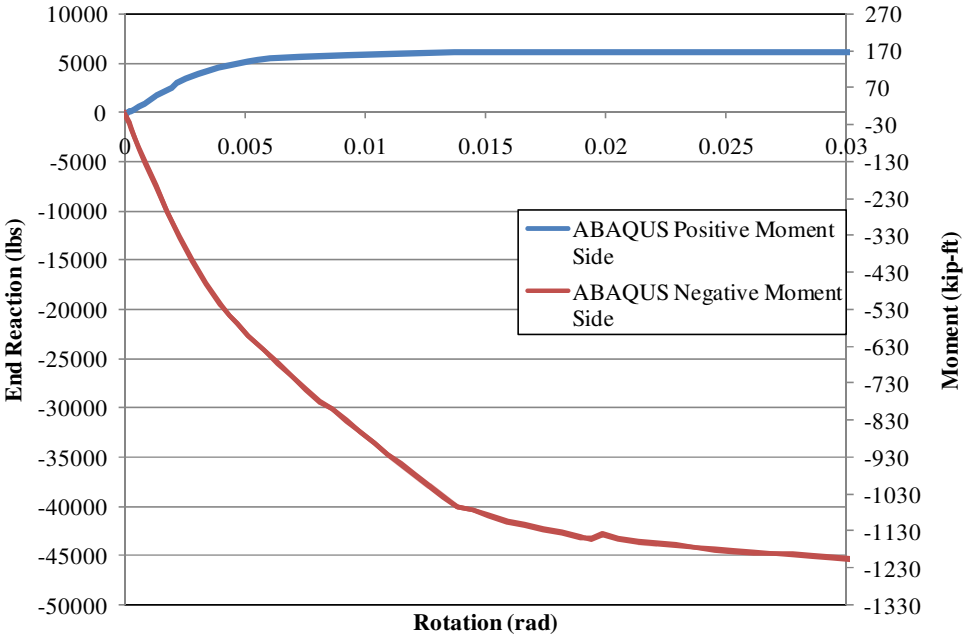


Figure 6.15. Girder end force vs girder end displacement response of the single girder test unit model in ABAQUS

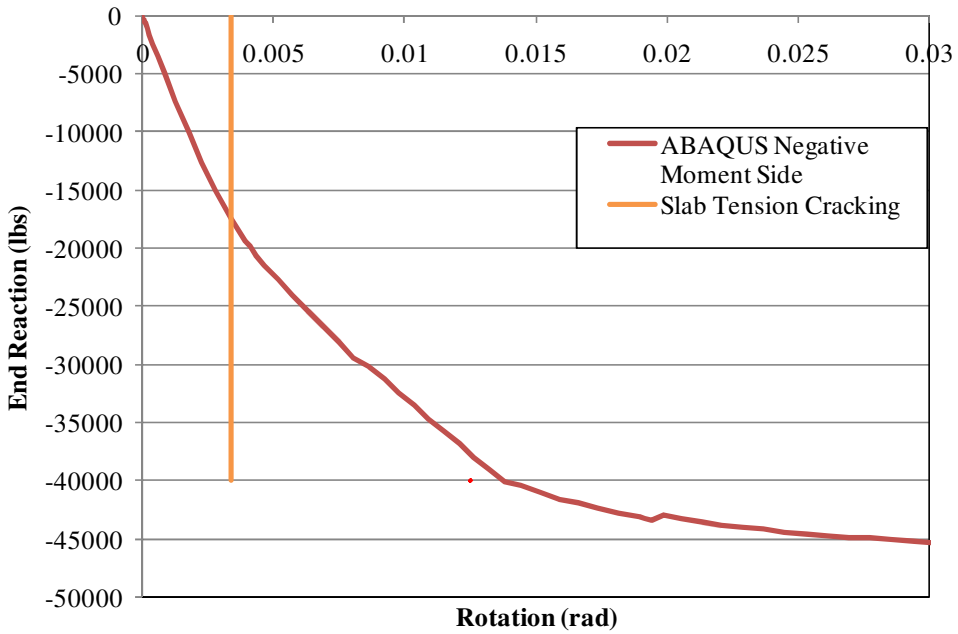


Figure 6.16. Negative moment investigation of the single girder test unit model

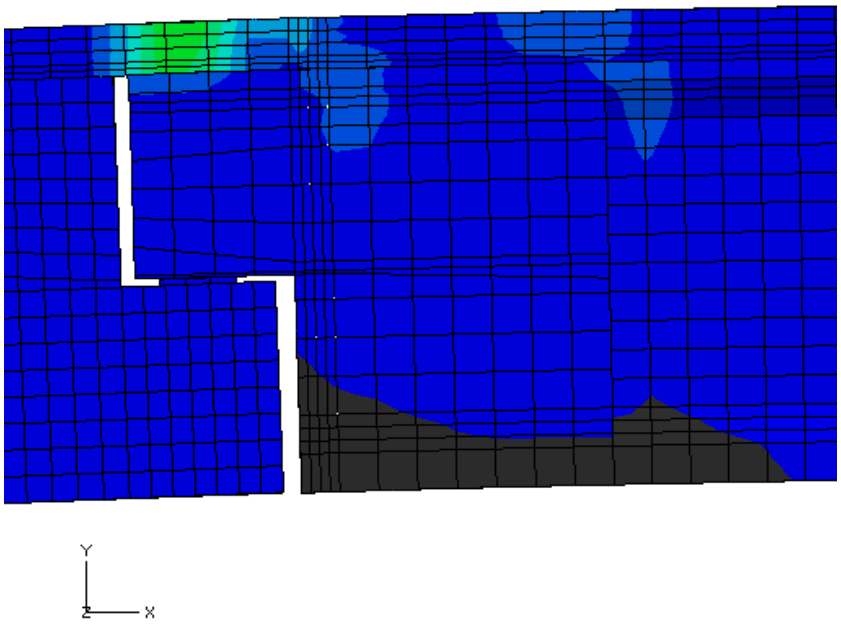


Figure 6.17. Location of concrete crushing of the girder on the negative moment side

On the positive moment side, after inspection at the specified rotation that the slab had cracked, the cap beam-to-diaphragm reinforcing bars and girder-to-diaphragm reinforcing bars had yielded. The girder-to-diaphragm connection began to soften at 0.00145 rad. with the bottom spring on each face of the girder first experiencing yielding. At a rotation of 0.00357 rad., 12 of the 20 springs have yielded so the response captured at the girder end continued to lose stiffness and eventually flattens out. Retrofitting the plastic hinge in the column after the seismic activity would not result in a fully functional bridge structure, and additional retrofits would be needed at the connection region to repair the damage experienced. Figure 6.18 provides the positive moment response of the girder-to-cap connection, in which the rotations corresponding to firs the slab cracking and yielding of two sets of what reinforcing bars are identified. The softening of the response was not apparent as the slab cracks since the cracking occurred above the girder dapped end-

to-cap beam interface, shown in Figure 6.19. Also, due to the concrete model in ABAQUS unable to allow for post cracking stress of concrete to soften to 0 psi., the drop in stiffness is not well defined.

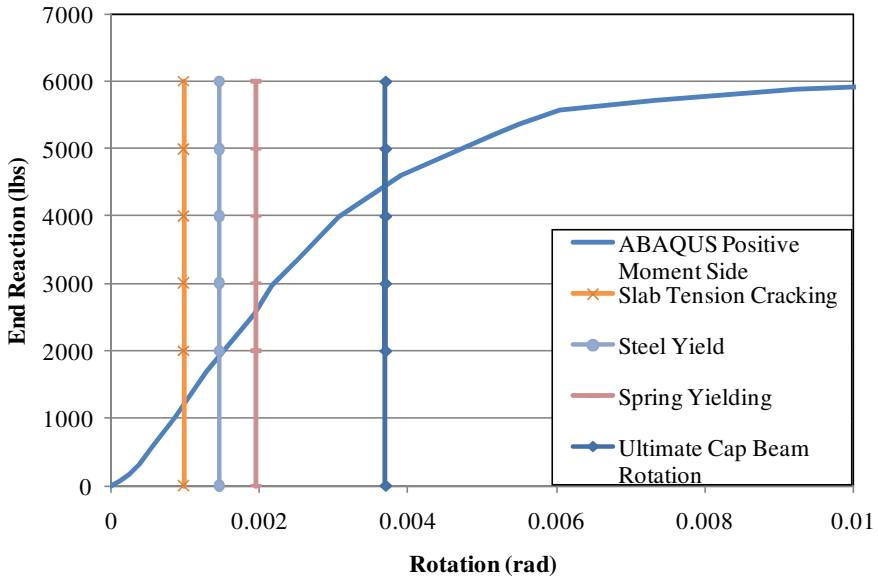


Figure 6.18. Positive moment vs. cap beam rotation of the test unit

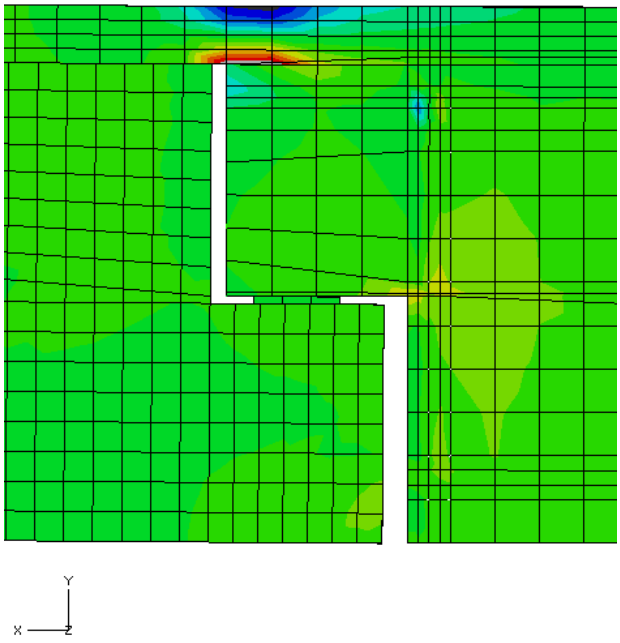


Figure 6.19. Positive moment connection slab cracking

The gap between the cap beam and girder was also monitored to obtain the opening of the gap between the girder and cap beam. In the multiple girder modeling presented later, the gap from the single girder model is compared with the gap opening recorded in the multiple girder models. The relative displacement between the girder and cap beam was captured by subtracting the relative displacements of each of the components separately. The resulting gap opening, occurring on the positive moment side, is presented in Figure 6.20. The gap opening was analyzed and at a rotation of 0.0032 rad. the stiffness of the gap softens. The change in stiffness occurred before the rotation where the reinforcing bars, discussed previously, began to yield. No significant change in the gap between the girder and cap beam on the negative moment side occurred during the analysis. The concrete compresses as the analysis runs resulting in a small reduction of 0.01 in the gap width due to compressing force transfer. Further comparisons of the negative moment side will be limited to analysis combinations where the response has changed.

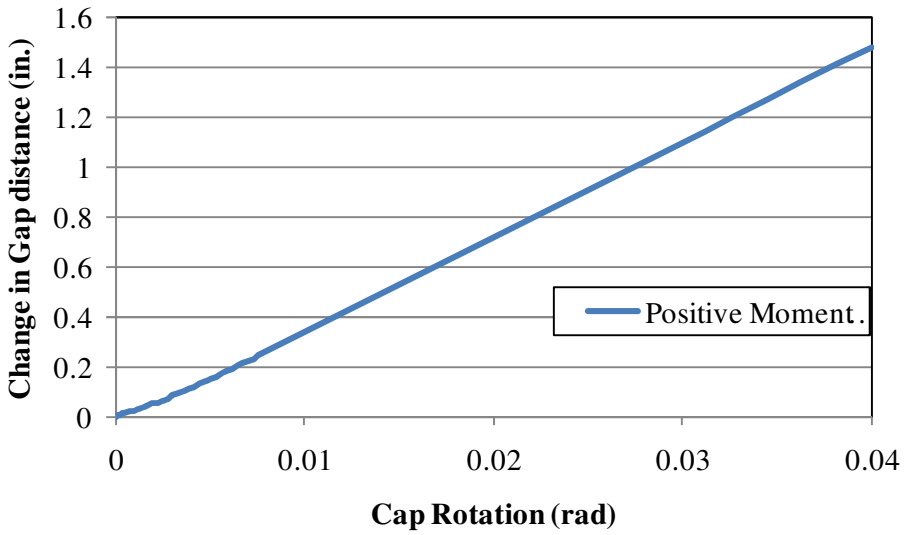


Figure 6.20. Gap displacement between the girder and cap beam in the single girder model

The effects of the slab, cap beam-to-diaphragm reinforcing bars and girder-to-diaphragm reinforcing bars are presented below in different analyses. The results are presented in Figure 6.21.

The response labeled "Single Girder" is the response previously captured and presented in Figure 6.18. The response labeled "Single Girder – no rebar" is an analysis where the reinforcing bars between the cap beam and diaphragm were removed. This combination will require the moment to be fully transferred through the deck slab and establish the moment resistance from the deck slab. At a cap beam rotation of 0.01 rad., the end reaction is 50% of the unmodified girder-to-cap-beam connection. The next analysis completed, labeled "Single Girder-rigid rebar", included the cap-to-diaphragm reinforcing bars but their material properties were changed to make them rigid. This analysis will not capture any effects from the cap-beam-to-diaphragm reinforcing bars but allow the girder-to-diaphragm reinforcing bars to yield. The resulting capacity from the "Single Girder-rigid rebar" analysis will include the deck slab capacity; therefore, the two responses would need to be subtracted to obtain the capacity from the girder-to-diaphragm connection only. From the figure, it can be seen that the deck slab and girder-to-diaphragm reinforcing bars are responsible for most of the response captured in the single girder analysis. The reinforcing bars between the cap beam and diaphragm contributed to limiting the capacity as the system yields but do not add any force capacity of the cap-beam-to-girder connection. The combination of the girder-to-diaphragm reinforcing bars removed was not completed as it seems intuitive that the only moment resistance would be the deck slab, similar to the analysis with the cap-beam-to-diaphragm reinforcing bars inactivated.

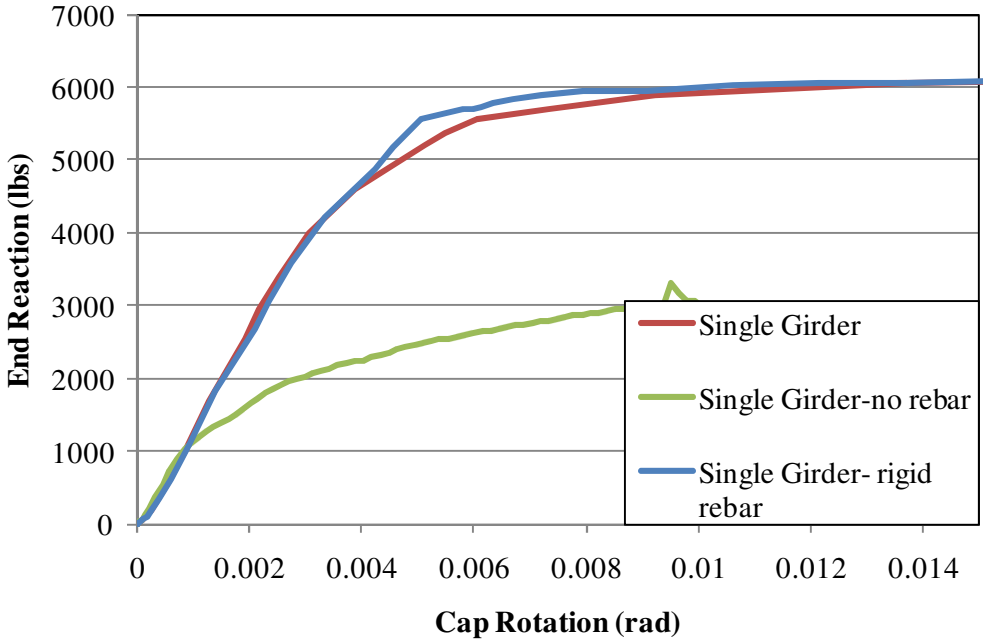


Figure 6.21. Influence of the cap-beam-to-diaphragm reinforcing bars on the response of the positive moment connection

### 6.4.3 Connection Properties

The properties for the spring to be modeled in the grillage model were developed from the single girder model where the interaction from additional girders would not alter the behavior of the connection. The properties were developed by finding the difference in rotation of the center of the cap from the rotation of the girder connection end.

An additional rotation was needed to create the connection behavior, the girder end rotation. However, the rotation was not provided as an output from ABAQUS, therefore a method had to be chosen to calculate the rotation of the girder end at the connection. Once the rotation of the girder connection end was calculated, the relative rotation between the cap beam and girder connection end was obtained. To calculate the girder connection end rotation, a node path was created in ABAQUS which when saved, outputs the results from every node that the path crosses. The path was created at

the center of the girder from the top of the slab to the bottom of the girder at the location of the connection, shown below in Figure 6.22.

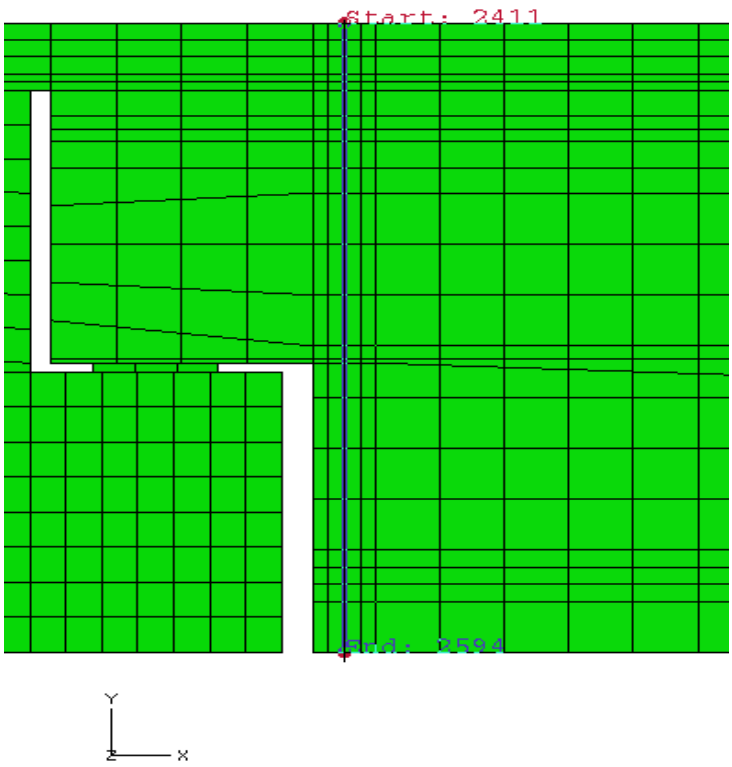


Figure 6.22. Node path location

Then the displacements along the path were saved at different analysis increments of cap rotation. The displacements where then plotted in Microsoft Excel for each increment and a linear trendline was drawn through the points. The slope was taken and inverted to obtain the rotation of the section. The inverted slope is able to be taken since the rotation is relatively small and the tangent of a small angle is the same as the angle itself. At the same increment step, the reaction of the restrained girder end was also recorded and multiplied by the distance from the connection to obtain the moment value, in kip-in, as needed for the grillage model. The resulting moment vs. rotation behavior of the girder-to-cap-beam connection is presented below in Figure 6.23.

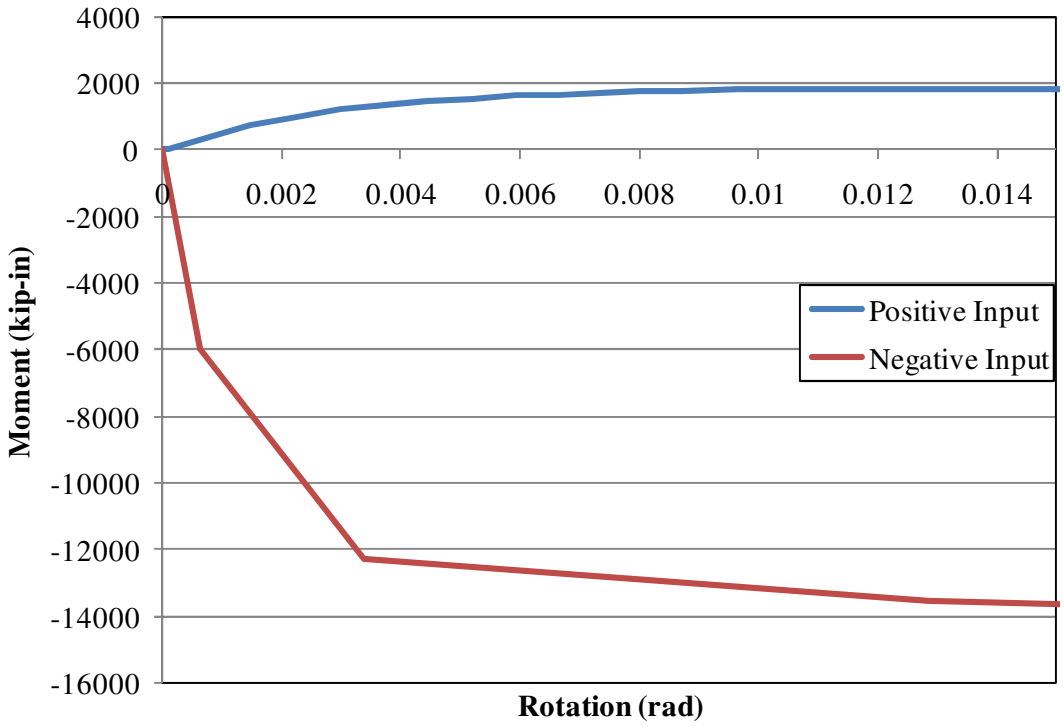


Figure 6.23. Moment vs. rotation behavior of the girder-to-cap-beam connection

### 6.4.4 Comparison to Grillage Model

With the connection properties obtained, a grillage model was developed replicating the same setup and boundary conditions as used in ABAQUS (Snyder, 2010). The girder end reaction vs. cap rotation was compared with the ABAQUS model and presented below in Figure 6.24. The positive moment connection matched well over the whole rotation. The initial stiffness from the grillage model was slightly softer than the ABAQUS results. The reason for the difference in stiffness was because the grillage model assumes the moment of inertia of the girders to be 70% of the gross value. The negative moment connection had larger percentage error along the whole rotation range. Similar to the positive moment connection, the girder stiffness was the factor that caused such a response. A further analysis was performed with the grillage model assuming 100% of the gross moment of inertia values for the girders. The response better predicted the initial stiffness. However, the gross moment

of inertia values led to the post cracking response from the grillage model to be significantly high. To better match the post cracking response, a moment of inertia value less than the initially assumed 70% of the girders must be used to soften the response.

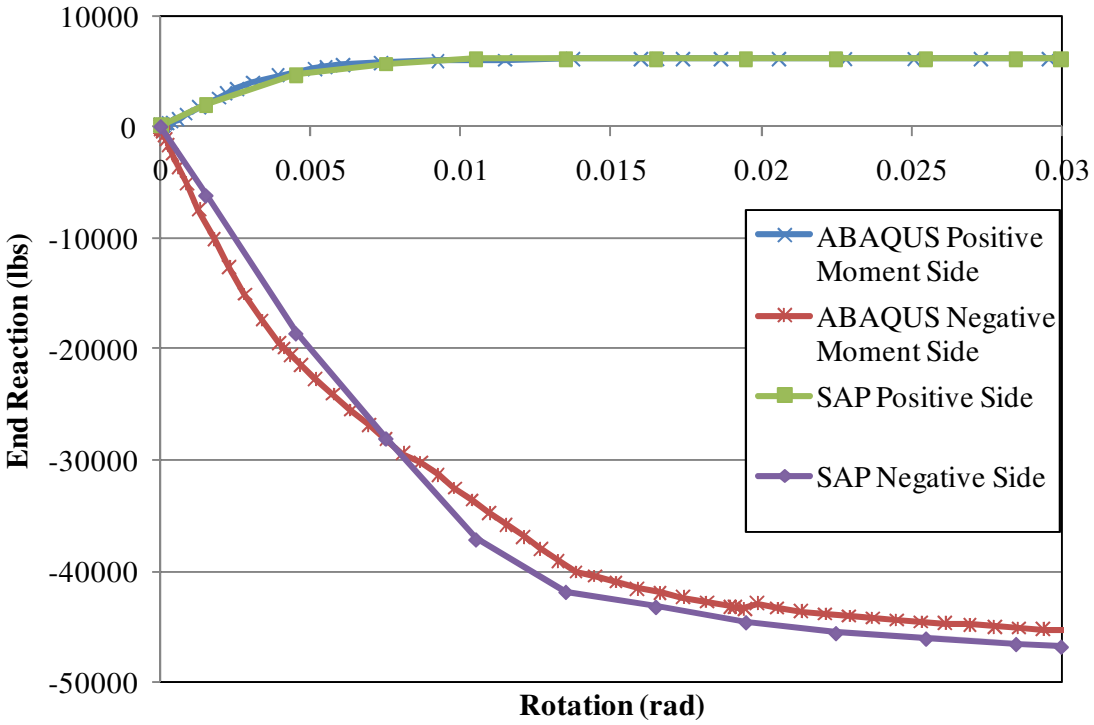


Figure 6.24. Comparison of the single girder model response from ABAQUS and the grillage model

## 6.5 Multiple Girder Model

### 6.5.1 Introduction

Once the connection behavior was obtained and validated in the grillage model the interaction between the girders, slab and diaphragms were investigated. The interactions would not be modeled initially in the grillage model and once the interactions were investigated and found to be contributing

the response of the section, steps were taken to implement the necessary components into the grillage model.

For this analysis, one-half of the width of the Test Unit was modeled by considering the symmetry about the centerline of the structure. To model this accurately, the boundary conditions discussed in Chapter 5 were used and shown below in Figure 6.25. The modeled structure consisted of two spans with 2 ½ girders in each span, one half of a cap beam and diaphragms. The rotation was applied at the face of the cap at the centerline of middle girder with the cap beam pinned across the length. The rotation was applied in this manner since the column was located under the center girder and as the Test Unit is pushed in the lab, the resistance from the column will cause the cap beam to rotate. Also, the moment along the cap beam will transfer to the column; therefore, the rotation was applied at the location of the column because that would be the point of highest resulting moment. From the grillage model, it was found that the ultimate rotation of the cap beam was .0037 rad. before the plastic hinge in the column fully develops. However, the analysis was completed with a rotation of .01 rad. so the nonlinear response could fully be developed. The information gained would be useful for the component testing that would be performed in the laboratory. The component testing would be performed by pushing the girder ends up and down until the connections were fully damaged to formulate the full response and provide information regarding the benefits of the proposed connection.

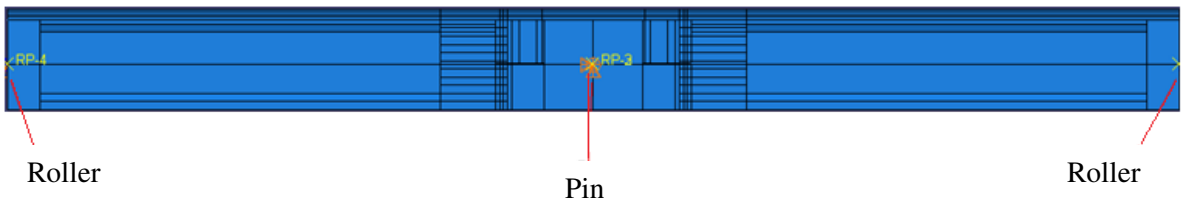


a) Cap beam and girder end boundary conditions

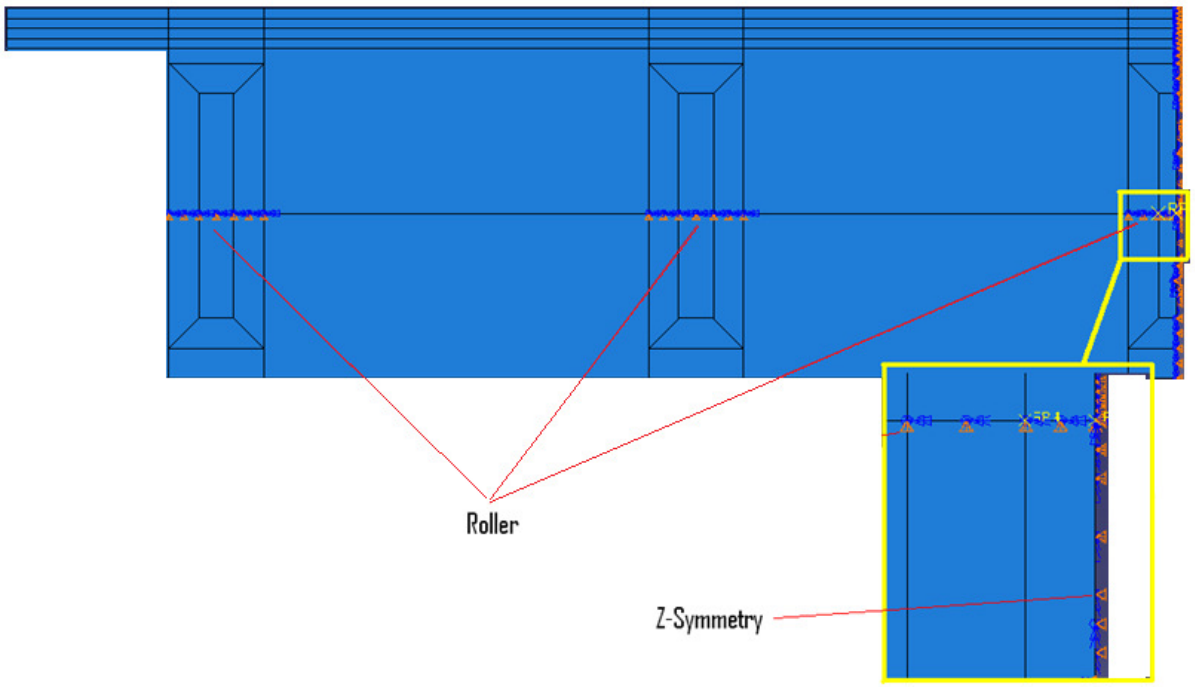


b) Girder end and symmetry boundary conditions

Figure 6.25. Boundary conditions for multi-girder model

### 6.5.2 Results

The 2 ½ girder model was first analyzed with the boundary conditions discussed above. However, the model was then broken down to try to eliminate the different interactions that are considered to be affecting the overall response. Some of the models were compared to the response from the grillage model to provide evidence that the detailed modeling could be replicated in the much simpler model. The grillage model was still being developed, though, so some of the analysis did not have comparisons completed. For the analysis, the rotation was completed to a value of 0.01 rad. to shorten the analysis time since most of the effects occur before then. The grillage model response will be denoted as dashed lines in all of the upcoming figures. The three mechanisms of failure discussed in the singled girder model will not be discussed for the comparison analyses with the grillage model as each of the effects from the three mechanisms has been captured in the spring developed for the grillage model.

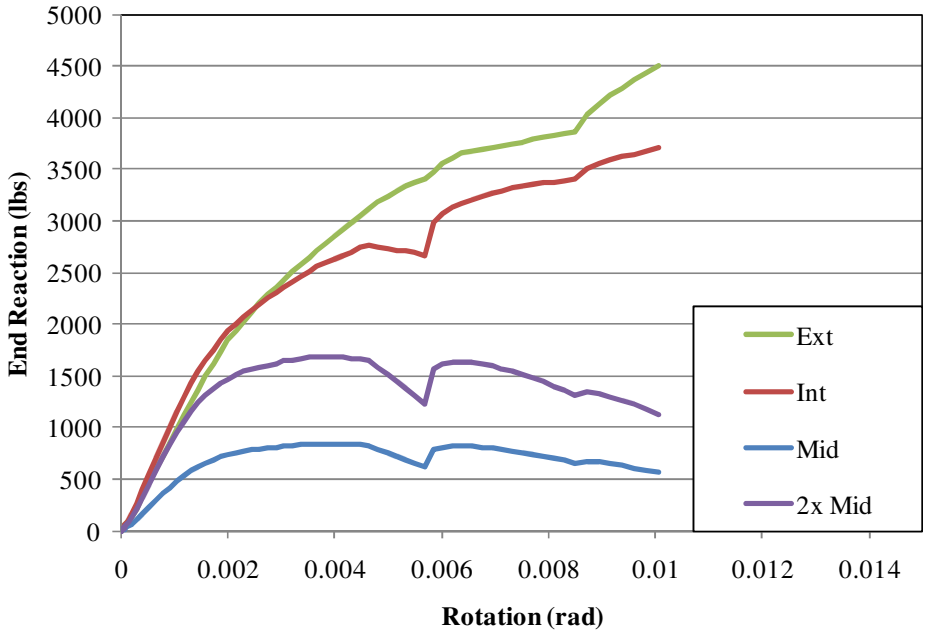


Figure 6.26. Initial multiple girder response

Initially, the full Test Unit was modeled and the response was obtained with no modifications to the components. The initial response is shown below in

Figure 6.26. The intermediate girder response is labeled below as "Int". The middle girder forces are shown on the graph as resulting from the model, labeled as "Mid", and doubled, labeled as "2x Mid". The forces are doubled because one-half the girder has been modeled due to symmetry. The exterior girder response is labeled in the graph as "Ext". It can be seen from the figure that the middle girder resists the least force at the ends of the girder then the intermediate and exterior girder. The initial stiffness values of all three girders match well until .0015 rad. of cap beam rotation. The change in stiffness was first noticed in the middle girder, then the intermediate girder. Further inspection of the model provided knowledge into possible reasons for the resulting response. At the rotation of .0015-.002 rad. the slab begins to crack between the middle and intermediate girder between the connection and the top of the cap beam stem. This was expected due to the observations

from the single girder model. To attempt to understand the behavior, additional analyses were performed and the information gathered will be used later to understand the behavior of this analysis.

#### *6.5.2.1 Elastic Cap Beam only*

The model was analyzed by modifying the cap beam to remain elastic. The original stiffness was used but the plastic action was removed from the material properties. The purpose was to capture the effects of the deck and end diaphragm on the force being transferred from the cap beam to the girder ends and not allow the cap beam cracking to affect the behavior of the system. The grillage model can be seen predicting higher forces then the ABAQUS model for the intermediate and middle girder, while the exterior girder is resisting less. The ABAQUS model still predicted a combined capacity of roughly 12,000 lbs, as does the grillage model. The gap displacements are presented in Figure 6.28. The middle girder gap followed the single girder analysis gap displacement closely, the only difference is middle girder gap was not as large at the end of the analysis but the difference was very small. The displacements of all three girders in this analysis have magnitudes that fall within a range of .05 in. The gap decreased at the intermediate girder and exterior girder, due to the greater distance from the location of applied rotation.

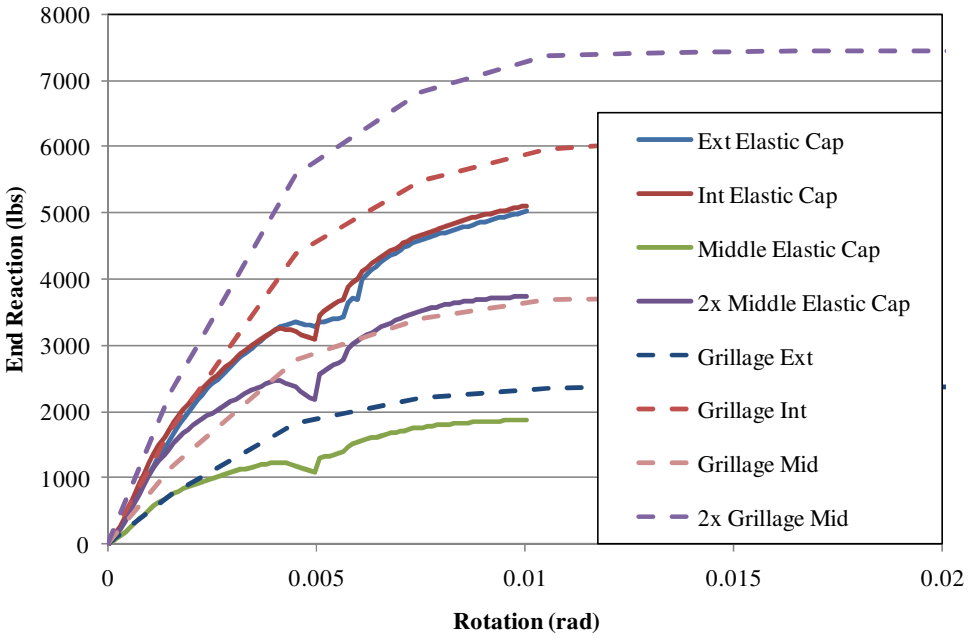


Figure 6.27. Comparison of ABAQUS and the grillage model with an elastic cap beam

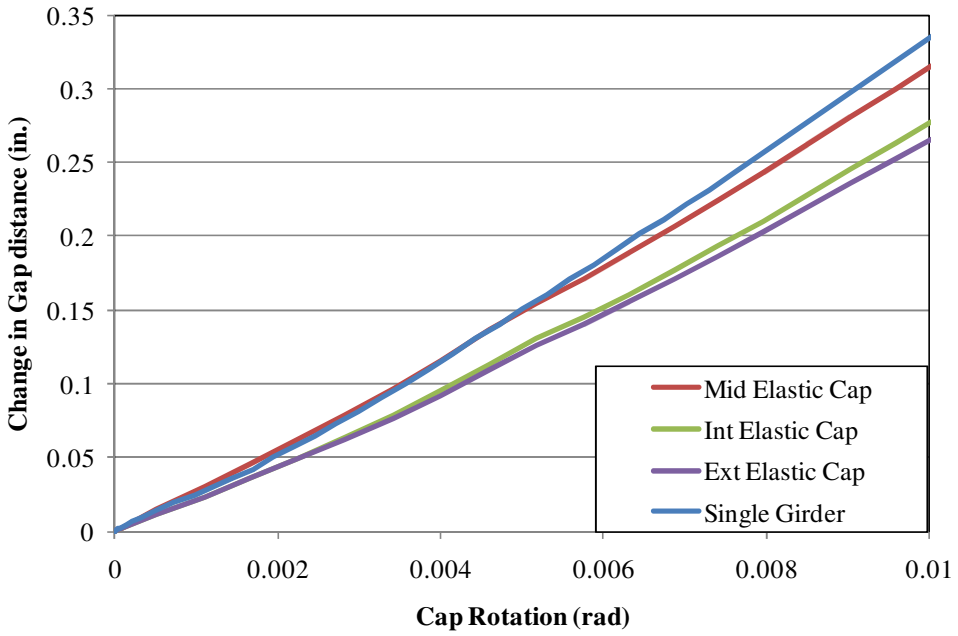


Figure 6.28. Comparison of gap openings in the ABAQUS model for the elastic cap only

*6.5.2.2 Sliced Deck and End Diaphragm, Elastic Cap Beam*

The first setup to be presented is the model with the deck slab and diaphragms sliced so the interaction between the girders would not be present and the cap beam elastic to eliminate any cracking of the concrete. The results are presented below in Figure 6.29 and Figure 6.30. The response of the intermediate girder is the largest, as expected, since in the model, it is the only girder with a connection on both faces. Both the middle girder and exterior girder have a connection on the one face in the model, the middle girder because only one face of the girder being modeled, due to symmetry, and the exterior girder because the diaphragm only extends to the interior face of the girder.

The two models predicted a similar response with this setup. The capacity and initial stiffness of each girder were similar. The ABAQUS model predicts a couple changes in the behavior that the grillage model does not capture. The difference in behavior between a rotation of 0.004 rad. and 0.008 rad. is not resulting from the cracking of the slab or yielding of any of the reinforcement. Further analyses were run to try to understand the behavior. The capacity from this analysis at 0.01 rad. is found to be 11,808 lbs.

Figure 6.31 below shows the gap opening of each girder. The gap opening from the single girder analysis is also presented on the graph for comparison. The middle girder initially has a smaller gap at each cap rotation. That was due to the rotation being applied directly at the centerline of the girder and not the between the girder. In the single girder analysis the rotation was applied two feet to each side of the girder but on both sides to create nearly uniform rotation. The intermediate girder gap is less than the middle girder but greater than the exterior girder which was expected due to the end reactions and the proximity to the location of applied rotation.

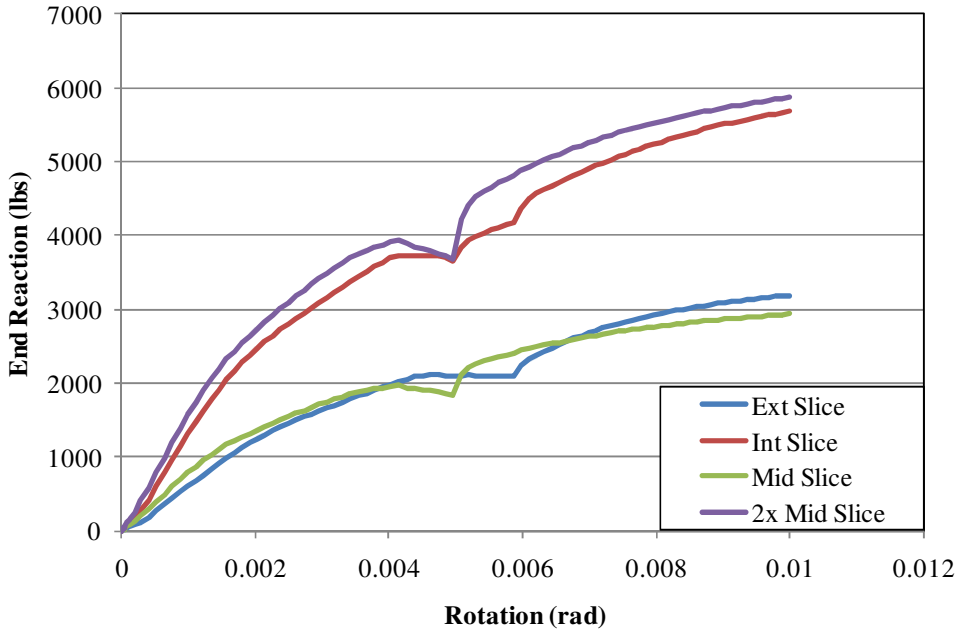


Figure 6.29. ABAQUS response for the sliced deck analysis

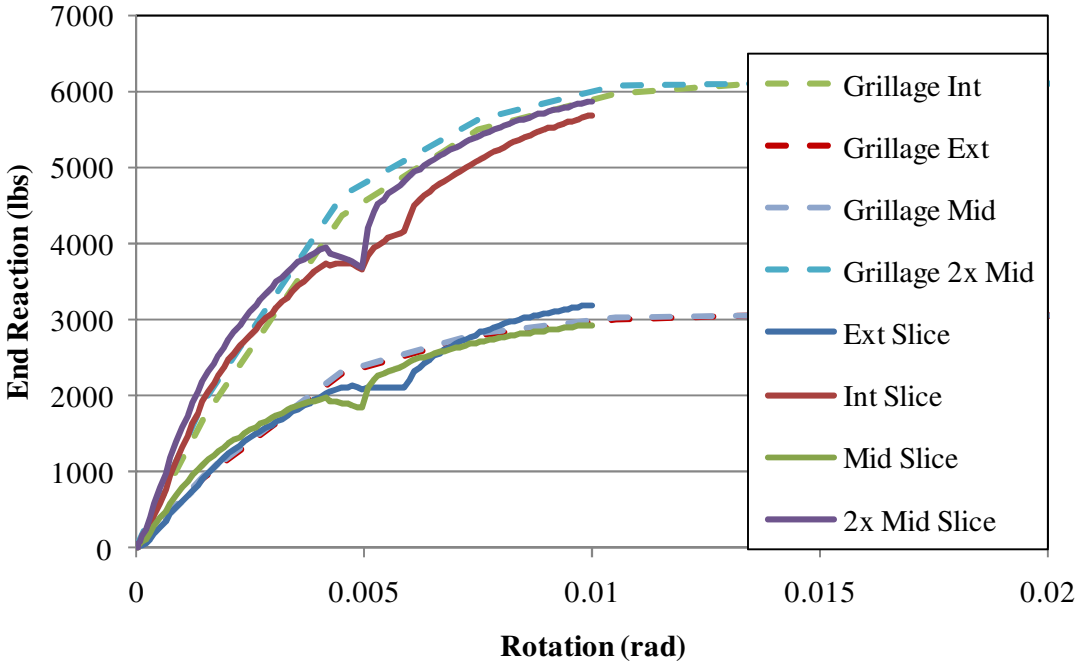


Figure 6.30. ABAQUS and grillage model comparison of the sliced deck analysis

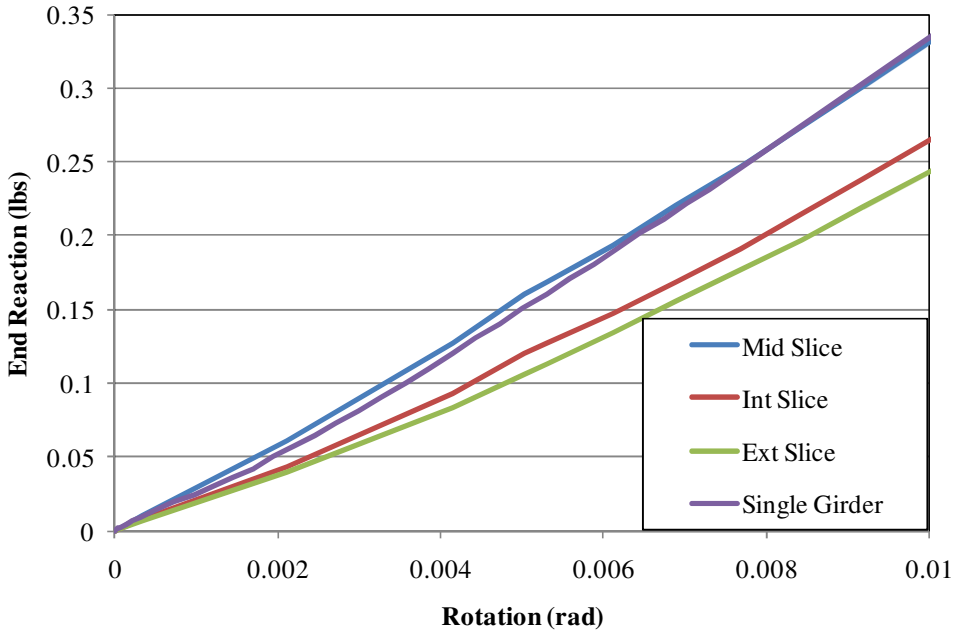


Figure 6.31. Gap opening between each girder of the sliced deck analysis

*6.5.2.3 Sliced Diaphragm only, Elastic Cap Beam 131*

The end diaphragm was the only piece sliced and the modification of the deck was removed to allow it to act as one piece and capture the effects of the girders due to the deck. The result is given in Figure 6.32. The slab causes the force to be transferred out to the exterior girder. By comparing the results in Figure 6.27 to this analysis, the middle girder drops significantly in the amount of force that is resisted. The exterior girder can be seen picking up the force from the middle girder. Another observation from the analysis was that the total capacity remains constant at a combined end reaction of 12,000 lbs, nearly identical to the previous analysis. The conclusion was drawn that the end diaphragm must transfer load into the middle girder and the grillage model should create a model to ensure that this effect is captured. Also, the drop and rise in forces still occurred between the rotations of 0.004 and 0.008 rad. as noticed in the previous analysis also.

Figure 6.33 provides the gap displacements of the three girders compared to the single girder model. The results are similar to the previous analysis. The moment transferred through the cap-beam-to-girder connections appear to be similar in each analysis at the same rotations. That concludes that the deck and end diaphragms are affecting the end reaction responses the most. Once the force is through the connection, the force appears to be transferred from the middle girder out to the exterior girder.

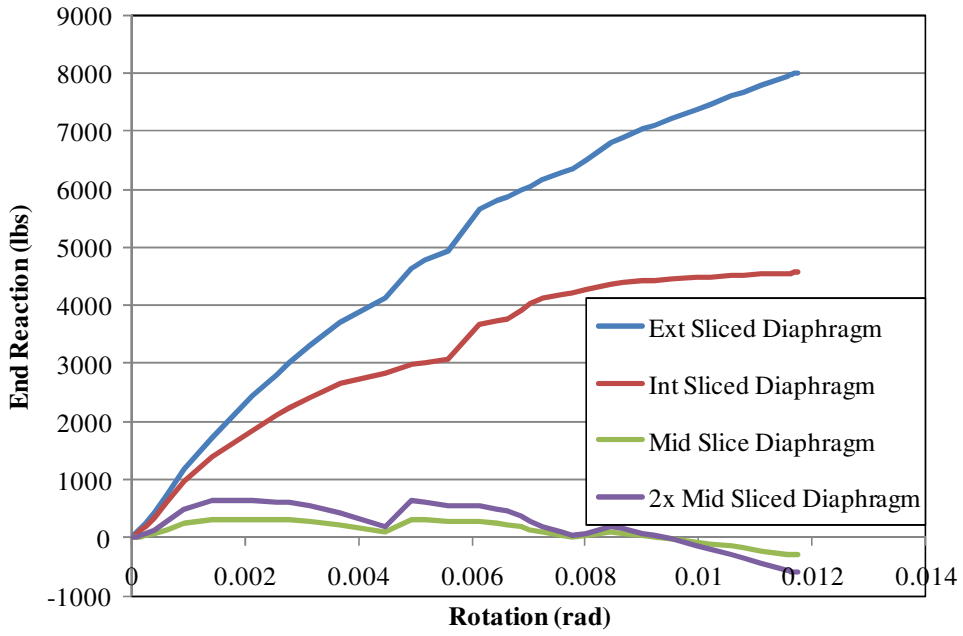


Figure 6.32. ABAQUS response of the analysis with the end diaphragms sliced

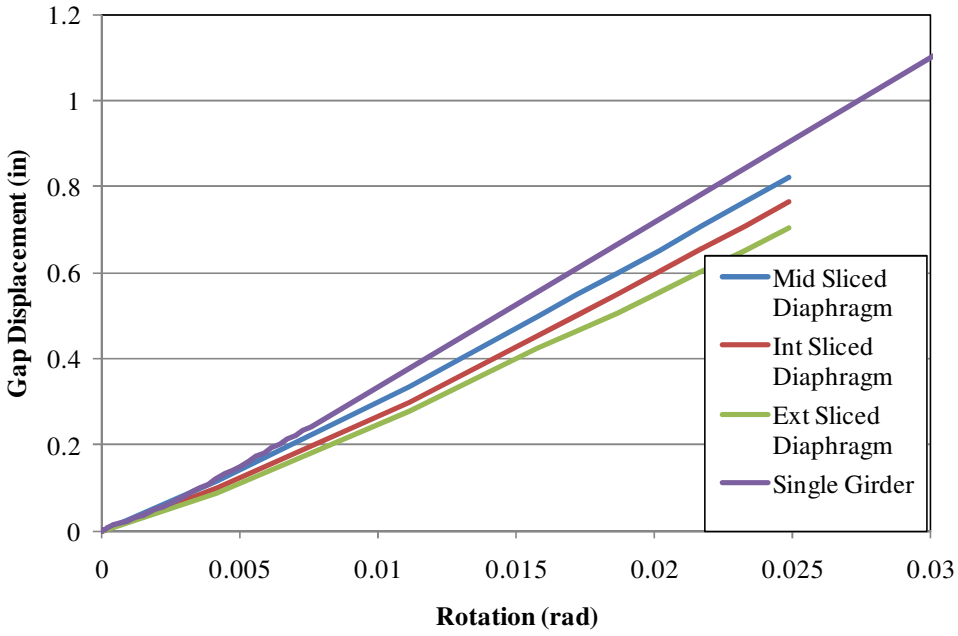


Figure 6.33. Gap displacements of the analysis with a sliced end diaphragm and elastic cap beam

*6.5.2.4 Elastic Cap Beam and Elastic Cap-Beam-to-Diaphragm Reinforcing Bars*

The drop and rise in stiffness between 0.004 and 0.008 rad. was apparent in all of the previous analyses. Since the cap-beam-to-diaphragm reinforcing bars yield at different locations, the behavior after yielding and through strain hardening was considered to cause the noted drop and rise in stiffness. Figure 6.34 below provides the response from ABAQUS to this analysis case. The change drop and rise in stiffness was not predicted in this analysis. The cap-beam-to-diaphragm reinforcing bars exceeded the yield strength between a rotation of 0.001 and .0016 but remained elastic due to the modification. The rotation at which the reinforcing bars yield is similar to that observed in the unmodified model. The effect of the reinforcing bars remaining elastic and providing more resistance at the larger rotations resulted in a smoother behavior. At the end of the analysis, the maximum stress in the reinforcing bars was over 200,000 psi which was much greater than the yield and ultimate strength of the reinforcing bar. The original model should be investigated to observe the

behavior of the cap-beam-to-diaphragm reinforcing bars at the questioned rotations. However, the combined end reactions still remain about 12,000 lbs.

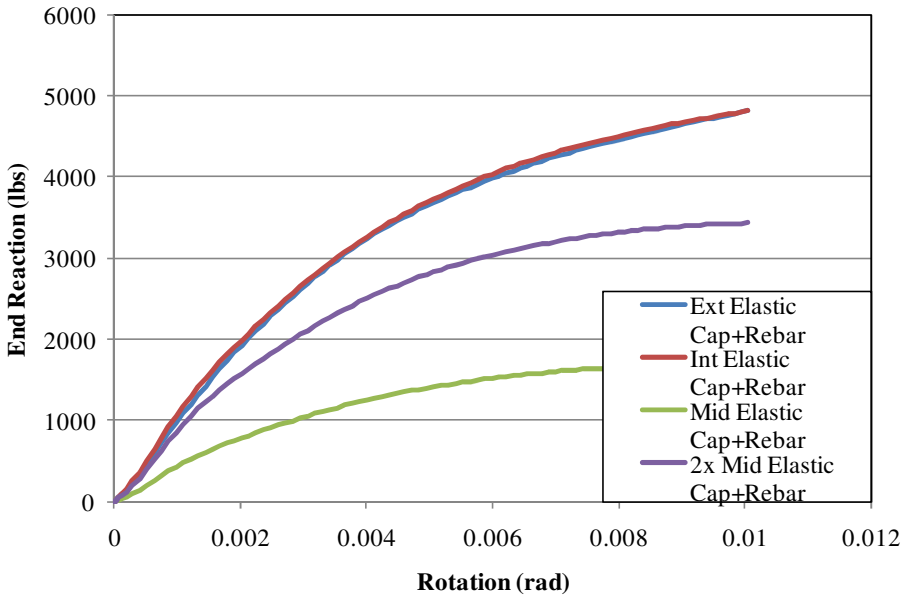


Figure 6.34. ABAQUS response to the elastic cap beam and cap-beam-to-diaphragm reinforcement

*6.5.2.5 Original Behavior*

The behavior predicted from the original model, which was design according to the Test Unit drawings and none of the pieces were modified. The response was given previously in Figure 6.26. After performing the previously discussed analyses, the model was inspected further to better understand the behavior.

The cap-beam-to-diaphragm reinforcing bars do not all yield at the same rotation as observed in the single girder model. The single girder model predicted that response since the cap beam was rotated from both ends and created a nearly uniform rotation. However, the rotation across the cap in the multiple girder models was not equal, but decreased along the cap. The first reinforcing bar began to yield at 0.00103 rad. while the last reinforcing bar began to yield at 0.0032 rad. It was observed

that the all three reinforcing bars between the middle and intermediate girder yield by a rotation of 0.00249 rad. Also, the bars placed closest to each girder were the girders with the highest stress and the bar in the middle measured less stress. The reinforcing bars were noticed in the current analysis and in some of the previous analyses to be yielding at different rotations. The grillage model must be designed to capture the transfer through the diaphragms to girder to better predict the overall behavior.

The cap-beam-to-diaphragm reinforcing bars also were noticed to affect the behavior of the system between the rotations of 0.004 rad. and 0.008 rad. in the previous models. The reinforcing bars were experiencing very high strains, 0.12 in./in. for the reinforcing bar closest to the middle girder, when the reinforcing bar closest to the exterior girder finally yielded. Once that occurred, the reinforcing bars reached the full capacity at strain hardening and were beginning to soften and drop in ability to withstand loads. The sequence of bars reaching the ultimate strength was similar to the yielding, starting between the middle girder and intermediate girder then between the intermediate girder and exterior girder. At the end of the analysis, the highest strain recorded was .275 in./in. At that strain, fracturing of the bar could be expected.

The behavior in which the force was being transferred to the exterior girder was then investigated. From the previous analyses, the deck appeared to have the greatest influence in the behavior. The principal compressive stress was plotted for the deck. Figure 6.35 shows only the region between the cap-beam-to-girder connection on the positive moment side of the cap beam to the girder ends. The middle girder is at the top of the figure and the exterior girder is on the bottom. It was observed a strut appears to be developing from the middle girder to the exterior girder. The compressive stress was present the full depth of the deck. In the grillage model, to capture this behavior a strut should be placed from the middle girder, just after the connection, to the exterior girder, prior to the end diaphragm. The thickness should be the thickness of the deck, 4 in. An

analysis was ran in which the deck slab was sliced between the girders except for the strut path suggested.

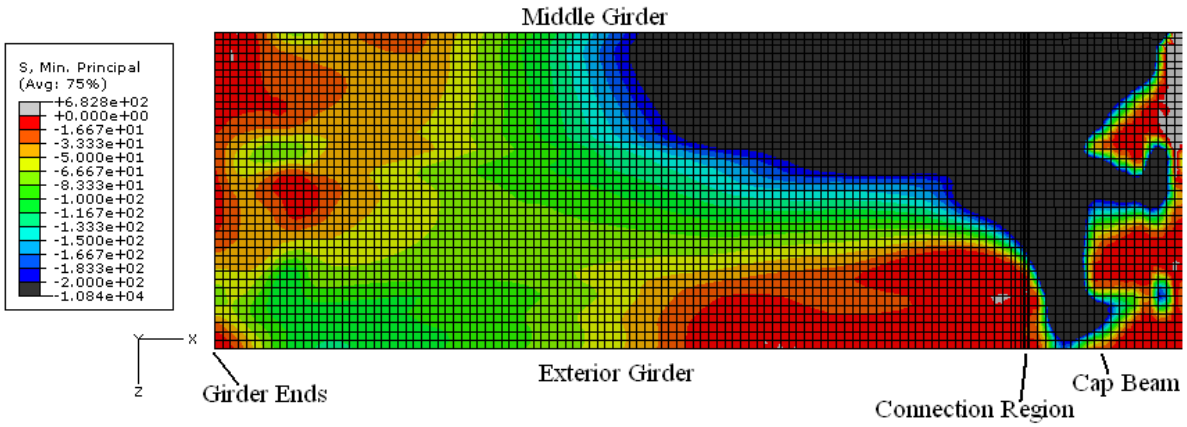


Figure 6.35. Principal compressive stress distribution

From the previous analysis cases with an elastic cap beam, the capacity from the combining the end reactions of each girder on the positive moment side was all about 12,000 lbs. The combined capacity was about double that of the single girder model. In the multiple girder model, there are two full girder-to-diaphragm connections. One connection at the intermediate girder and the middle girder and exterior girder combine to make the second connection. Therefore, with an elastic cap beam, the section resisted the same amount as two single girder models. However, in the actual test unit case, the capacity at the rotation 0.01 rad. was only 8,600 lbs. The cap beam must be cracking and causing a drop in stiffness of the positive moment side of the cap beam. To capture the behavior, the grillage model must include nonlinear behavior in the cap beam. To provide the necessary response in the grillage model, the cap beam must behave in such a manner as presented below in Figure 6.36. The moment vs. rotation behavior presented was captured by modeling the cap beam, diaphragm and deck. The width was taken as 60 in. which was the distance from the end of each cap beam ledge. The height was taken from the bottom of the cap beam to the top of the deck, 38 in. All

the cap beam reinforcement was included. The resulting piece that was analyzed is shown below in Figure 6.37.

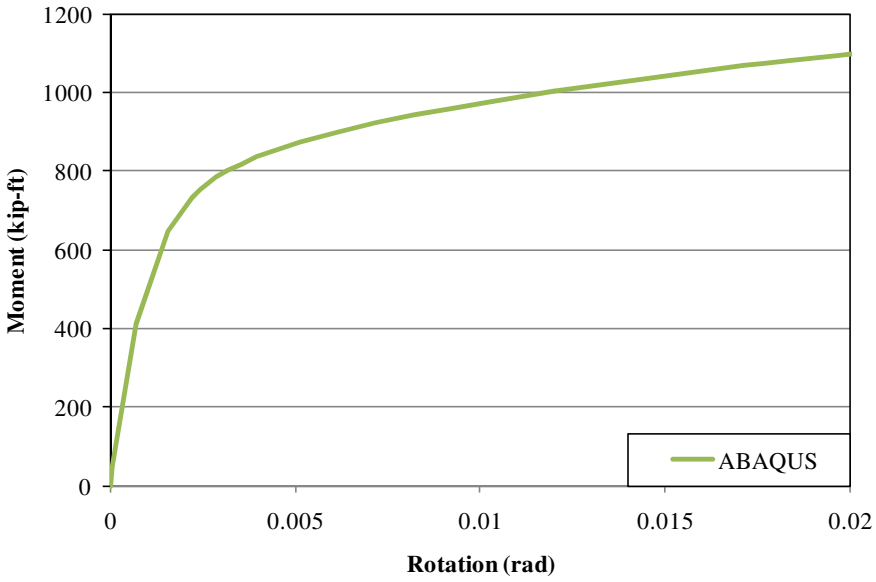


Figure 6.36. Cap beam moment vs. rotation behavior from ABAQUS

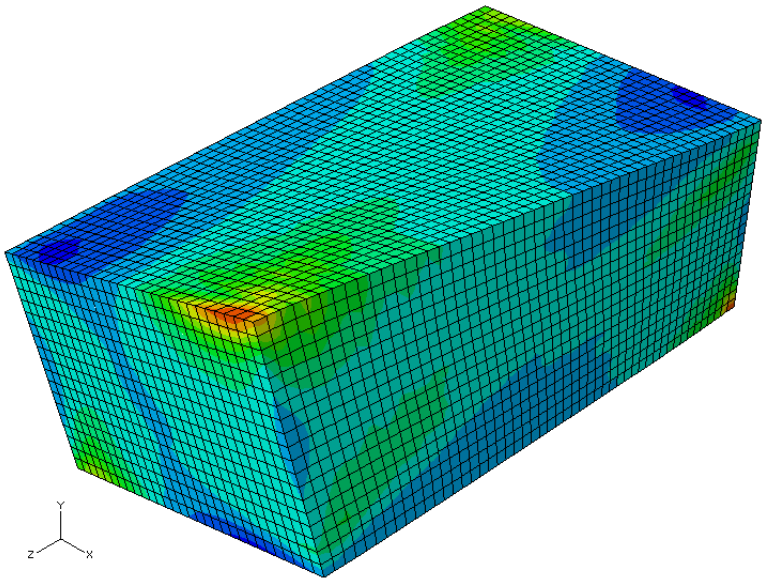

Figure 6.37. Cap beam element used for torsion analysis

## 6.6 Proposed Connection

### 6.6.1 Overview

The proposed connection that was tested consisted of an unstressed prestressing placed the length of the modeled test unit in ABAQUS and grouted in the girders and cap beam. In the actual test unit that will be built for testing, the strand will be placed from the cap beam to the girder end on one side only, as shown in Figure 6.38, to allow for the new and existing connection to be tested in one setup. Information will be presented below providing evidence as to why the grouting was necessary along the length of the girder. The purpose of the connection is to contribute to the positive moment capacity in the girder-to-cap-beam connection.

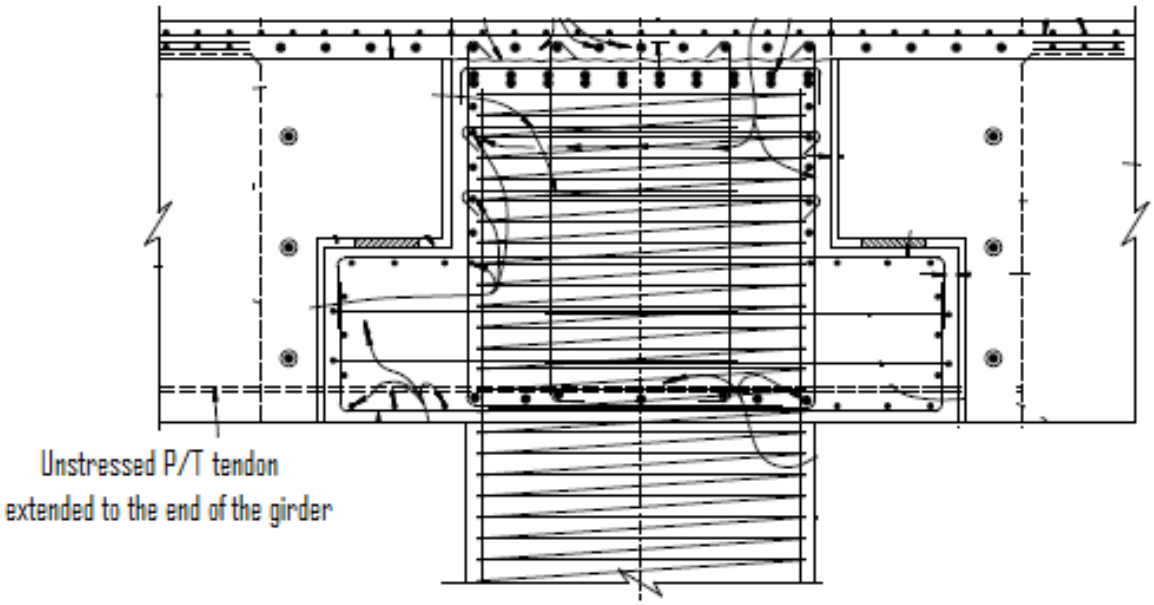


Figure 6.38. Test unit detail for the unstressed prestressing strand

The strand was first placed along the length of the test unit and the vertical and transverse displacements were constrained at key points along the path: girder ends and cap beam edges. Once the analysis was completed, the displacement of the girder and strand along the length of the girder

was checked to see if additional points of constraints were needed. Additional points of constraint would have been needed if the strand displaced a greater distance than the radius of the duct it is designed to be placed in. The response of the existing connection is given below in Figure 6.39. In Figure 6.40, the response of the unstressed, ungrouted prestressing strand is shown. The comparison of the responses is presented in Figure 6.41.

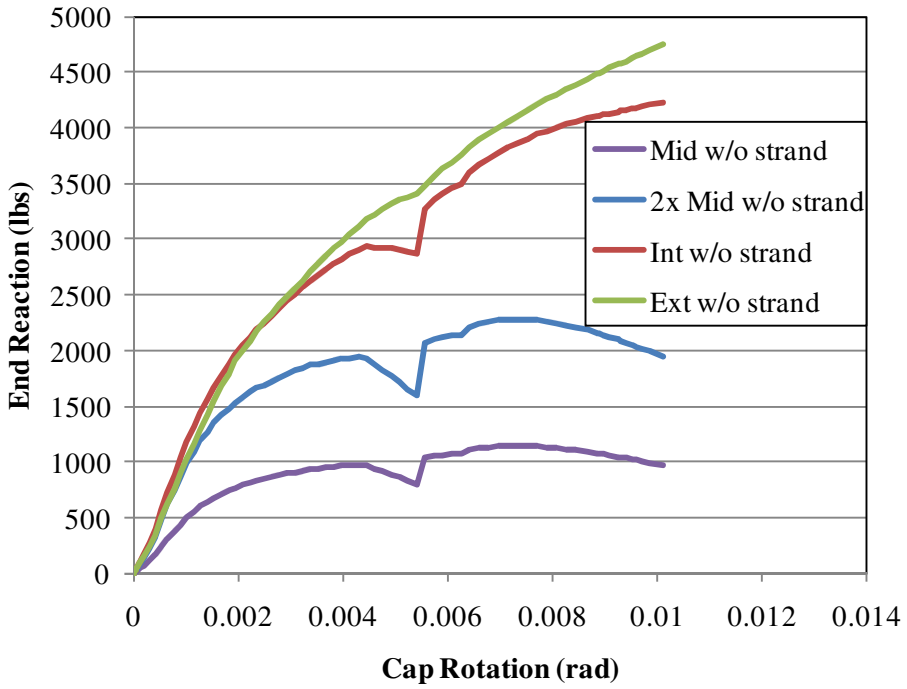


Figure 6.39. Multiple girder cap beam rotation vs. girder end reaction response without the proposed strand

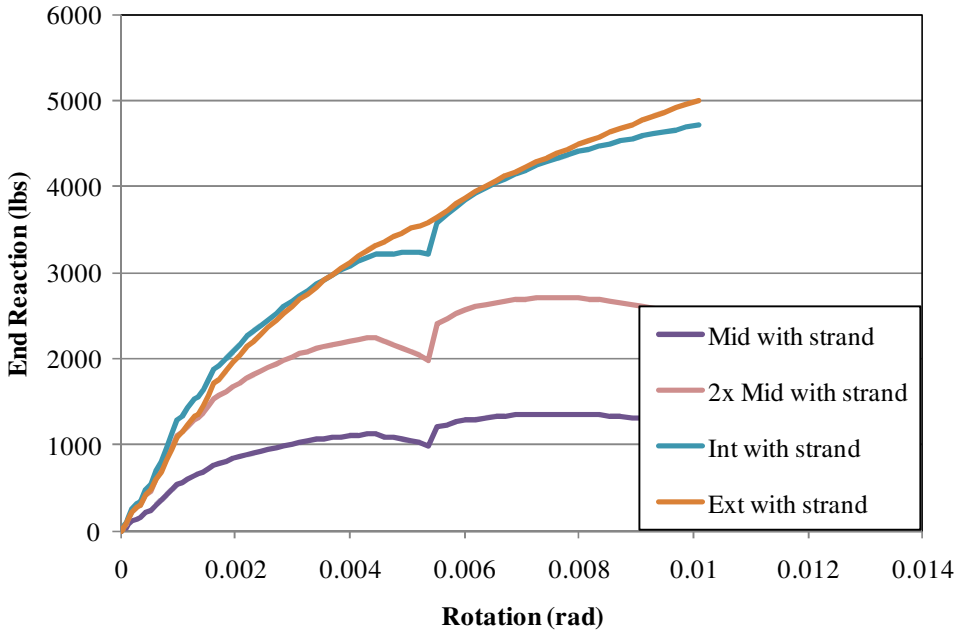


Figure 6.40. Multiple girder cap beam rotation vs. girder end reaction response with the proposed strand ungrouted

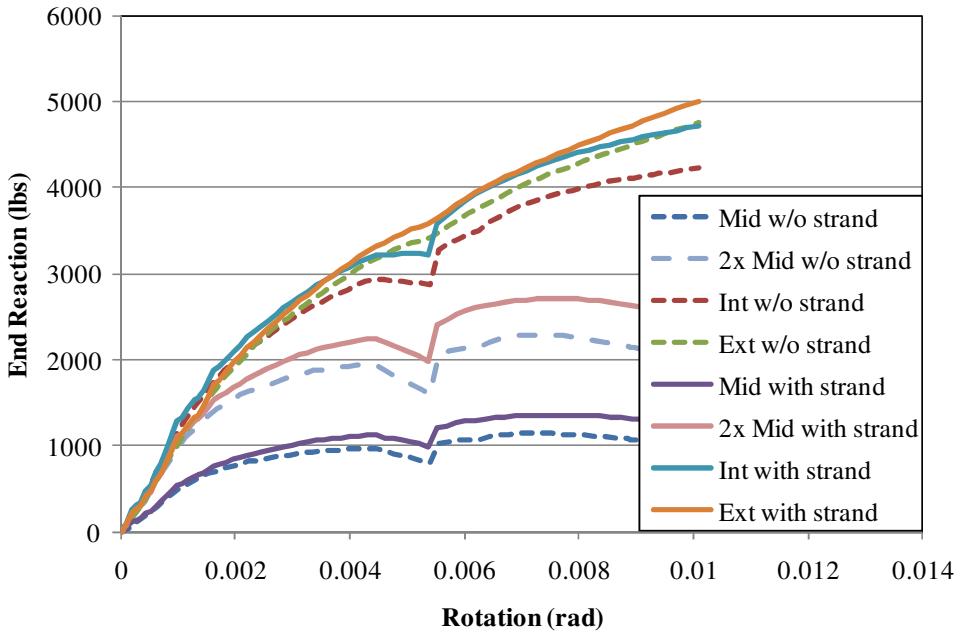


Figure 6.41. Comparison of the effectiveness of the ungrouted strand

The additional capacity from the ungrouted strand is minimal after a comparison of the two responses. To understand the response, the gap displacements were then compared at each of the girders. For all the girders, the change in gap opening was negligible. The displacement comparisons are presented in Figure 6.42. With the gap displacements, the strain in the strand was calculated and compared to the value from the model. For the center girder, the gap displacement at a rotation of .01 rad was 0.28 in. and the strand was unrestrained a length of 320 in. The resulting strain was calculated to be 0.000875 in./in. Multiplying the strain by the elastic modulus of the prestressing steel, a stress of 25.375 ksi was obtained. The next step was to check the analysis model to see if the values were the same. From the ABAQUS model, the strain was 0.0075 in./in. and a resulting stress of 21.3 ksi. The calculated values were higher than the model predicted but within 15%.

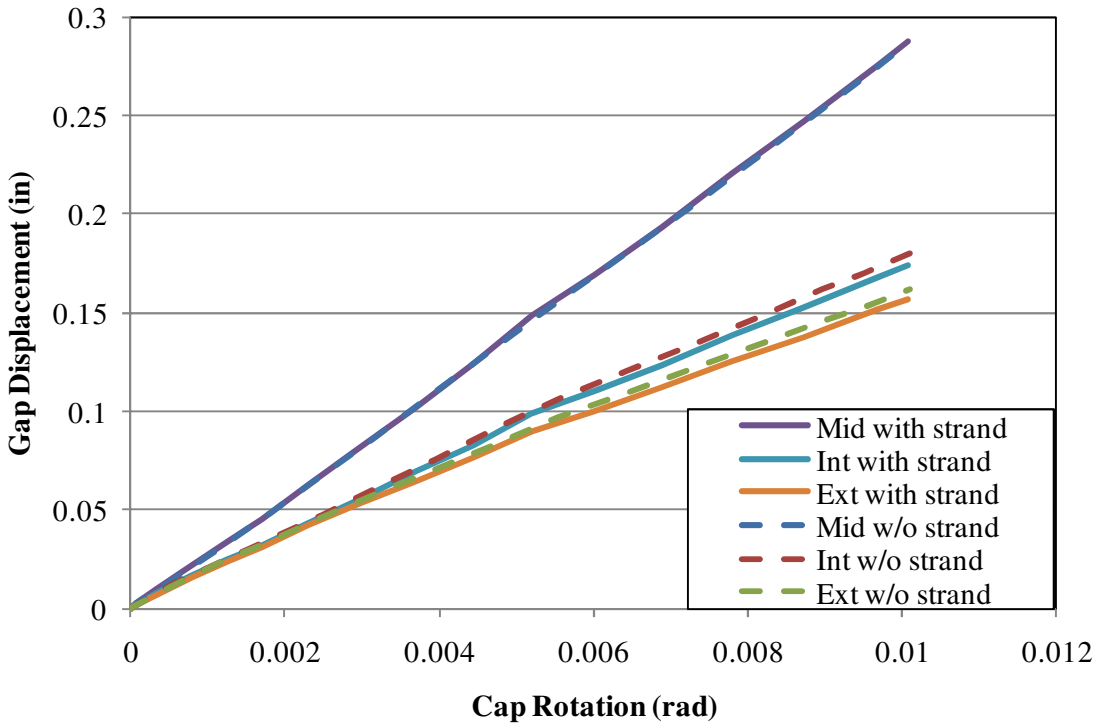


Figure 6.42. Comparison of gap openings between the current connection and unstressed, ungrouted prestressing strand connection

With the strain and stress comparison completed, the additional moment capacity was then calculated. From the ABAQUS model the distance from the neutral axis to the prestressing strand was obtained, 22 in. The distance from the neutral axis to the top of the slab was also obtained, 16 in. To calculate the additional moment, the force in the strand was found from the stress and multiplied by the distance to the centroid of the compression force. The distance to the centroid of the compression force, 32.33 in., was calculated by adding the distance of the steel from the neutral axis to 2/3 the height of the compression depth. The resulting compression force was estimated to be at 2/3 the height because the additional moment capacity calculation was performed to obtain a quick estimate of the amount of additional capacity would be generated to verify the model was predicting an accurate response. The steps taken to obtain the additional end reaction from the middle girder are presented below. Table 6.1 provides the values for all three girders.

$$\varepsilon = \frac{0.28\ in.}{320\ in.} = .000875\ \frac{in.}{in.}$$

$$\sigma = 0.000875 \frac{in}{in} * 29000\ ksi = 24.94\ ksi$$

$$F = 24.94\ ksi * 2 * (0.085\ in^2) = 4.24\ kips$$

$$Add'l\ Moment\ Capacity = 4.24\ kips * \frac{32.33\ in.}{12} = 11.42\ \ kip - ft$$

$$Add'l\ End\ Reaction = \frac{11.42\ kip - ft.}{27\ ft.} = 0.43\ kips$$

Table 6.1. Additional girder end reaction from ungrouted connection

| | | Displacement | Strain | Stress | Force | Add'l Moment | Add'l End Reaction |
|---|---|---|---|---|---|---|---|
| | | in. | in./in. | ksi | kips | kip-ft | kips |
| Girder | Middle | 0.28 | 0.000875 | 25.38 | 4.31 | 11.62 | 0.43 |
| | Intermediate | 0.18 | 0.000563 | 16.31 | 5.55 | 14.94 | 0.55 |
| | Exterior | 0.16 | 0.0005 | 14.50 | 4.93 | 13.28 | 0.49 |

The additional end reactions combined (1.47 kips) are larger than the analysis prediction of 1.017 kips, the reason for the discrepancy was the neutral axis was measured at the middle girder and used for all three connections. However, the calculations show that the unstressed strand is ineffective in providing a positive moment connection. The next step was to suggest a change that would make the connection more effective. The suggestion was to grout the strand along the full length. By doing this, the strain in the strand would increase since the gap displacement would be acting over a much shorter length of strand. Since the strand would be full grouted and there are no gaps along the strand, the length of strand effective in resisting the gap opening would be the length of strain penetration. The strain and stress was obtained from the analysis with the fully grouted strand and were significantly higher than previously, 0.02 in./in. and 241.7 ksi, respectively. The resulting force from the strands at the middle girder cap-beam-to-girder connection was 41.089 kips. The response from ABAQUS is presented below in Figure 6.43. The capacity of the connection more than doubles, going from a combined end reaction of 9.948 kips to 23.415 kips. The capacity was calculated from the Middle, Intermediate and Exterior girders. The doubled middle girder capacity was not used. The capacity required to be resisted for the plastic hinge was 650 kip-ft., which was half of the required value of 1300 kip-ft. obtained from the grillage analysis. The proposed connection capacity will exceed the required values at 0.0018 rad. of cap rotation. At that rotation, the reinforcing bars between the cap beam and diaphragm, along with the girder-to-diaphragm connections remain elastic. The cap-to-diaphragm reinforcing bars yield at 0.002 rad. and the girder-to-diaphragm connection

yields at 0.005 rad. The proposed unstressed strand remains elastic until a rotation of 0.0055 rad. At that rotation, the moment capacity of the model was 1416 kip-ft. That is for 2 ½ girders, not the full 5 girders that would contribute to the formation of the plastic hinge. Therefore, the proposed unstressed, grouted prestressing strand would be sufficient in providing the additional resistance for the plastic hinge to form in the column during a seismic loading. With the capacity sufficient, the damage would be primarily in the column, as the column would be more cost effective and require a shorter time to repair than repairing the superstructure, which is desired by the capacity design philosophy.

The comparison of girder openings was then compiled and presented in Figure 6.44. The gaps are much smaller with the strand, as expected. The strands are grouted fully along the length and are embedded within the girder, diaphragm and cap beam. This allows for the strand to be fully effective in resisting the gap opening that was occurring in the previous analyses.

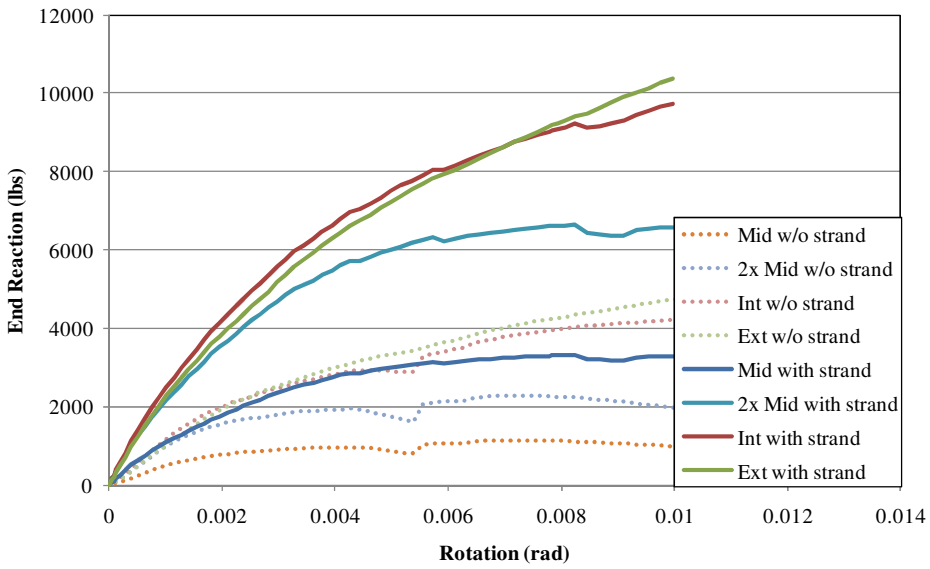


Figure 6.43. Comparison of gap openings between the current connection and unstressed, fully grouted prestressing strand connection

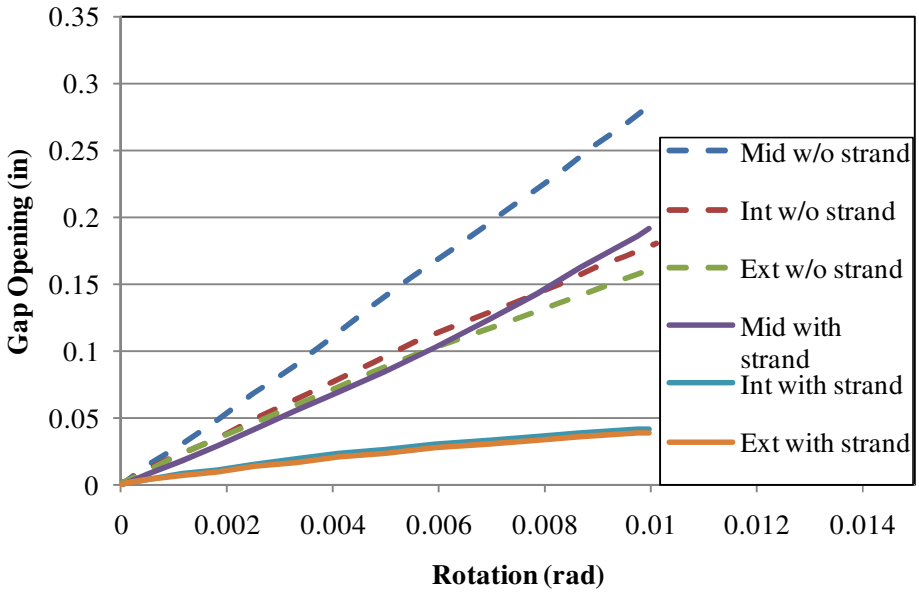


Figure 6.44. Gap displacements of the girders with and without the proposed strand

### 6.6.2 Test Unit connection response validation

The actual test unit protocol is to displace the girder ends in a cyclic manner in the longitudinal direction of the bridge to generate the moment in the cap beam from the column. All the previously mentioned effects were captured by rotating the cap at the column centerline where the moment would be transferred to the column. To verify that rotating the cap beam end will provide the same results as the testing protocol, one-half of an elastic column, with the same effective cross section as the grillage model used for the test unit, was modeled in the ABAQUS model. The effective cross section was obtained from the idealized moment-curvature analysis response of the plastic hinge section. The radius of the cross-section was taken as 11.33 in. The modulus of elasticity for the elastic concrete was 3604996 psi, which corresponds to 4 ksi concrete. With the column in place, the girders remained on rollers while the cap beam pinned boundary condition was removed. One end of the girders was displaced laterally to the maximum displacement before the

model could not converge. The modeled test unit with the column is shown in Figure 6.45 and Figure 6.46, and the displaced shape is shown in Figure 6.47.

The model was analyzed to compare three different connection setups. The first setup was with the current, unretrofitted cap-beam-to-girder connection on both sides of the cap beam which is referred to as the as-built setup. Second, the analysis was performed with one connection to include the unstressed, prestressing strand placed from one end of the girders to the opposite edge of the cap beam, referred to as the testing setup, as shown in Figure 6.38, since the test unit will be detailed in that way for the scaled testing. The third analysis was performed with the strands placed the full length of the test unit, since the retrofitted connection will be grouted from one end of the bridge structure to the opposite end, referred to as the full connection.

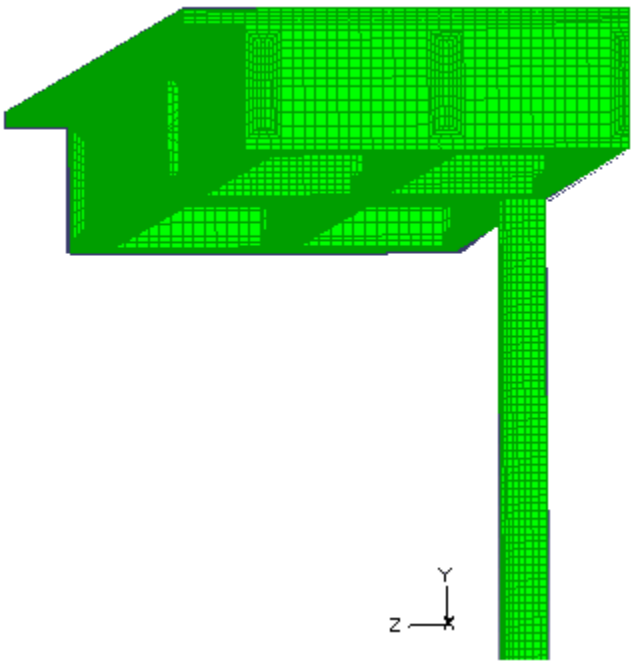


Figure 6.45. Angled view of test unit model with column

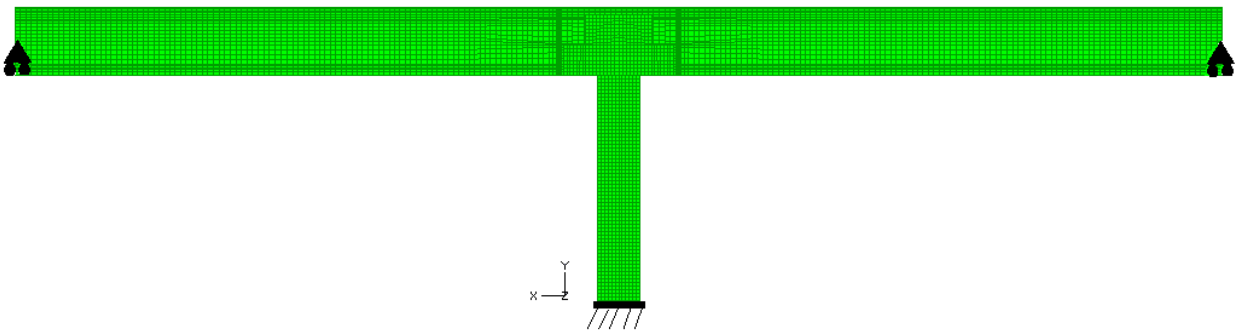

Figure 6.46. Side view of test unit model with column showing the boundary conditions

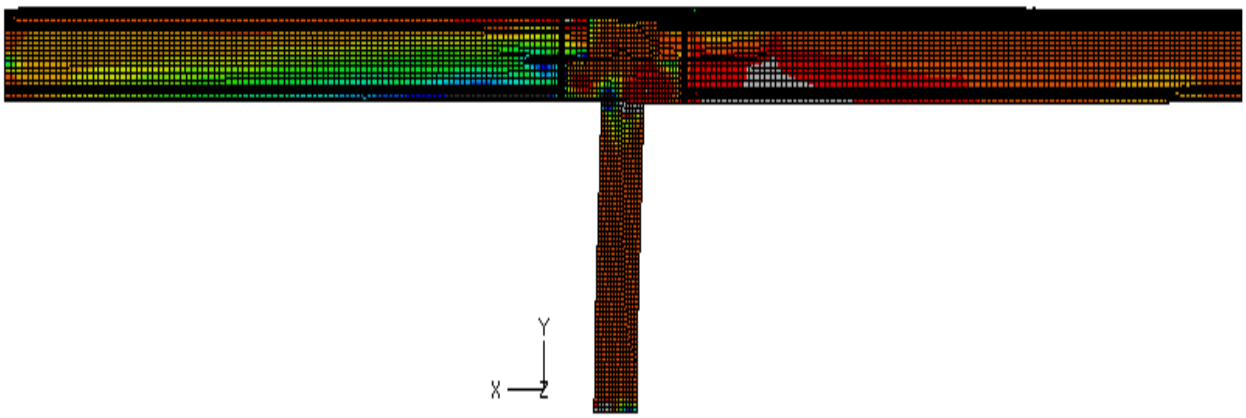

Figure 6.47. Displaced shape with stress contours

Previously, an analysis was performed to take into consideration the effect of the strand on the moment capacity of the girder-to-cap beam connections. The strand was expected to greatly improve the moment capacity; however, the main purpose of this analysis was to capture the effects the strand would have on the current force distribution between the girders. The connection performance of the as-built case is given in Figure 6.48 and Figure 6.49. The performance will be compared to the other two connection cases.

The full connection case is shown in Figure 6.50 and Figure 6.51. The as-built case is shown in the figures as the dashed lines. The end reactions increase significantly on the positive moment side of the cap beam since the moment capacity in the connection has increased due to the prestressing strand. The gap displacement was decreased significantly when compared to the as-built case, similar response was shown in Figure 6.44 corresponding to the cases compared previously. One observation to note was the resistance of negative moment side decreased due to the significant increase in the positive moment cap-beam-to-girder connection stiffness. Another observation in the response is the exterior girder no longer resists the most load on the positive moment side in the testing setup case. The unstressed strand yields at a rotation of 0.0044 rad. where the moment resistance from both connections was 1062 kip-ft. The moment required to create a plastic hinge was 650 kip-ft. The proposed connection would be more than sufficient in developing the plastic hinge and remain effective in future seismic attacks.

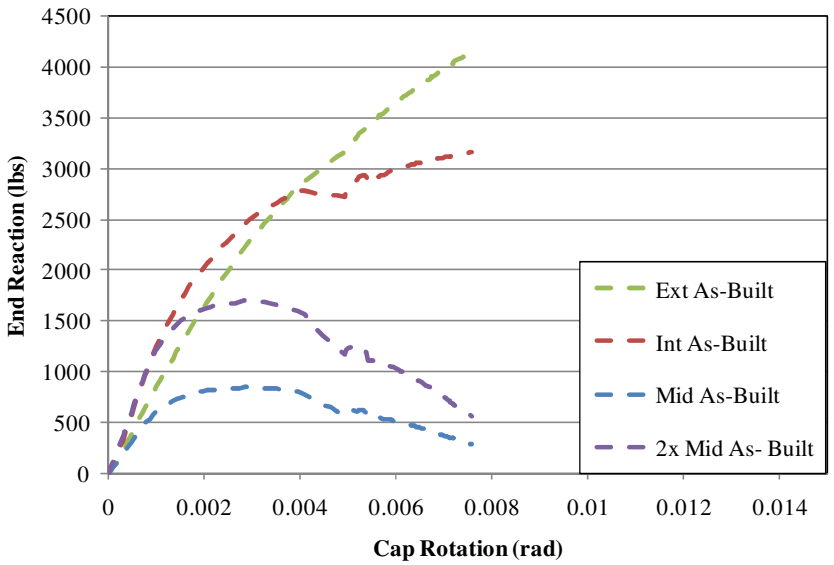


Figure 6.48. End reaction of the positive moment connect side from the as-built case

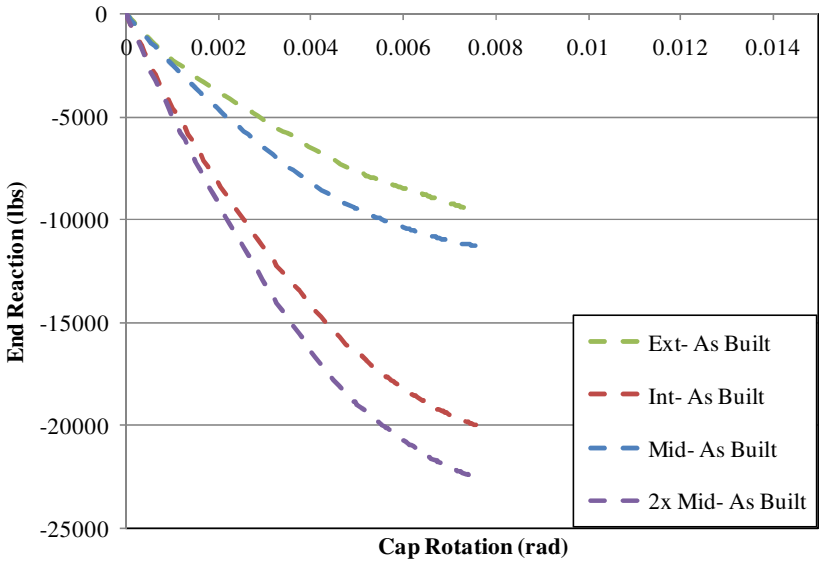


Figure 6.49. End reaction of the negative moment connection side from the as-built case

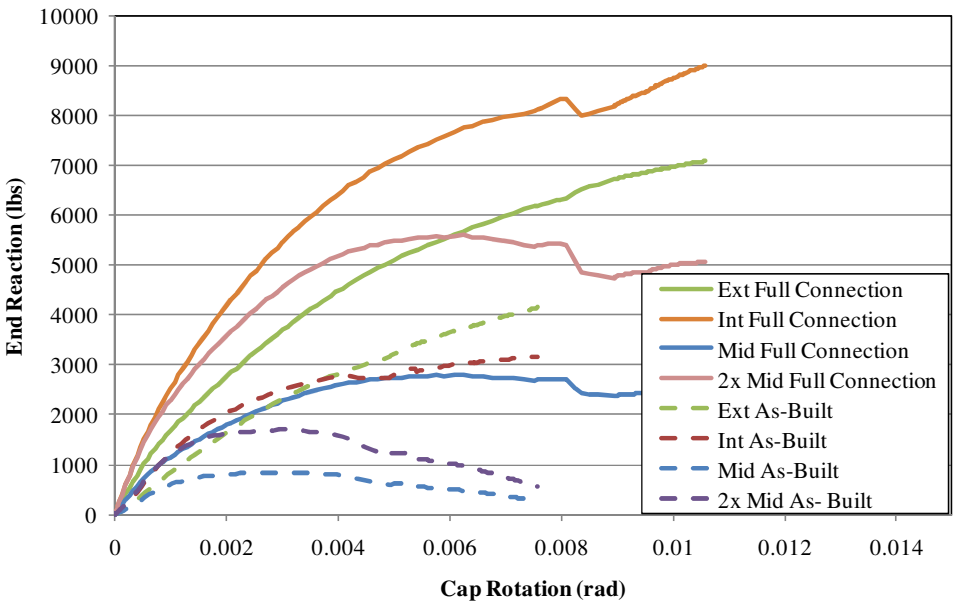


Figure 6.50. End reaction comparison of the positive moment connection side of the as-built and full connection

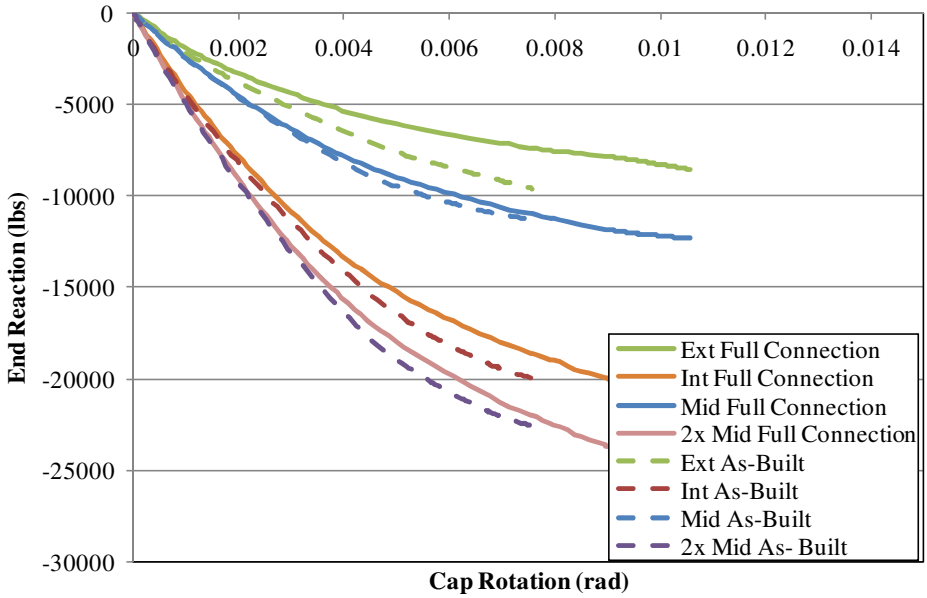


Figure 6.51. End reaction comparison of the negative moment connection side of the as-built and full connection

The third case, the testing setup, is shown below in Figure 6.52 and Figure 6.53 when the proposed connection resists the positive moment. The analysis was performed to ensure that the response from the test unit was properly capturing the response from a system with the full connection and the existing connection.

To make the comparison the results from the full connection analysis were plotted on the respective graphs. The comparison of the connection behavior on the positive moment side of the cap beam between the full connection and testing setup until a cap rotation, resulting from the lateral displacement, are nearly identical. At a rotation of 0.008 rad. the full connection setup drops in capacity slightly. The drop occurs right after the strands exceed 240,000 psi and at that stress, the stress-strain stiffness behavior of the prestressing steel becomes significantly softer. The cap beam rotation where the behavior changes between the two setups would not be achieved in the lateral load testing because the plastic hinge would've formed much sooner and once the plastic hinge is formed

any further rotation of the cap beam would not occur. On the negative moment side, the resistance provided in the testing setup will be less than in the full connection. The full connection includes the strand which would affect the connection stiffness since the strand would resist an additional force when in compression. However, through a rotation of 0.005 rad., the difference in the end reactions is minimal and the plastic hinge should is expected to be fully developed prior to that rotation. The difference in the response after 0.005 rad. was due to the strand continuing to resist the load in an elastic manner as the concrete in the diaphragm between the girder and cap beam begins to crush. With the strand present, the additional load is resisted and the cap beam does not rotate as much. Therefore referring to Figure 6.53, since the full connection resists less load than the as built connection, the test set up also will provide less moment resistance than the as built connection. However, the difference in the resistance was small in magnitude and the overall behavior was unchanged. The test setup should capture a comparable behavior of a bridge structure with the proposed unstressed prestressing strand included in the girder-to-cap-beam connection on both sides of the cap beam.

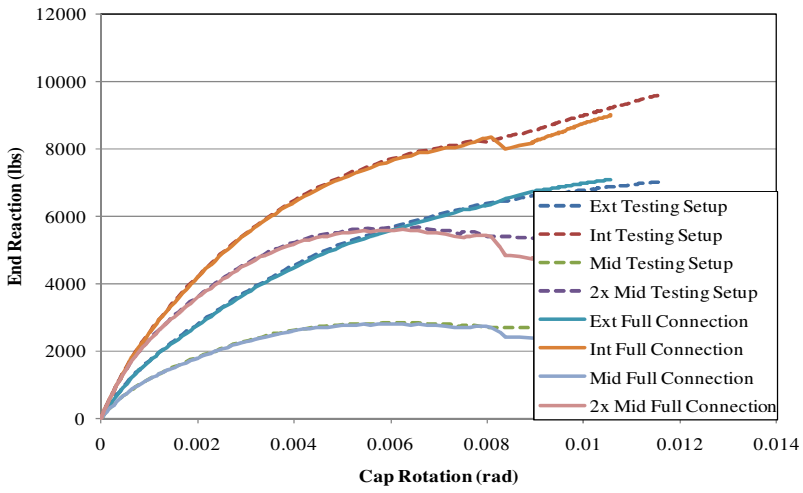


Figure 6.52. End reaction comparison of the positive moment connection side of the testing setup and full connection

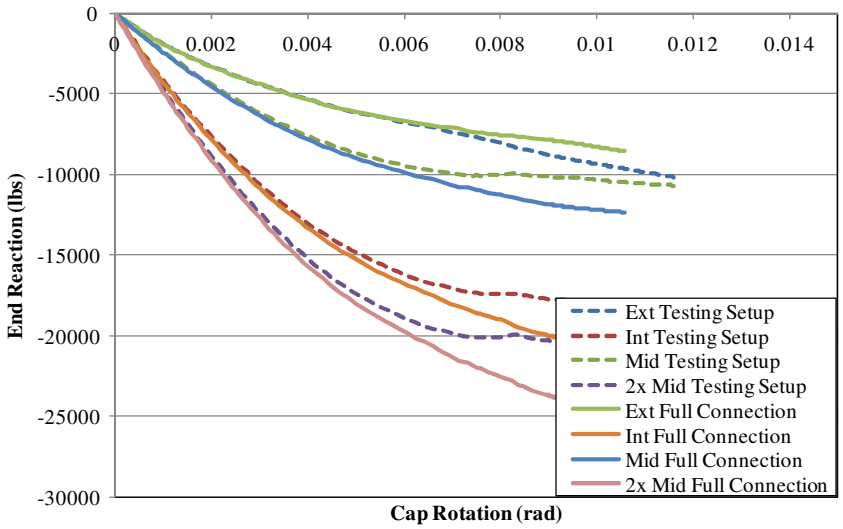


Figure 6.53. End reaction comparison of the negative moment connection side of the testing setup and full connection

# Chapter 7. CONCLUSION

The following are the conclusions that were provided from the analytical investigation presented in the previous chapter:

- The damaged plasticity model in ABAQUS is capable of modeling the effect of confinement on concrete. However, the unconfined material properties had to be modified to allow for the confined results to match closely.
- However, the concrete material property is unable to accurately model the tensile behavior of concrete under flexure. The tensile stress cannot be reduced to zero stress after cracking due to convergence problems.
- The behavior of the current cap-beam-to-girder connection of an inverted-tee cap beam bridge with precast girders results from the capacity of the deck slab in parallel with the cap-beam-to-diaphragm reinforcing bars and the girder-to-diaphragm reinforcing bars acting in series.
- The current connection would cause concrete in the deck to crack, the cap-beam-to-diaphragm reinforcing bars to yield and the girder-to-diaphragm bars to yield. Once the reinforcing bars yield, the moment capacity achieved from the post-yielding strength of the bars may be enough to create a plastic hinge in the top of the column.
- A proposed connection would ensure the moment capacity in the cap-beam-to-girder region to be sufficient in resisting the required moment to form a plastic hinge in top and bottom of the column.

- The proposed connection consists of an unstressed, grouted prestressing strand placed in the bottom web of the precast girders and through the cap beam. Grouting is required to develop the additional moment capacity.
- The deck of the bridge has a large affect on the behavior and distribution of forces between the girders. The middle girder connection resists the most moment, according to the gap displacement between the cap beam and girder, but the girder end reaction measures the least force. The deck develops a strut which transfers the force from the middle girder out to the exterior girder. Consideration needs to be taken in the grillage model to capture the affect.
- The end diaphragms on the Test Unit actively transfer the force from the exterior girder back into the middle girder and intermediate girder. Consideration also needs to be taken in the grillage model to capture the affect.
- The assumed girder stiffness in the grillage model influences the resulting stiffness in the system initially and after yielding. The assumed girder stiffness values must be developed by incorporating the respective moment demands from the analysis.

With the above recommendations for the grillage model and the proposed connection the large-scale testing can be performed with a degree of confidence. The proposed connection should perform well to adequately develop the plastic hinge and the test setup should allow for the response of the two connections to be captured. The full testing results will be presented with recommendations for future work in the future report (Snyder, 2010).

# BIBLIOGRAPHY

AASHTO. (2003). *LRFD bridge design specifications, 3rd Ed.* Washington, D.C.

Abdalla, K. M., Alshegeir, A., & Chen, W. F. (1996). Analysis and Design of Mushroom Slabs with a Strut-Tie Model. *Computers and Structures , 58* (2), 429-434.

ACI Committee 318. (2005). *ACI 318-05: Building Code Requirements for Structural Concrete and Commentary.* Farmington Hills, MI: ACI.

Almer, K., & Sanders, D. (2007, November). *23th US - Japan Bridge Engineering Workshop.* Retrieved January 2009, from Public Works Research Institute: http://www.pwri.go.jp/eng/ujnr/tc/g/pdf/23/23-8-2sanders.pdf

Alshegeir, A., & Ramirez, J. (1992). Computer Graphics in Detailing Strut-Tie Models. *Journal of Computing in Civil Engineering , 6* (2), 220-232.

Bentley Systems, Inc. (2008). CONSPAN Rating v. 8.0.

Biggs, R. M., Barton, F., Gomez, J., Massarelli, P., & McKeel, W. J. (2000). *Finite Element Modeling and Analysis of Reinforced-Concrete Bridge Decks.* Charlottesville: Virginia Department of Transportation.

Caltrans. (1995, October). *Bridge Design Aids.* Retrieved May 2008, from California Department of Transportation: http://www.dot.ca.gov/hq/esc/techpubs/manual/bridgemanuals/bridge-design-aids/bda.html

Caltrans. (1995). *Bridge Design Aids.* Sacramento.

Caltrans. (2003). *Bridge Design Specifications.* Sacramento.

Caltrans. (2006). *Seismic Design Criteria.* Caltrans, Sacramento.

Caltrans. (2006). *Seismic Design Criteria, v. 1.4.* Sacramento.

Chen, W.-F., Yamaguchi, E., Kotsovos, M., & Pan, A. (1993). Constitutive Models. *Finite Element Analysis of Reinforced Concrete Structures II* , 36-117.

Chowdhury, M. R., & Ray, J. C. (1995). Further Considerations for Finite-Element Analysis. *Journal of Structural Engineering , 121* (9), 1377-1379.

Dassault Systemes Simulia Corporation. (2008). *ABAQUS v6.8* . Providence, RI.

Federal Highway Administration. (2008). *National Bridge Inventory*. Retrieved January 2009, from Department of Transportation: http://www.fhwa.dot.gov/BRIDGE/nbi/ascii.cfm?year=2008

Freyermuth. (1969). Design of Continuous Highway Bridges with Precast, Prestressed Concrete Girders. *PCI Journal* , 14-39.

Harisis, A., & Fardis, M. (1991, March). Computer-Aided Automatic Construction of Strut-and-Tie Models. *Structural Concrete* , 533-538.

Hastak, M., Mirmiran, A., Miller, R., Shah, R., & Castrodale, R. (2003). State of Practice for Positive Moment Connections in Prestressed Concrete Girders Made Continuous. *Journal of Bridge Engineering* , 267-272.

Hillerborg, Modeer, & Petersson. (n.d.). Analysis of crack formation and crack growth n concrete by means of fracture mechanics and finite elements.

Holombo, J., Priestley, M. N., & Seible, F. (1998). *Longitudinal Seismic Response of Precast Spliced-Girder Bridges.* San Diego: University of California, San Diego.

Internation Federation of Structural Concrete. (2007). *Seismic Bridge Design and Retrofit - Structural Solutions* (Vol. 39). Lausanne, Switzerland: FIB.

Lee, J., & Fenves, G. (1998). Plastic-Damage Model for Cyclic Loading of Concrete Structures. *Journal of Engineering Mechanics , 124* (8), 892-900.

Lubliner, J., Oliver, J., Oller, S., & Onate, E. (1989). A plastic-damage model for concrete. *Internation Journals of Solids and Structures , 25* (3), 299-326.

Ma, Z., Chaudhury, S., Millam, J., & Hulsey, J. L. (2007). Field Tests and 3D FE Modeling of Decked Bulb-Tee Bridges. *Journal of Bridge Engineering , 12* (3), 306-314.

Miller, R., Castrodale, R., Mirmiran, A., & Hastak, M. (2004). *Connection of Simple-Span Precast Concrete Girders for Continuity.* Washington, DC: National Cooperative Highway Research Program.

Mosalam, K., Naito, C., & Khaykina, S. (2002). Bidirectional Cyclic Performance of Reinforced Concrete Bridge Column-Superstructure Subassemblies. *Earthquake Spectra , 18* (4), 663-687.

Park, H., Kim, Y., & Uhm, T. (2005). Direct inelasitc strut-tie model using secant stiffness. *J. Korean Concrete Institute , 17* (2), 201-212.

Patty, J., Seible, F., & Uang, C.-M. (2002). *Seismic response of integral bridge connections.* Univ. of California, San Deigo, Dept. of Structural Engineering.

Prabha, P., Seetharaman, S., Arul Jayachandran, S., & Marimuthu, V. (2007). *RUM 2007 Papers.* Retrieved March 2009, from Simulia: http://www.simulia.com/locations/india/rum_07_papers.html

Priestley, M. J., Seible, F., & Calvi, G. M. (1996). *Seismic Design and Retrofit of Bridges.* New York: John Wiley & Sons, Inc.

Priestley, M., Seible, F., & Calvi, G. (1996). *Seismic Design and Retrofit of Bridges.* New York: John Wiley & Sons, Inc.

Roylance, D. (2001, February). *Mechanics of Materials* . Retrieved March 2009, from Massachusettes Institute of Technology Open Coursework: http://ocw.mit.edu/NR/rdonlyres/Materials-Science-and-Engineering/3-11Mechanics-of-MaterialsFall1999/7F1B1AAF-92A4-48A8-AB55-24CF00601799/0/fea.pdf

Salmons, J., & McCrate, T. (1977). Bond Characteristics of Untensioned Presetressing Strand. *Journal of Prestressed Concrete Institute , 22* (1), 52-65.

Schlaich, J., & Schafer, K. (1991). Design and Detailing of Structural Concrete Using Strut-and-Tie Models. *The Structural Engineer , 69* (6), 113-125.

Snyder, R. (2010). *Grillage model analysis of the girder-to-cap beam connection of an inverted-tee cap beam bridge structure designed for seismic loadings.* Iowa State University. Masters degree thesis in progress.

Sritharan, S., Vander Werff, J., Abendroth, R., Wassef, W., & Greimann, L. (2005). Seismic Behavior of a Concrete/Steel Integral Bridge Pier System. *Journal of Structural Engineering* , 1083-1094.

State of California. (2007). *Age Profile for California Bridges*. Retrieved January, from California Department of Transporation: http://www.dot.ca.gov/hq/structur/strmaint/agegroup.pdf

Tadros, M., Ficenec, J., Einea, A., & Holdsworth, S. (1993). A New Technique to Create Continuity in Prestressed Concrete Members. *PCI Journal* , 30-37.

Tjhin, T., & Kuchma, D. (2002). Computer-Based Tools for Design by Strut-and-Tie Method: Advances and Challenges. *ACI Structural Journal , 99* (5), 586-594.

TRC/Imbsen Software Systems. (n.d.). WinRECOL, v. 5.0.2.

TRC/Imbsen Software Systems. (n.d.). XTRACT.

U.S. Department of Transportation: Federal Highway Administration. (2008). *National Bridge Inventory*. Retrieved January 2009, from Department of Transportation: http://www.fhwa.dot.gov/BRIDGE/nbi/ascii.cfm?year=2008

Yun, Y. M. (2000). Computer Graphics for Nonlinear Strut-Tie Model Approach. *Journal of Computing in Civil Engineering , 14* (2), 127-133.

Yun, Y. M., & Kim, B. H. (2008). Two-Dimensional Grid Strut-Tie Model Approach for Structural Concrete. *Journal of Structural Engineering , 134* (7), 1199-1214.

# Appendix A. PROTOTYPE DRAWINGS

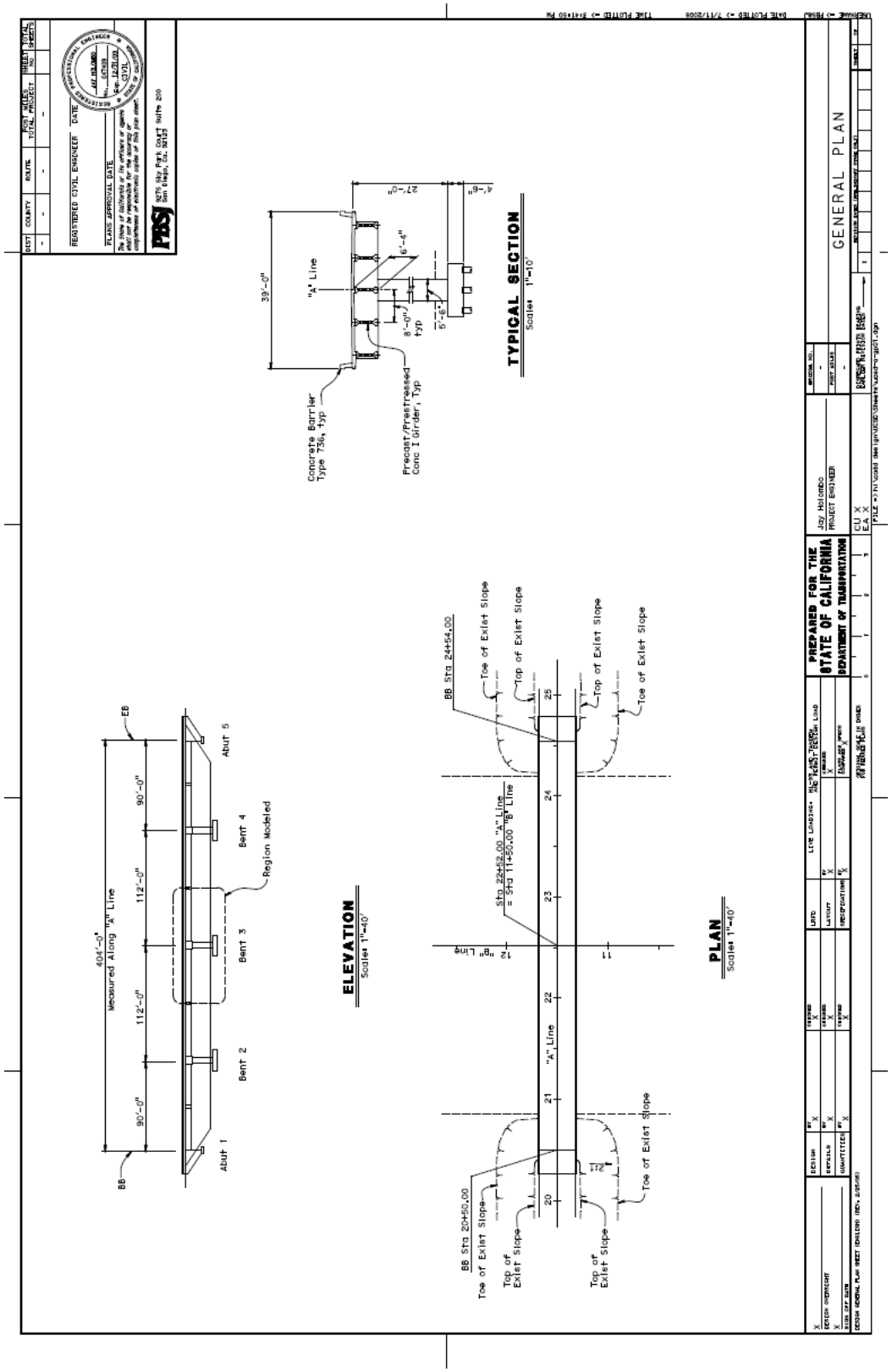


Figure A.1. Prototype drawing 1 of 7

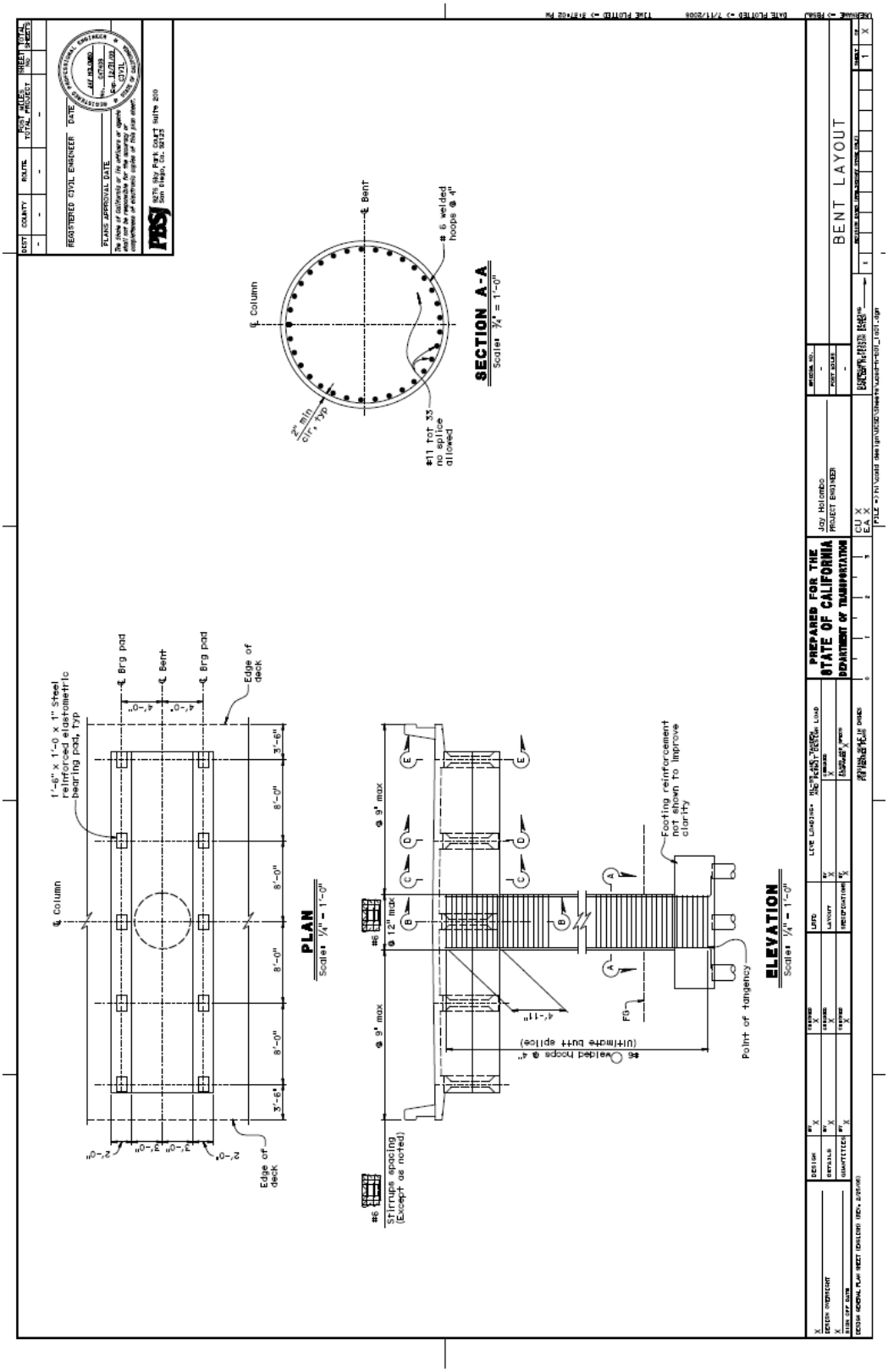


Figure A.2. Prototype Drawing 2 of 7

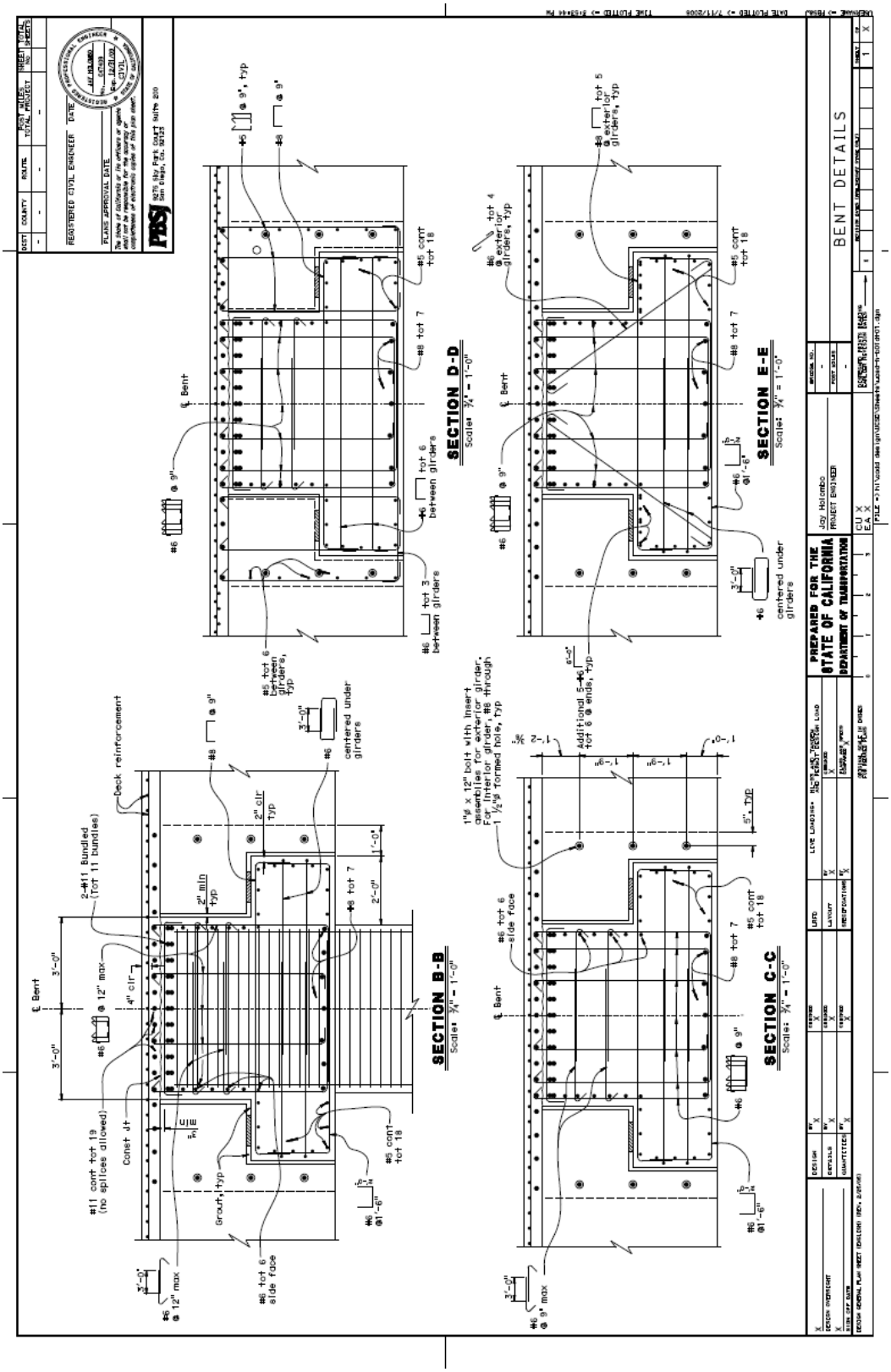


Figure A.3. Prototype drawing 3 of 7

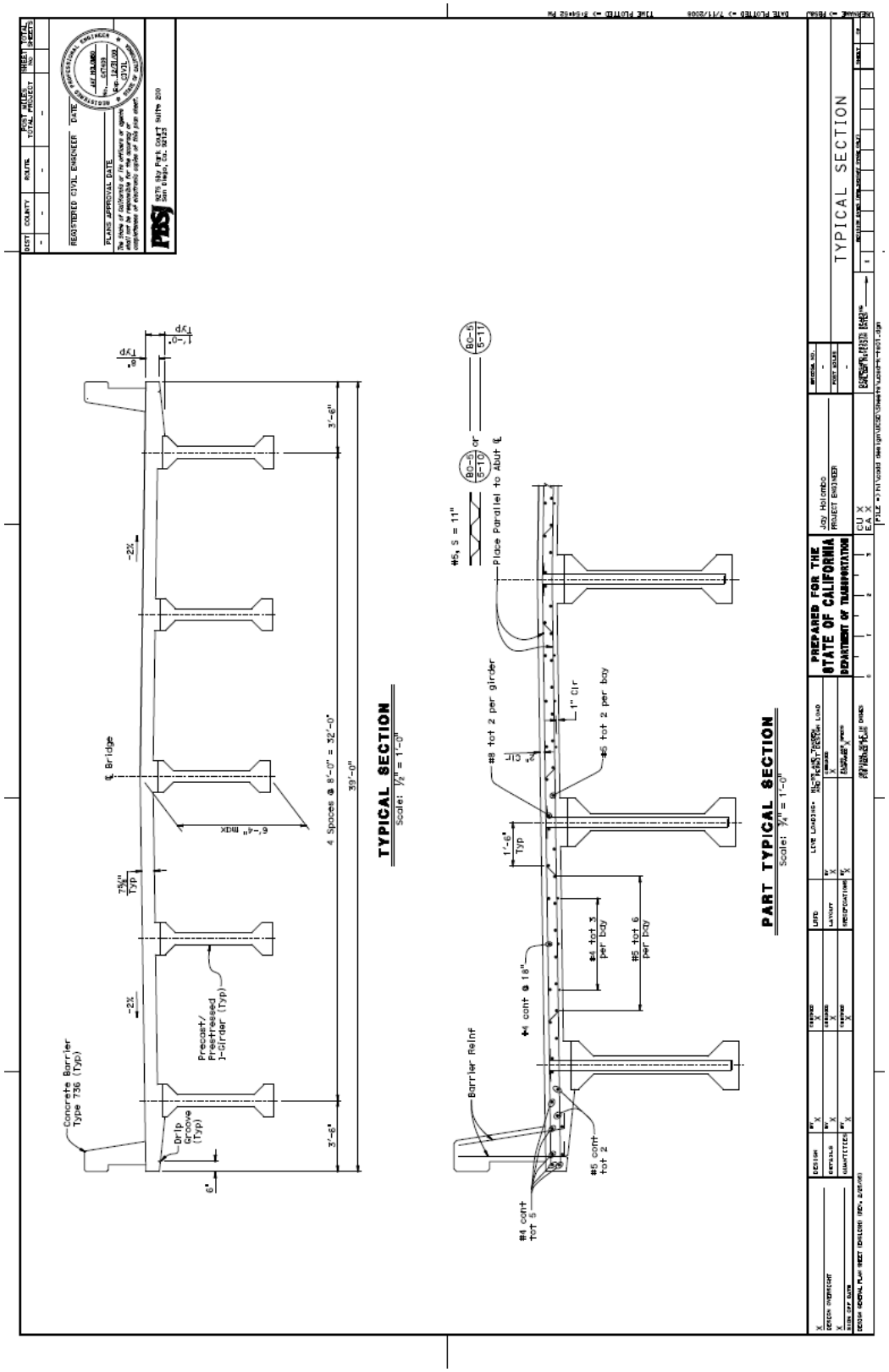


Figure A.4. Prototype drawing 4 of 7

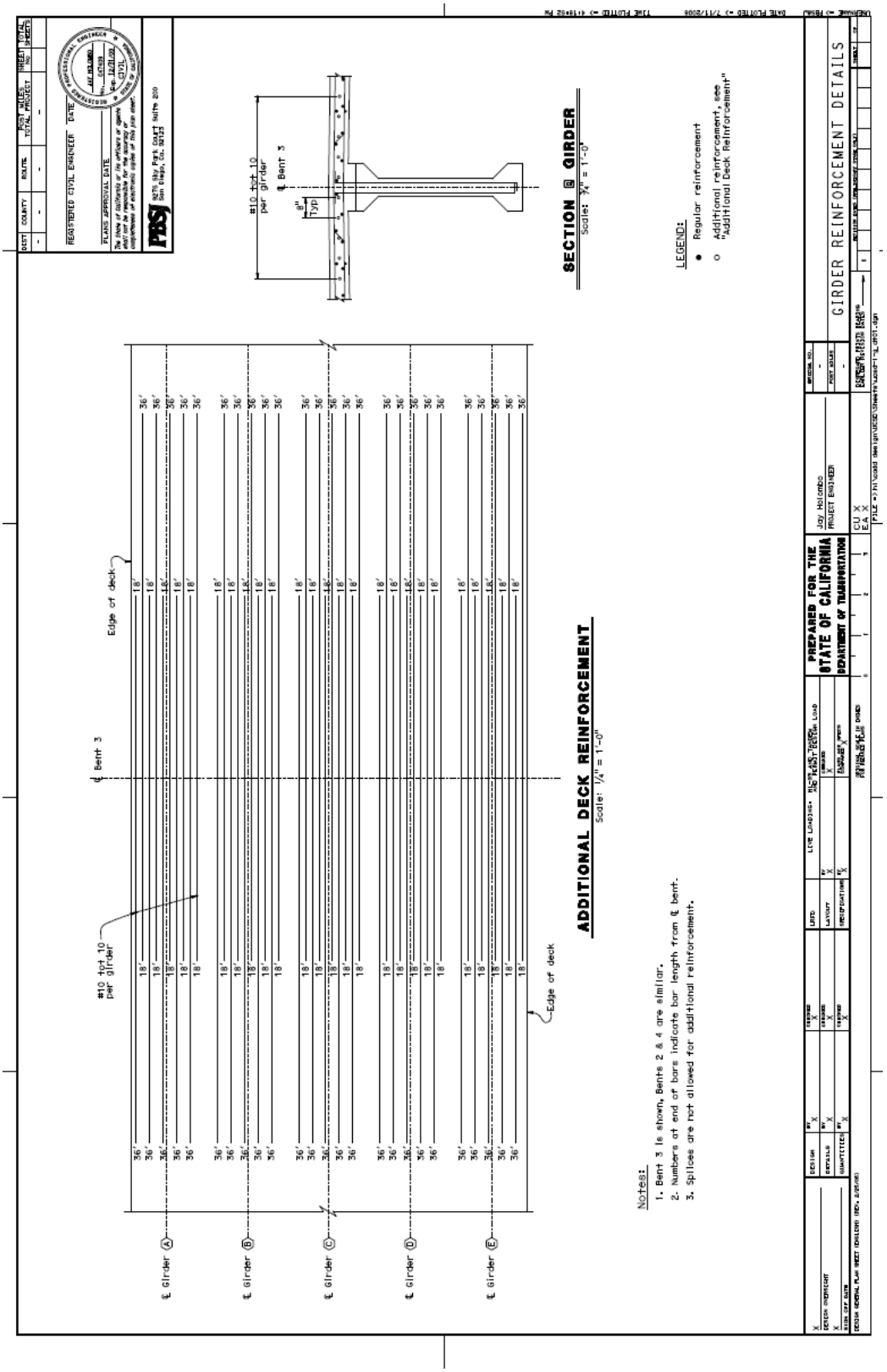


Figure A.5. Prototype drawing 5 of 7

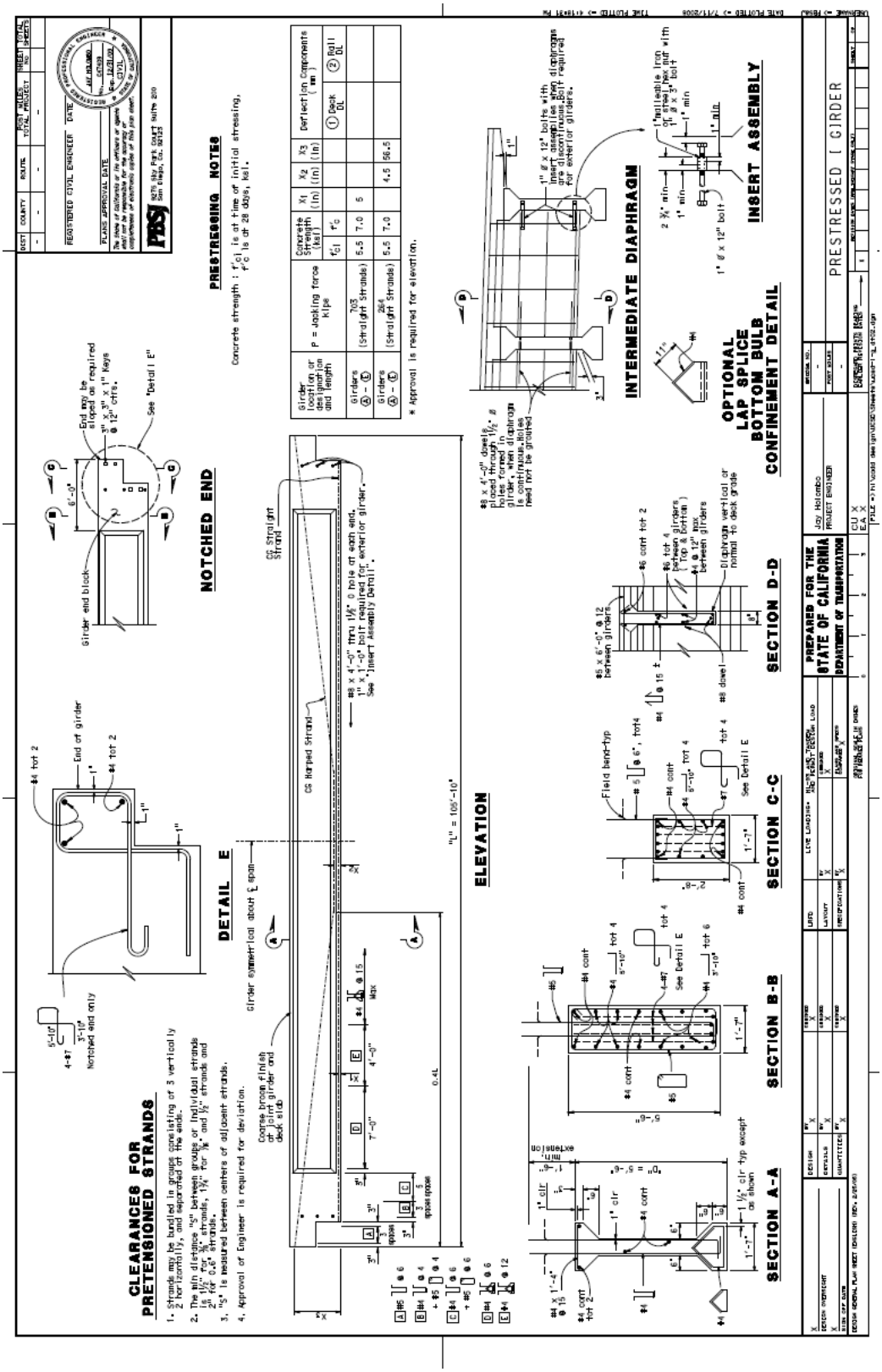


Figure A.6. Prototype drawing 6 of 7

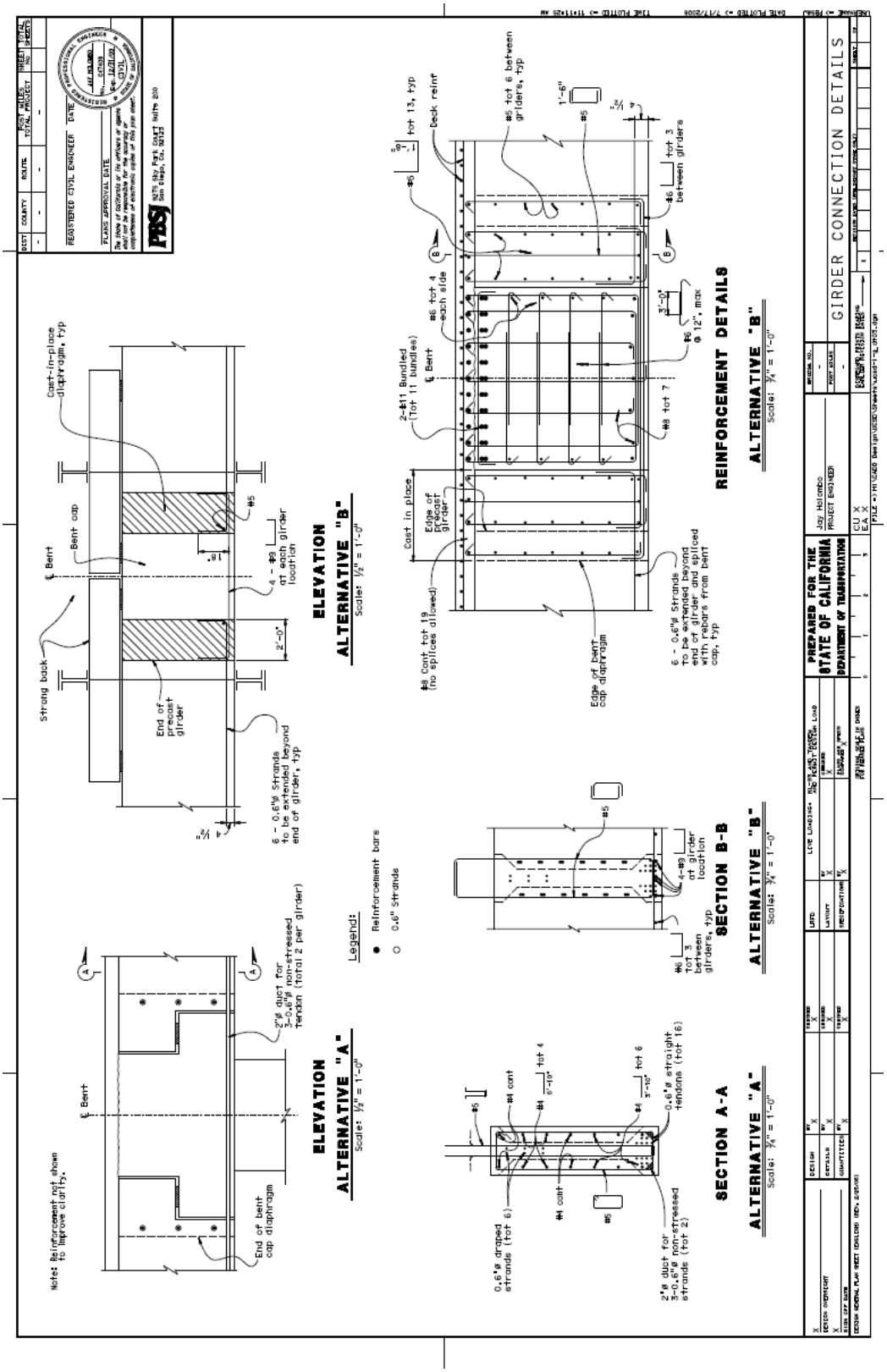


Figure A.7. Prototype drawing 7 of 7

# Appendix B. TEST UNIT DRAWINGS

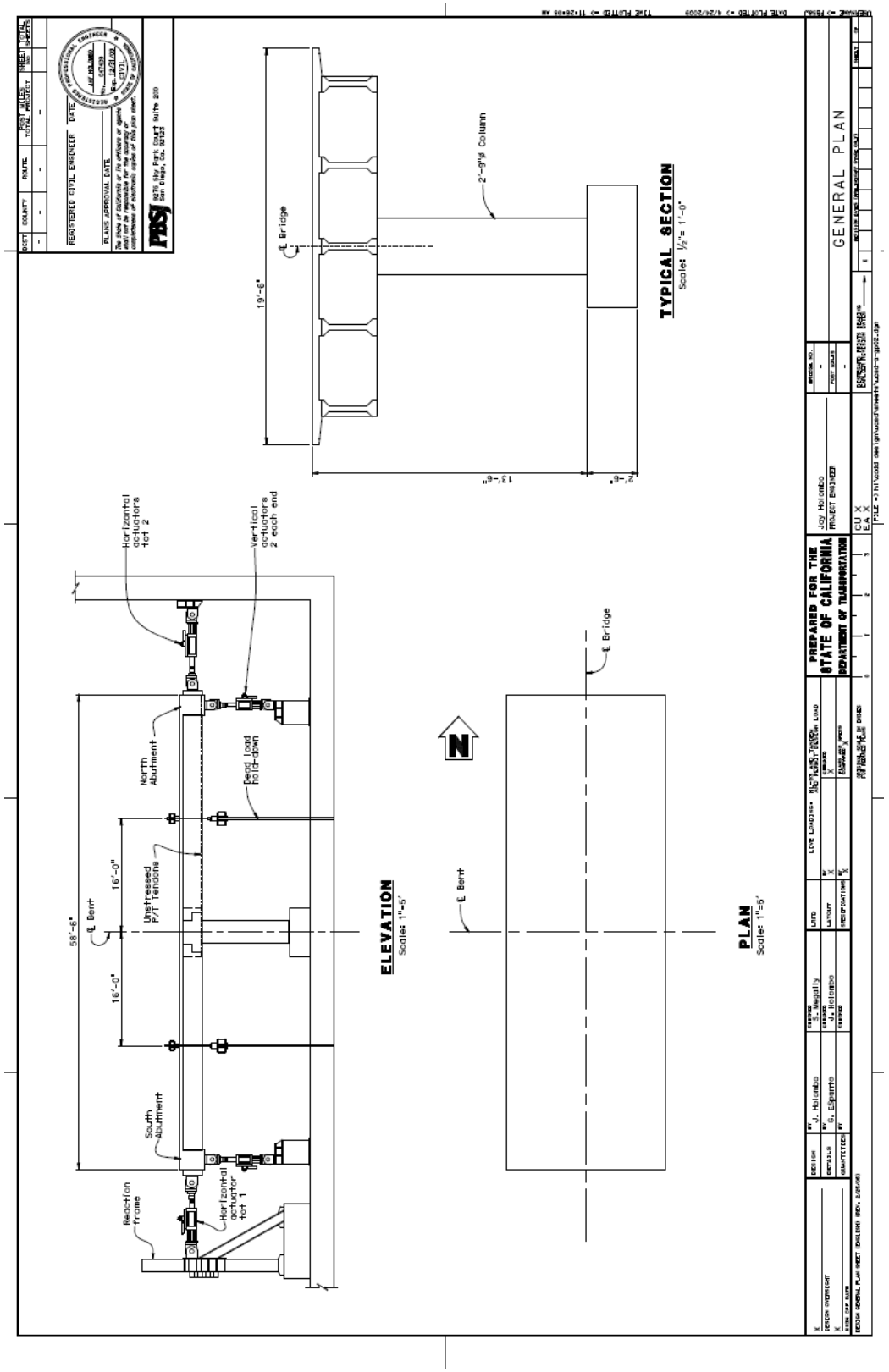


Figure B.1. Test unit drawing 1 of 7

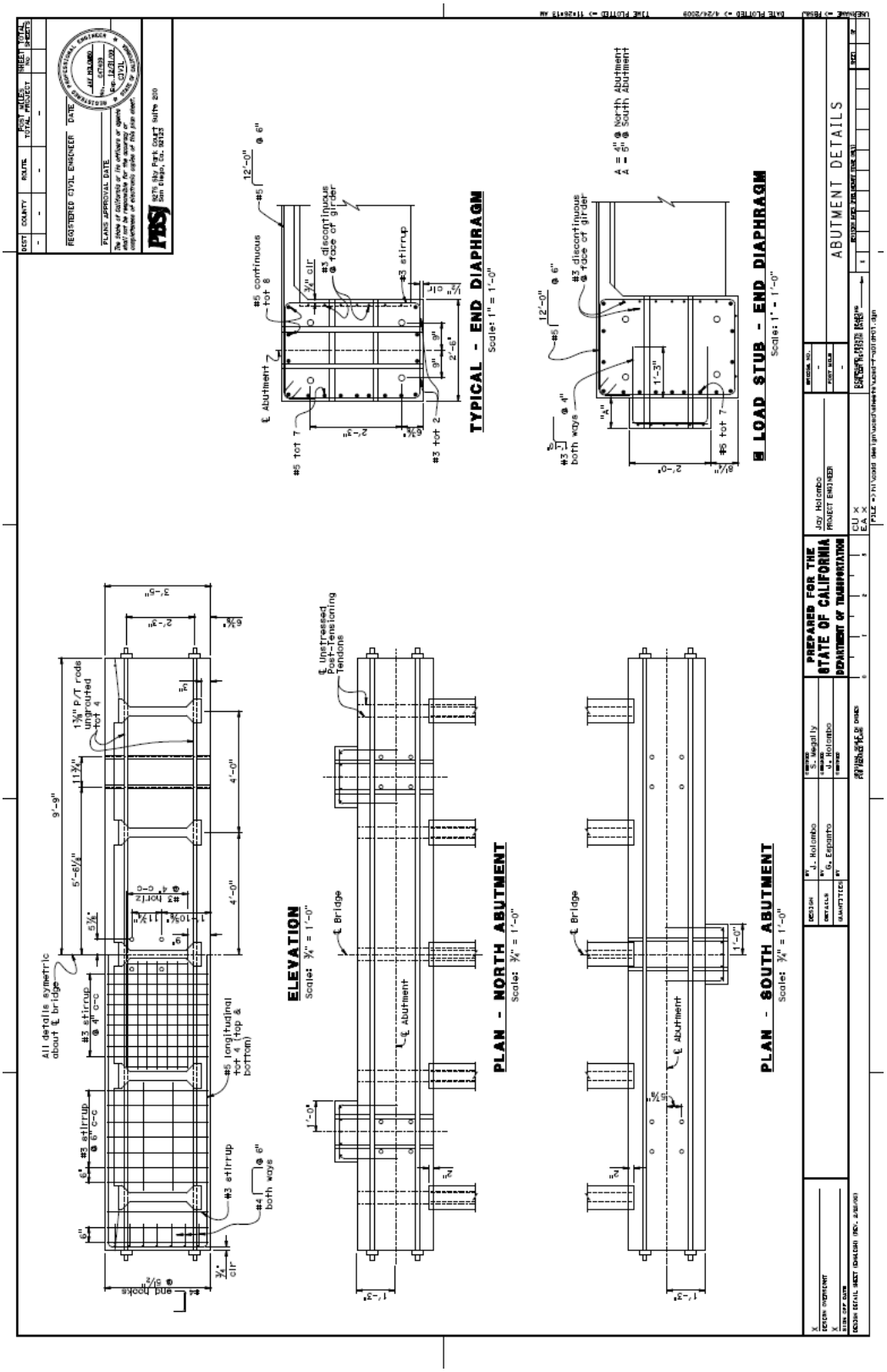


Figure B.2. Test unit drawing 2 of 7

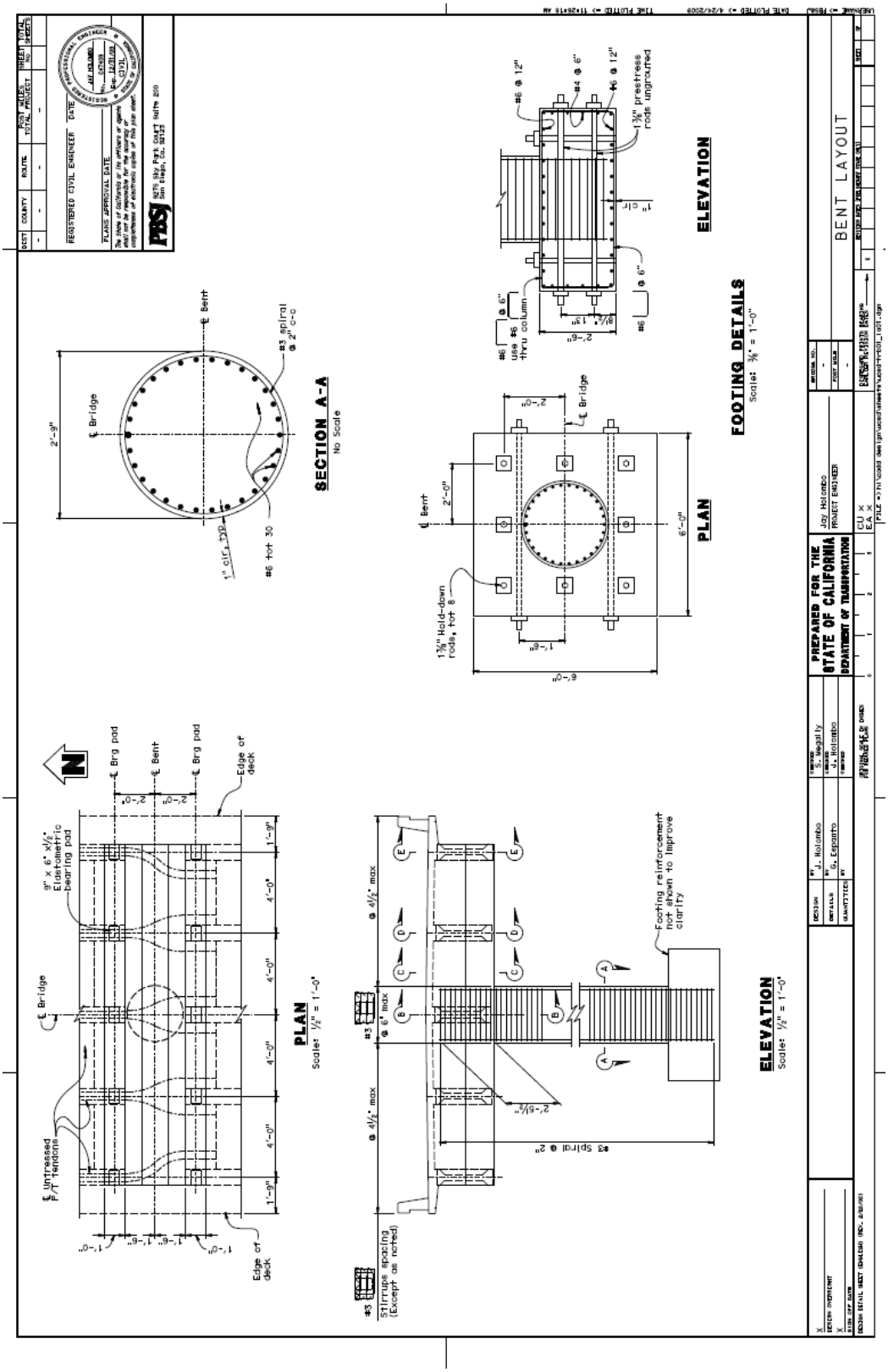


Figure B.3. Test unit drawing 3 of 7

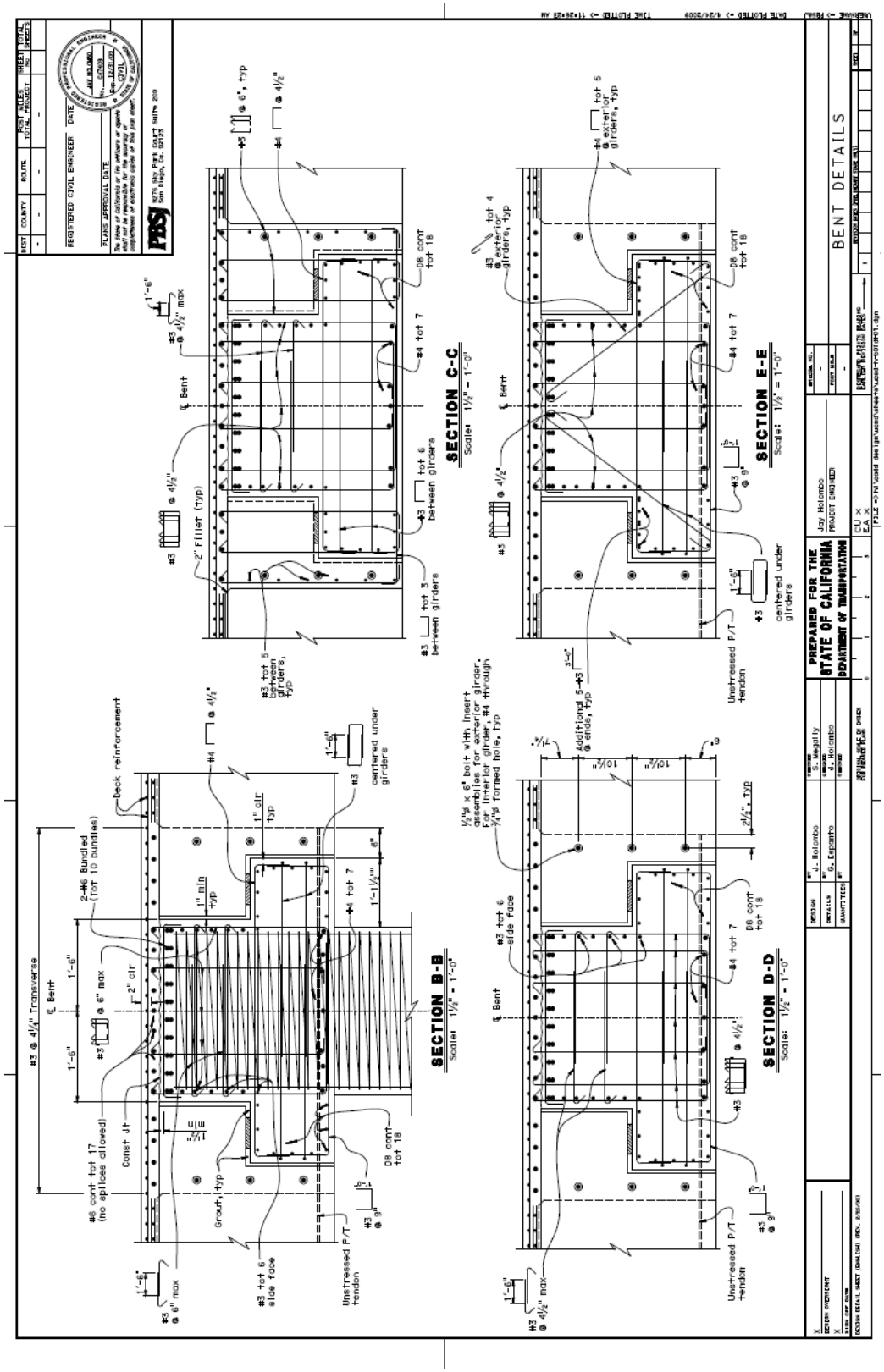


Figure B.4. Test unit drawing 4 of 7

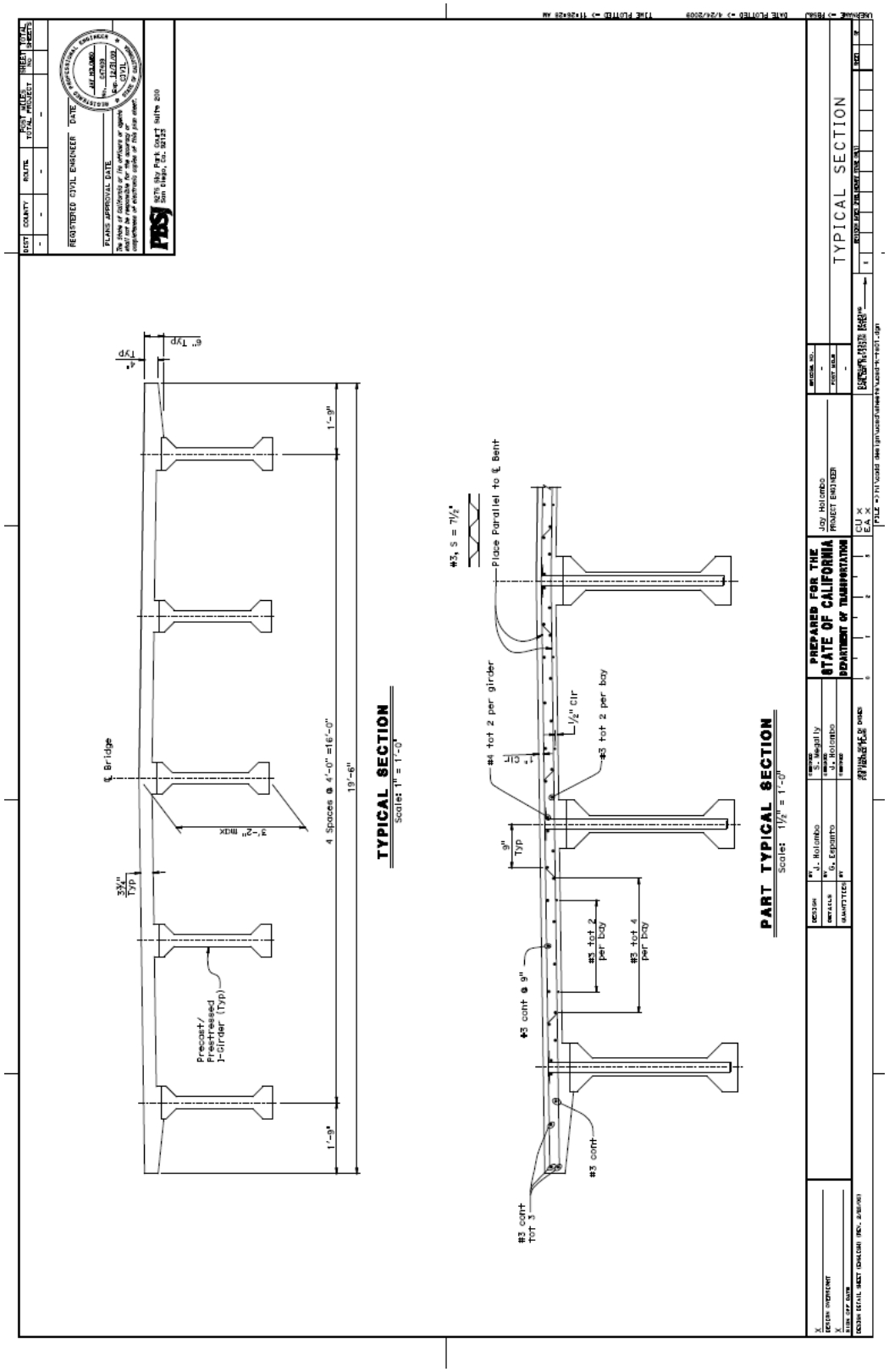


Figure B.5. Test unit drawing 5 of 7

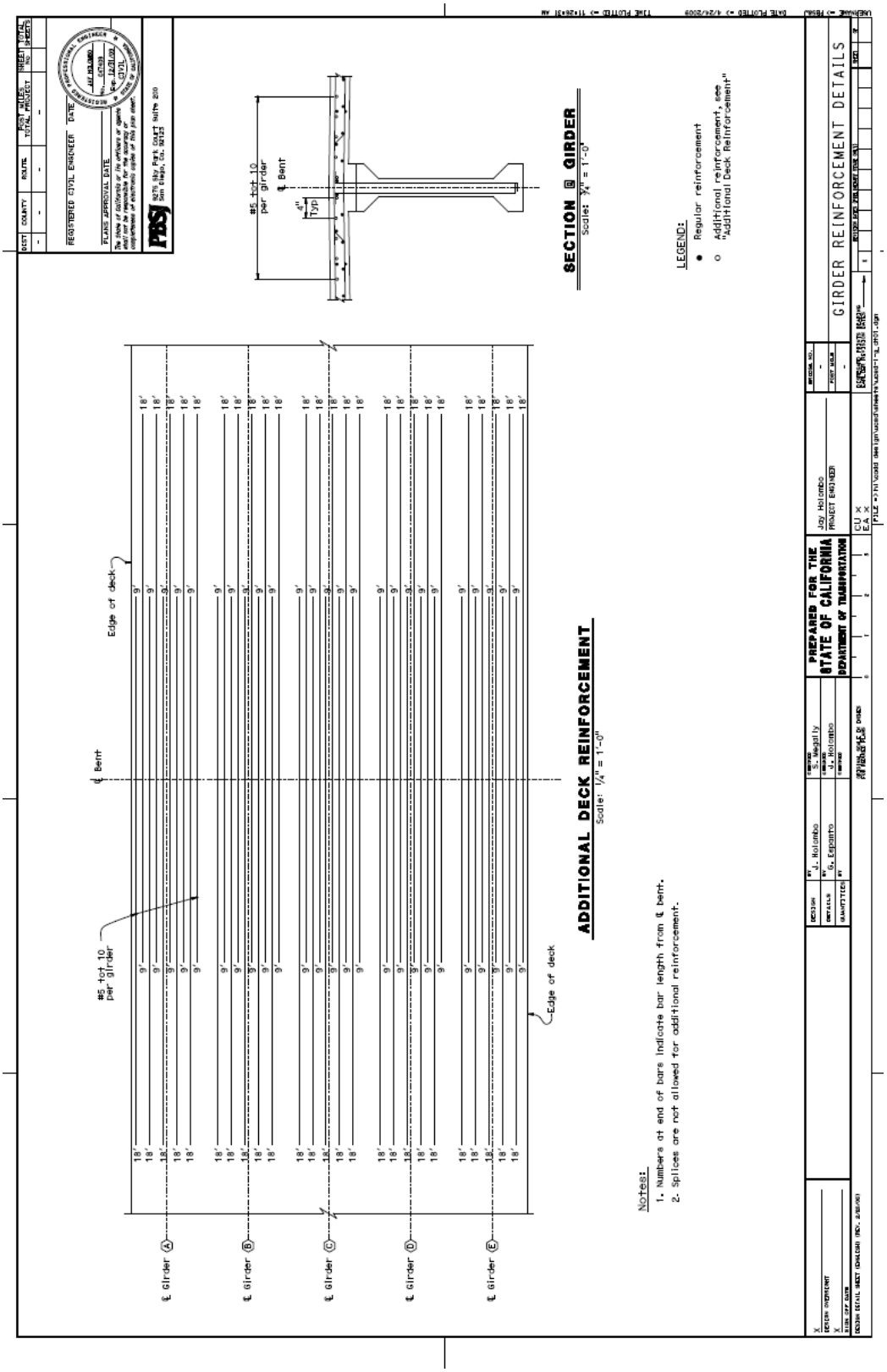


Figure B.6. Test unit drawing 6 of 7

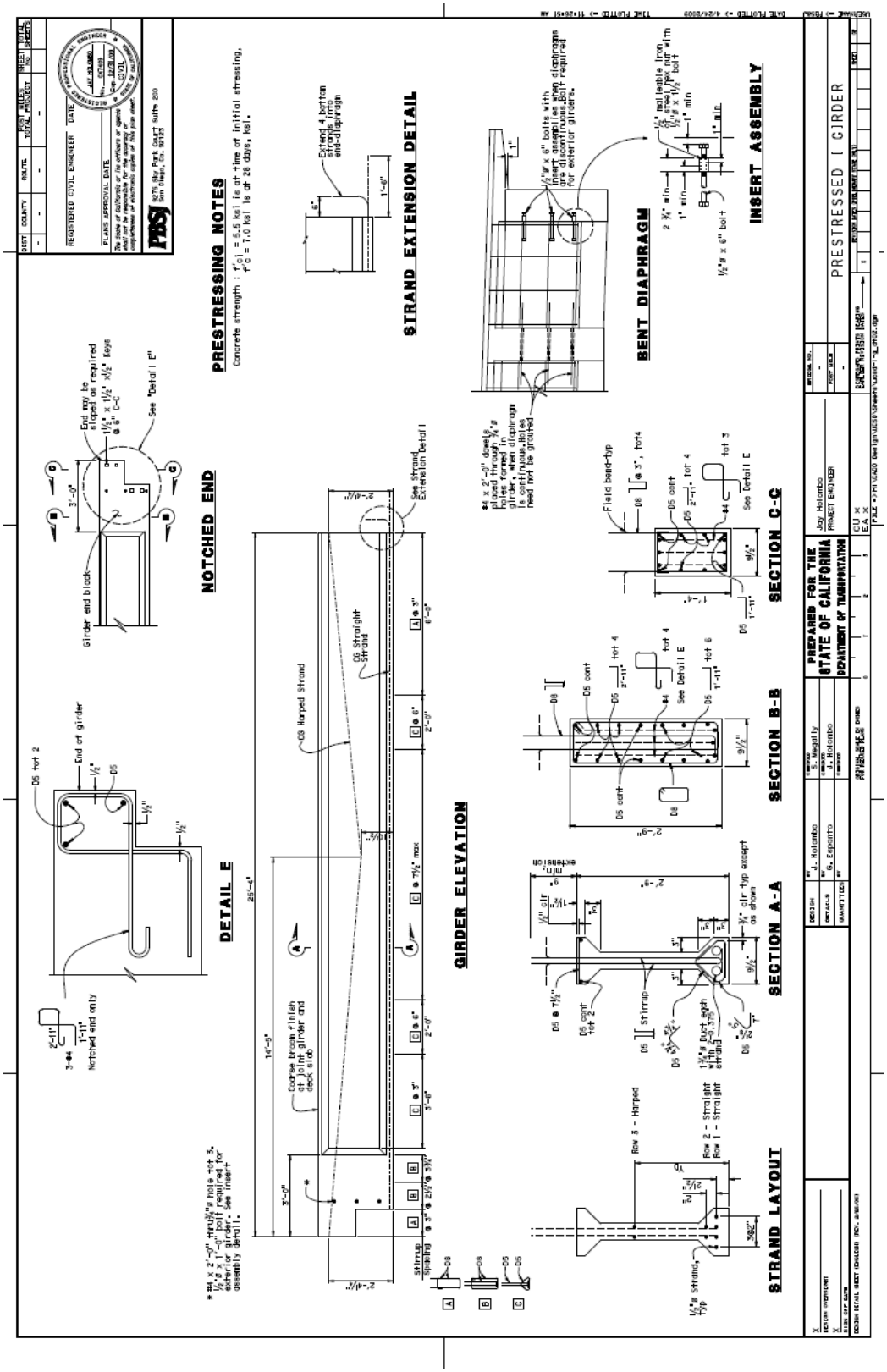


Figure B.7. Test unit drawing 7 of 7

# Appendix C. MATERIAL PROPERTIES

| 4.5 ksi Concrete | |
|---|---|
| Dilation Angle | 32 |
| Eccentricity | 0.1 |
| fbo/fco | 1.16 |
| K | 0.666 |
| viscosity Paramter | 0 |
| | |
| E | 3605000 psi |
| | |
| Compressive Stress (psi) | Inelastic Strain |
| 1600 | 0 |
| 2450 | 0.0005 |
| 3000 | 0.0011 |
| 4500 | 0.0035 |
| 4400 | 0.0059 |
| 3900 | 0.0089 |
| 3300 | 0.0145 |
| 2800 | 0.0195 |
| 2400 | 0.0245 |
| 2000 | 0.0295 |
| 400 | 0.0495 |
| | |
| Tensile Stress (psi) | Cracking Strain |
| 100 | 0 |
| 200 | 2.77E-05 |
| 300 | 5.55E-05 |
| 400 | 8.32E-05 |
| 497 | 0.000110125 |
| 300 | 0.04 |

a) 4.5 ksi concrete

| 7 ksi Concrete | |
|---|---|
| Dilation Angle | 32 |
| Eccentricity | 0.1 |
| fbo/fco | 1.16 |
| K | 0.666 |
| viscosity Paramter | 0 |
| | |
| E | 4768962 |
| | |
| Compressive Stress (psi) | Inelastic Strain |
| 2400 | 0 |
| 4800 | 0.0005 |
| 7153 | 0.001 |
| 7000 | 0.0035 |
| 6500 | 0.0059 |
| 6000 | 0.0089 |
| 5000 | 0.0145 |
| 4200 | 0.0195 |
| 3400 | 0.0245 |
| 2500 | 0.0295 |
| 400 | 0.0495 |
| | |
| Tensile Stress (psi) | Cracking Strain |
| 132 | 0 |
| 264 | 2.77E-05 |
| 396 | 5.54E-05 |
| 528 | 8.30E-05 |
| 627 | 0.000103796 |
| 400 | 0.04 |

b) 7 ksi concrete

Table C.1. Concrete material properties

| Prestressing Steel | |
|---|---|
| E | 28500000 |
| | |
| Yield Stress | Plastic Strain |
| 200000 | 0 |
| 240000 | 0.002982 |
| 270000 | 0.042982 |

a) Prestressing Steel

| Reinforcing Bar Steel | |
|---|---|
| E | 29000000 |
| | |
| Yield Stress | Plastic Strain |
| 60000 | 0 |
| 68000 | 0.02 |
| 90000 | 0.08 |
| 80000 | 0.25 |
| 1000 | 0.3 |

b) Reinforcing Bar Steel

Table C.2. Steel material properties